Neurophysiological mechanisms of functional lateralization in the human auditory networks

by
Neeraj kumar

Thesis submitted to

National Brain Research Centre

for the award of

Doctor of Philosophy in Neuroscience

National Brain Research Centre

Gurugram, Haryana

CERTIFICATE

This is to certify that the thesis titled **"Neurophysiological mechanisms of functional lateralization in the human auditory networks"** is the result of work carried out by **Neeraj Kumar** in the Division of Cognitive and Computational Neuroscience Division, National Brain Research Centre, Manesar, Haryana, India towards requirements for M.Sc.- Ph.D. Integrated degree.

The work presented herein is original and has not been submitted previously for the award of any degree or diploma to National Brain Research Centre (Deemed-to-be University) or to any other University. The work is as per guidelines given by National Brain Research Centre (Deemed-to-be University) and is a record of candidate's own efforts.

Prof. Arpan Banerjee
(Supervisor)

Prof. Krishanu Ray
(Director, NBRC)

Place: Manesar

Date:

DECLARATION BY THE CANDIDATE

I, **Neeraj Kumar**, hereby declare that the work presented in the form of this thesis was carried out by me under the guidance of **Prof. Arpan Banerjee** at the Division of Cognitive and Computational Neuroscience Division, National Brain Research Centre (Deemed-to-be University) Manesar, Haryana, India.

I declare that no part of the thesis contains any plagiarised material. Any previously published or other material sourced from anywhere else has been appropriately attributed to the source. I also declare that no part of this thesis has been previously submitted for the award of any degree or diploma to National Brain Research Centre (Deemed to be University) or to any other university.

Place: Manesar Neeraj kumar

Date:

Dedicated to my Grandparents Sh. Bakshi Ram and
Smt. Chanda Devi for their unconditional love

ACKNOWLEDGEMENT

At the culmination of this profound journey, I find myself humbled and profoundly grateful for the support, guidance, and companionship of numerous individuals who have played pivotal roles in shaping my PhD experience.

Firstly, I am profoundly grateful to Prof. Arpan Banerjee for his pivotal role in my academic journey during my PhD. Coming from a biology background, I was introduced to the captivating world of computational neuroscience through your lectures during coursework. It was this introduction that not only opened new horizons for me but also paved the way for an incredible opportunity to join his lab. Throughout my time in Prof. Banerjee‘s lab, his mentorship has been nothing short of inspiring. Having Arpan's cabin located just next door was like having a treasure trove of solutions within arm‘s reach. Thank you, Arpan, for being an exceptional mentor and for sharing your knowledge and insights generously. Your guidance has been and will be a guiding light on the academic path of mine. I extend my heartfelt thanks to my co-supervisor, Dr. Dipanjan Roy for his capable guidance and for being a goldmine of academic literature.

I am thankful to the past and present Directors of the NBRC for their generous provision of resources. I extend my heartfelt appreciation to the members of my doctoral committee, Dr. Dipanjan Roy, Prof. Soumya Iyengar, and Prof. Anindya Ghosh Roy for their constructive criticism and valuable feedback that has enriched the quality of this work.

I extend my sincere appreciation to Dr. Nivethida for her invaluable introduction to tACS and her guidance in establishing the tACS set-up. I would like to express my gratitude to Mr. Jitender Ahlawat, the Technical Officer and Satpal, for his

indispensable support in recording MRI and DWI data. My heartfelt thanks go to all the participants who willingly and enthusiastically became a crucial part of this study.

I am deeply thankful to Mr. Amit Jaiswal for generously providing the initial EEG dataset, which served as the foundation for this research. I am grateful to previous lab members Vinodh, Shrey and Tamesh for brain stimulating discussions that introduced me to the engineering perspective, broadening my horizons and enriching my approach to this research. I would like to express my appreciation to Dida for his thought-provoking discussions about science in general. A special mention to Abhishek and Nisha for engaging in enlightening discussions about philosophy, history, religion, and everything else under the sun. These conversations surely broadened my intellectual horizons in countless ways. I extend my thanks to Anagh for his invaluable insights into computational modeling, although discussion with him extended beyond this realm. I would like to express my gratitude to my other lab friends, Varun, Amit Naskar, Gargi, Pratika, Azman, Ritu, Suman da, Priyanka Chakraborty, Vinsea, and Ankit. Your camaraderie, support, and shared enthusiasm have made my research journey more enjoyable and memorable.

I want to take a moment to appreciate my dear batchmates, Meenakshi, Dr Gaurav, Surajit, Himali, Sarbani di, Shruti and Utsav who have been an integral part of this journey. Together, we have faced the challenges, celebrated the milestones, and shared the countless late-night study sessions that have brought us closer as a group. Your unwavering support, friendship, and the unique bond we've formed have made this academic experience truly special. Most importantly Meenakshi for being a lifeline in NBRC. Your unwavering support have been the cornerstone of my strength throughout this journey. Your presence has made every challenge more manageable and every success more meaningful. Thank you for being my source of inspiration and for sharing this remarkable journey with me.

I would like to extend a heartfelt thankyou to my childhood friends, Nitin and Yogender. Your presence, even from afar, has made this endeavor all the more meaningful.

Last but certainly not least, I want to express my profound gratitude to my family. Your unwavering support, patience, and encouragement have been the bedrock of my journey. Your belief in me has been my constant source of strength, and I am forever grateful for your love and understanding.

Neeraj Kumar

September 2023

"If I have seen further,

it is by standing on the shoulders of giants."

Isaac Newton

Contents

List of Tables

List of Figures

Chapter 1

Introduction

Hearing, the remarkable ability to perceive sound, stands as one of the fundamental senses that enrich our human experience. From the soft whispers of a loved one to the grandeur of a symphony orchestra, the auditory world surrounds us with a symphony of sound. Our auditory system, an engineering marvel, plays a central role in translating these vibrations into meaningful sensations, allowing us to connect with the world and each other in profound ways. Its core comprises a cluster of miniature acoustical sensors, densely packed into a space barely larger than a pea. These sensors possess the ability to detect vibrations at the atomic level, responding with a speed that far surpasses even our visual photoreceptors. This remarkable sensitivity to auditory cues enables rapid orientation of the head and body to unfamiliar stimuli, particularly those outside our immediate field of vision. Despite our strong visual tendencies, human communication heavily relies on the auditory system; in fact, the loss of hearing can have more profound social consequences than vision loss. Beyond speech, the auditory system plays a fundamental role in appreciating the aesthetics of music, representing one of the most sophisticated forms of human expression. Given its crucial importance and intricate workings, audition remains a captivating and vital mode of sensation.

1.1 The structure of the auditory system

The auditory system‘s functional range extends from the ears to the frontal lobes, with increasing complexity observed as we move up the nervous system's hierarchy. It begins with the transmission of sound waves through the peripheral auditory system, where the external ear funnels sound vibrations to the middle ear and then to the inner ear. In the inner ear, the cochlea converts sound vibrations into electrical signals that travel along the auditory nerve to the brainstem. At the brainstem, the auditory nerve fibers synapse with neurons in the cochlear nucleus [Yu and Young, 2000], the first station of auditory processing (see Fig. 1.1). From here, information is relayed to the superior olivary complex, which helps in sound localization, and the inferior colliculus, which integrates auditory signals from both ears. The auditory pathway then ascends to the thalamus, specifically the medial geniculate body (MGB), which serves as a major mediating station for auditory information [Aitkin et al., 1981]. From the MGB, the auditory signals are projected to the auditory cortex in the temporal lobe [Kandel and Schwartz, 2014]. The primary auditory cortex, located in the superior temporal gyrus, is responsible for basic auditory processing, such as frequency and intensity discrimination [Kaas and Hackett, 2000b]. Beyond the primary auditory cortex, the auditory pathway branches into multiple auditory association areas [Kaas et al., 1999]. These higher-order areas process more complex aspects of sound, including speech comprehension, sound recognition, and musical perception [Zatorre and Belin, 2001]. The auditory association areas also interact with other sensory and cognitive areas of the brain, contributing to multisensory integration and higher-level cognitive processes related to sound [Hackett, 2011]. In the current thesis, my work is centred around the cortical auditory processing.

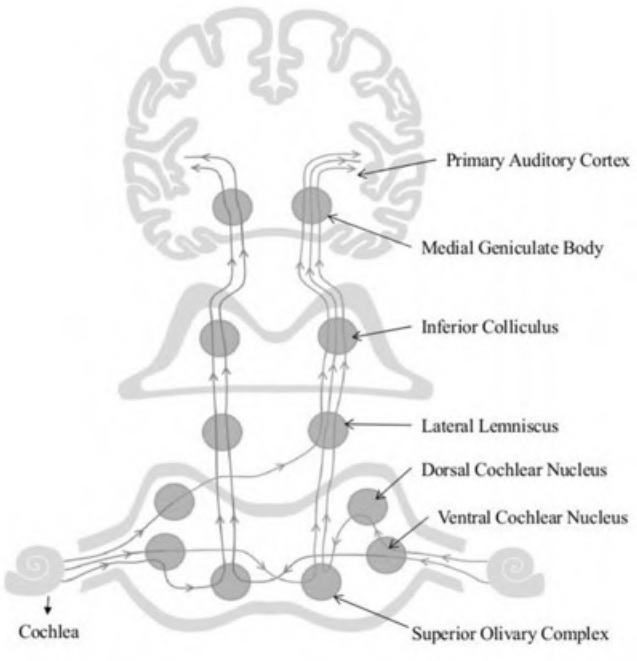

Figure 1.1: Schematic representation of central auditory pathway and main nuclei of brain stem. The shown ascending strucutral pathway extend from the cochlear nucleus to the primary auditory cortex. The pathway includes crossing at the lower brain stem level and thereby contralaterally dominant in subsequent representation. Adapted from [Jayakody et al., 2018].

1.1.1 Primary Auditory Cortex

Located in the superior temporal gyrus of the temporal lobe, the primary auditory cortex is the first stage of cortical auditory processing [Kaas et al., 1999]. Here, the ascending auditory signals received from the thalamus undergo initial processing, laying the foundation for cortical processing. The primary auditory cortex exhibits tonotopic organization, where neurons are arranged according to their preferred frequency response [Rauschecker et al., 1995, Pantev et al., 1989]. This spatial arrangement allows for efficient frequency discrimination, enabling us to distinguish between various pitches and tones. Within the primary auditory cortex, neurons respond selectively to specific acoustic features, such as the duration and intensity of sounds [Rauschecker et al., 1995]. Additionally, PAC is involved in encoding of pitch, temporal envelope, and spectral content, transformation into percepts and

subsequent communication within the auditory system. This selectivity helps in perceiving temporal patterns, essential for speech recognition and rhythm appreciation in music [Luo et al., 2006, Zeng et al., 2005]. Additionally, the primary auditory cortex is involved in binaural processing, integrating auditory inputs from both ears to facilitate sound localization, a crucial aspect of spatial hearing. As information progresses through the primary auditory cortex, it interacts with neighbouring auditory association areas, marking the transition from basic sound analysis to more intricate auditory processing [Hackett, 2015]. These higher-order regions play a pivotal role in extracting meaning from auditory stimuli, recognizing familiar sounds, and engaging in complex auditory tasks like language comprehension and music perception. Moreover, the primary auditory cortex is not solely limited to auditory processing. It interacts with other cortical regions, including those responsible for selective attention, working memory, and emotional processing [Plakke and Romanski, 2014, Kaas and Hackett, 2000a]. Such cross-modal interactions underscore the integrative nature of auditory perception, enriching our understanding of the broader cognitive implications of sound processing.

At the initial stage of cortical processing of auditory information, a hierarchical organization unfolds, encompassing several functionally distinct fields [Pandya and Sanides, 1973, Pöppel, 1997]. The first level comprises core primary areas, composed of potentially two areas, AI and R, each exhibiting a specific pattern of tonotopic organization and koniocortical histological features (See Fig. 1.2). Functionally, these primary-like areas play a crucial role in basic auditory analysis, such as frequency discrimination and intensity coding [Rauschecker et al., 1995]. The primary auditory cortex is densely interconnected and surrounded by the lateral belt cortex, comprising the antero-lateral belt (AL), middle-lateral belt (ML), and caudal-lateral (CL) belt [Kaas and Hackett, 2000b]. These lateral belt regions host three separate tonotopic regions with frequency reversals that separate them.

Compared to primary auditory cortical neurons, which primarily respond to relatively simple acoustic elements like pure tones, neurons in the lateral belt association cortex prefer more complex stimuli, such as band-passed noise and vocalizations. These lateral belt areas are part of the secondary auditory association cortex. The secondary cortex regions exhibit a lower density of staining for the calcium-binding protein parvalbumin [Hackett, 2011]. Neurophysiological studies have delved into the complex auditory and multisensory responses of the belt regions, shedding light on their role in higher-order auditory processing, sound recognition, and the integration of auditory information with inputs from other sensory modalities [Aitkin et al., 1981, Rauschecker et al., 1995]. These interconnected belt areas then project to a lateral parabelt region, consisting of two or more fields, which have limited direct connections with the core (Fig. 1.2). The pattern of connections clearly distinguishes between rostral and caudal regions. Caudal core field A1 exhibits moderate connections with the caudal belt and parabelt fields while being mainly associated with the surrounding belt fields and the rostral auditory core field (R). The rostral auditory core field (R) displays weak connections to both the rostral and caudal belt and parabelt fields, as well as to RTp, but has moderate connections with A1 and the RT. RT (region T) shows connections with the rostral belt fields and the adjacent field RTp. RTp demonstrates a unique connectivity pattern involving lateral and ambiguous connections with the temporal pole, rostral belt, and parabelt fields. The resulting connectivity pattern forms a recurrent and interactive network with numerous parallel paths and both direct and indirect connections. Notably, the suprathreshold activation of the parabelt neurons are mostly carried by the belt inputs rather than thalamic inputs. These intricate connections and functional differentiations between the primary auditory cortex, lateral belt cortex, and parabelt auditory cortex contribute to the complex auditory processing network [Rauschecker et al., 1995].

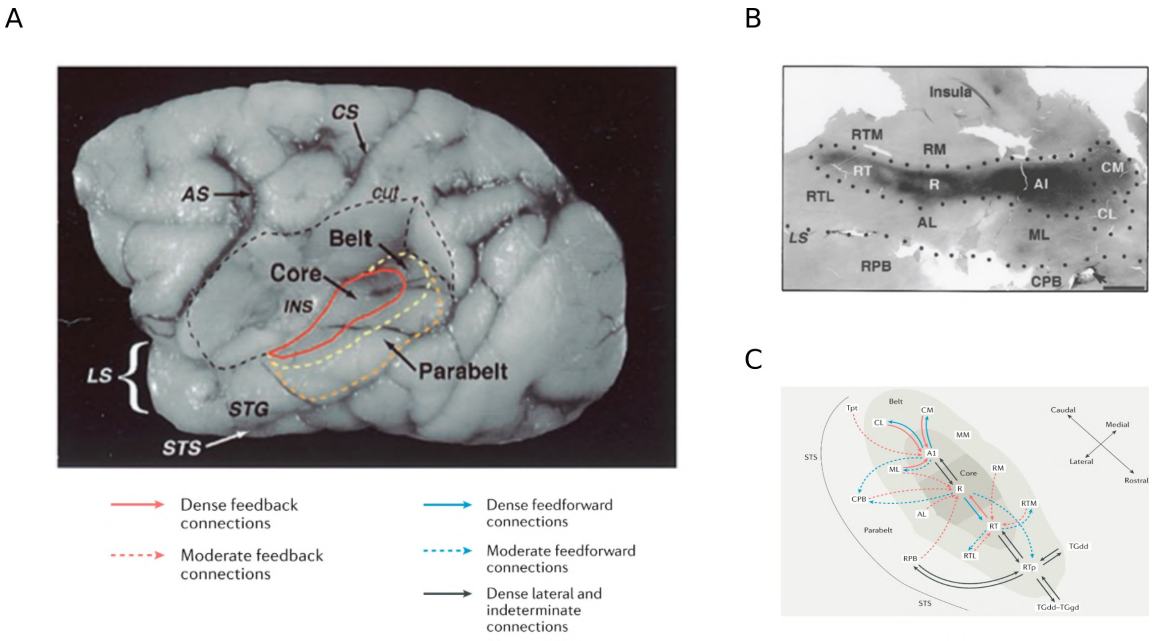

Figure 1.2: Auditory cortex and its intrinsic connections: (A) Lateral view of the macaque cerebral cortex Dorsolateral view of the brain after removing the overlying parietal cortex, exposing the ventral bank of the lateral sulcus and insula. The approximate locations of the core region (solid red line), caudal and lateral portions of the belt region (dashed yellow line), and the parabelt region (dashed orange line) are shown. The medial portion of the belt region and the rostral pole of the core in the ventral circular sulcus are not visible. Dashed black line defines portion of cortex cut away. AS, arcuate sulcus; CS central sulcus; INS, insula; LS, lateral sulcus; STG superior temporal gyrus; STS, superior temporal sulcus. (B) Architectonic fields by parvalbumin immunohistochemistry of auditory cortex. The core fields are the most darkly stained. The caudal belt fields are moderately dark. [Kaas and Hackett, 2000a] (C) A schematic image illustrating the connectivity of different core auditory regions [Jasmin et al., 2019].

The parabelt fields along with belt, in turn, establish connections with more distant cortex in the superior temporal gyrus, superior temporal sulcus, and prefrontal cortex [Plakke and Romanski, 2014, Kaas and Hackett, 2000b]. Each early cortical area receives a distinctive combination of inputs from multiple thalamic nuclei. Notably, the ventral nucleus of the medial geniculate complex primarily projects to areas in the core region, the dorsal divisions broadly project to the belt and parabelt regions, and the medial nucleus projects extensively to all three regions. Consequently, the auditory cortex in mammals is confined to adjoining areas in the temporal region,

as observed in various mammalian species.

1.1.2 Information Flow Beyond Auditory Cortex: Connections with higher-order regions

Beyond the primary auditory cortex, the flow of auditory information extends into an intricate and specialized network of interconnected regions, contributing to a myriad of auditory functions and interactions with other cognitive processes [Plakke and Romanski, 2014, Kaas and Hackett, 2000b]. This complex pathway involves the lateral belt cortex, the parabelt auditory cortex, and connections with frontal and temporal regions. The auditory information is processed through two main streams known as the ventral and dorsal streams, which originate from opposite ends of the auditory belt [Plakke and Romanski, 2014]. The rostral parabelt connects with the more rostral portions of the superior temporal gyrus, likely serving mainly auditory functions. Similarly, the caudal parabelt connects with the cortex of the caudal end of the superior temporal gyrus, also implicated in auditory processing. This organization of processing streams extends further into the prefrontal regions (See Fig. 1.3). The rostral principal sulcus, inferior convexity, and the lateral orbital cortex, including orbital and ventrolateral areas of the prefrontal cortex, are connected with the rostral superior temporal gyrus, the rostral belt, and the rostral parabelt. On the other hand, dorsolateral regions like the dorsal periarcuate cortex and the caudal principal sulcus, along with a small connection with caudal inferior convexity, are connected with the caudal belt and caudal parabelt. Notably, the connections to the prefrontal cortex are stronger in late auditory cortex, suggesting a cascade of lighter to stronger projections to the prefrontal cortex from early to late auditory processing regions. This arrangement implies separate processing pathways for spatial (where) and non-spatial auditory information (what). Further supporting

this notion, distinct anatomical projections from different auditory regions to prefrontal targets suggest that the auditory regions are associated with functions akin to the visual domain, where DLPFC and VLPFC are responsible for visuo-spatial and visual object processing, respectively. The parabelt also projects to four major regions of the frontal lobe, including the cortex near or within the frontal eye field, which is significant for directing gaze toward objects of interest, as spatial locations often correlate with visual interest. Moreover, the orbitalfrontal cortex, a multimodal region involved in assigning value to stimuli and the reward system, also responds to auditory stimuli [Hackett, 2011].

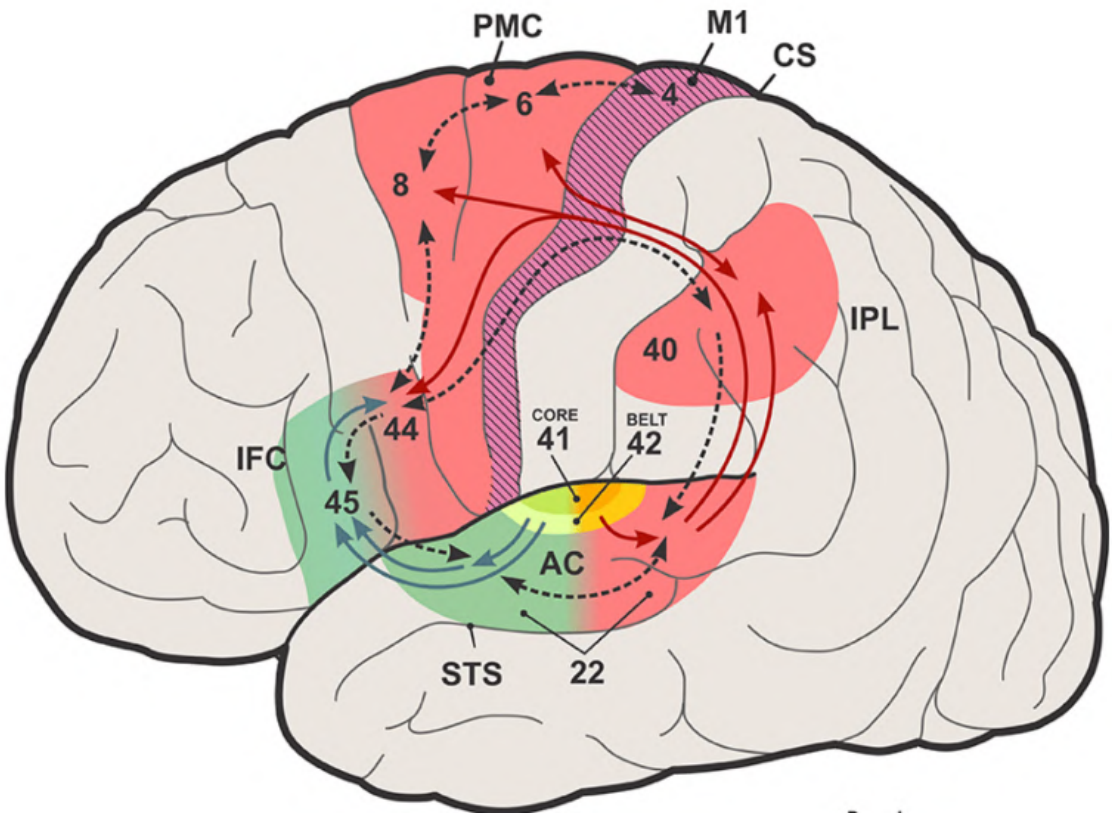

Figure 1.3: Processing streams efferents from auditory cortex [Rauschecker, 2021].

Furthermore, in humans, the auditory processing beyond the primary cortex becomes even more complex and intricate. As we ascend the hierarchy of the auditory

pathway, the anatomical connections among different regions become highly specialized and nuanced, far from a streamlined process. However, the challenge lies in the limitations of directly studying these connections in humans. To truly comprehend the intricate flow of auditory information to the prefrontal cortex, a fundamental prerequisite is understanding which parts of the temporal lobe are indeed auditory-responsive. This crucial knowledge remains elusive, leaving the organization of the human auditory cortex somewhat uncertain and sketchy. Further advancements in non-invasive neuroimaging techniques, such as functional magnetic resonance imaging (fMRI) and electroencephalography (EEG), offer hope for investigating human auditory processing with higher resolution. By combining these methods with innovative paradigms and computational models, we could unravel the complex network of auditory connections, filling in the gaps in our understanding of auditory processing in the human brain. This pursuit holds promise not only for enriching our knowledge of auditory cognition but also for advancing our comprehension of the broader mechanisms underlying human sensory and cognitive functions.

1.2 Functional representation of auditory system

When we conduct experiments to study how the brain responds to tasks we often observe distinct deflections in brain activity compared to the baseline or background neural activity. These deviations aren‘t just fluctuations but specific patterns of neural responses that provide valuable insights into the brain‘s information processing mechanisms. We employ a set of quantifiable and parameterized measures to decipher the intricacies of underlying brain processing and the corresponding neuronal configurations at play during auditory tasks. In essence, these *metrics* serve as the analytical instruments to decode the functional and structural attributes of the brain‘s response to auditory stimuli. For instance, these metric are often used to

quantify the magnitude, timing, and spatial distribution of neural responses. There are various metrics and measures used to study and quantify different aspects of brain function and information processing.

- Electroencephalography (EEG) Metrics: EEG measures electrical activity of synchronised postsynaptic potentials of pyramidal neurons using electrodes placed on the scalp. Metrics derived from EEG include:
  - Neural oscillations: rhythmic patterns of neural activity categorized into frequency bands such as delta, theta, alpha, beta, and gamma.
  - Event-Related Potentials (ERPs): electrical responses of the brain that are transient but time-locked to the onset of the stimulus.
- Functional Magnetic Resonance Imaging (fMRI) Metrics: Blood oxygen level-dependent (BOLD) signal is readily used to identify activated brain regions during tasks or at rest.
- Functional Connectivity: Statistical inter-dependencies in activity between different brain regions. Assess how different brain regions communicate and interact, often using measures like coherence, cross-correlation, or graph theory metrics.
- Neurophysiological Metrics: These include measures like spike rate, synaptic activity, and firing patterns, elucidating the electrical properties and activity of neurons and neural networks.

Given the temporal nature of sound, neural oscillations in particular serves as a crucial approach to understanding auditory processing [Giraud and Poeppel, 2012]. Neural oscillations synchronize with the temporal patterns of auditory stimuli, forming the basis of auditory perception [Ding et al., 2015]. These oscillations encode

various sound attributes, such as pitch, timbre, and rhythm, and their synchronization enables the brain to decode complex auditory information.

1.2.1 Neural oscillations

Neural oscillations, also known as brain rhythms or brainwaves, are rhythmic patterns of synchronized electrical activity generated by the collective behaviour of large populations of neurons in the brain. These oscillations occur across a wide range of frequencies, from slow oscillations in the delta band (0.5 - 4 Hz) to faster gamma oscillations (30 - 100 Hz). Each frequency band is associated with specific cognitive and behavioural states, reflecting the dynamic nature of neural processing [Kösem and van Wassenhove, 2017a, Kösem and van Wassenhove, 2017b]. The rhythmic firing of neurons within specific brain regions leads to the emergence of oscillatory patterns, which can propagate and synchronize across functionally related brain areas. Neural oscillations serve as a temporal code, providing a framework for the precise timing of neuronal firing and communication [Roß et al., 2002, Buzsáki and Chrobak, 1995, Ding et al., 2017]. They play a fundamental role in the organization and coordination of brain networks, facilitating the integration of information across different brain regions. Synchronization of neural oscillations is thought to enhance the efficiency of information processing and communication, allowing for the integration of distributed sensory inputs and the binding of different features of stimuli into coherent perceptual experiences.

Mechanistic basis of neural oscillations The mechanistic basis of neural oscillations lies in the interactions between excitatory and inhibitory neurons within neural circuits, as well as the intrinsic properties of individual neurons and the connectivity patterns between brain regions [Buzski, 2006, Hutcheon and Yarom, 2000, Wang, 2010]. Several key mechanisms contribute to the generation, synchroniza-

tion, and regulation of neural oscillations. Reciprocal synaptic connections between neurons within a network facilitate the synchronization of neural firing, creating positive feedback loops that allow for the propagation of oscillatory activity across functionally related brain regions. Additionally, gap junctions, enabling direct electrical coupling between neurons, contribute to the synchronization of neural oscillations [Buzsáki and Wang, 2012]. Neurons possess intrinsic membrane properties, such as ion channel conductances and time constants, that influence their firing patterns. Some ion channels exhibit resonance at specific frequencies, promoting rhythmic firing and contributing to the generation and maintenance of oscillatory activity. Pacemaker neurons are a specialized group of neurons with intrinsic rhythmic firing patterns, acting as local oscillators. They can drive oscillatory activity within their local circuitry and synchronize with neighbouring neurons, contributing to larger-scale neural oscillations. The architecture and connectivity of neural circuits play a vital role in shaping the frequency and synchronization of oscillatory activity. The coordinated activity of large populations of neurons within specific brain circuits and networks gives rise to neural oscillations across a range of frequencies [Buzsáki and Draguhn, 2004]. Neural oscillations can also be modulated by external inputs and sensory stimuli [Lakatos et al., 2019]. Sensory inputs can entrain and phase-lock neural oscillations, aligning them to the timing of external events. Additionally, neuromodulators, such as dopamine and serotonin, can modulate the excitability of neurons and influence the strength and timing of oscillatory activity.

Neural oscillations during speech and music processing

Neural oscillations play a critical role in the processing of speech and music in the brain, facilitating the efficient and coherent communication of auditory information. Different aspects of speech and music processing are associated with specific neural oscillatory patterns, reflecting the dynamic nature of these cognitive functions

[Gnanateja et al., 2022]. During speech processing, neural oscillations in the theta and alpha frequency bands (4 - 8 Hz and 8 - 13 Hz, respectively) are particularly relevant [Baar et al., 2000]. Theta oscillations have been linked to the segmentation and parsing of speech sounds, helping the brain to identify meaningful units in continuous speech [Giraud and Poeppel, 2012]. They are thought to contribute to speech comprehension and language processing by enabling the temporal organization of phonemes and words. Alpha oscillations, on the other hand, are involved in inhibiting irrelevant sensory inputs, fostering focused attention on speech stimuli [Klimesch, 2012]. They help filter out background noise and enhance the perception of speech sounds, especially in noisy environments. Alpha oscillations are also associated with anticipatory processing, predicting upcoming speech content and facilitating speech comprehension. In music processing, neural oscillations in the gamma frequency range (30 - 100 Hz) play a prominent role. Gamma oscillations are thought to be crucial for the integration of different musical elements, such as melody, rhythm, and harmony [Malekmohammadi et al., 2023]. They enable the binding of these elements into a coherent musical experience, allowing the brain to process and appreciate complex musical patterns. Moreover, neural oscillations are involved in cross-modal interactions during both speech and music processing. For example, in speech processing, visual inputs from lip movements during lip-reading can entrain and phase-lock with auditory oscillations, enhancing speech comprehension [Kumar et al., 2016]. Similarly, in music processing, visual cues from musicians‘ gestures can synchronize with auditory oscillations, enhancing the emotional and cognitive impact of the musical experience. In the motor cortex, research has shown that beta oscillations are involved in the entrainment of movement to a regular beat [Fujioka et al., 2015, Chang et al., 2018]. This can be observed in the form of increased beta power in the motor cortex when people tap their foot or move along to a rhythm. Overall, neural oscillations play a fundamental role in the efficient

processing and integration of auditory information during speech and music perception. The dynamic interplay between different frequency bands enables the brain to segment, organize, and bind auditory elements, contributing to the rich and nuanced experience of speech and music. Understanding the neural oscillatory mechanisms involved in speech and music processing provides valuable insights into the neural basis of human communication and creativity. Moreover, this knowledge has practical implications for improving speech and music processing in individuals with communication disorders or hearing impairments.

These neural oscillatory responses are known to align with the temporal structure of speech, known as *neural entrainment* observed in the brain during speech processing [Riecke et al., 2018, Lakatos et al., 2019, Ding et al., 2015]. It refers to the synchronization of neural oscillatory activity with the rhythmic patterns present in speech signals. When we listen to speech, the brain actively aligns its neural responses to the temporal structure of the incoming speech sounds. This synchronization allows the brain to precisely track the rapid changes in speech sounds, such as phonemes and syllables, which are crucial for understanding the meaning and intent conveyed in the spoken language. The process of neural entrainment is not passive but rather dynamic and interactive. The brain‘s oscillatory activity adapts and tunes itself to the timing and rhythm of the speech stream in real-time [Roß et al., 2002, Pöppel, 1997]. As a result, neural responses become optimally poised to capture and process relevant speech information, ensuring efficient speech comprehension. Neural entrainment is particularly prominent in brain regions involved in speech processing, such as the auditory cortex and the superior temporal gyrus. These regions demonstrate heightened activity in response to specific speech rhythms and exhibit enhanced neural synchronization during speech perception [Ding et al., 2015]. Moreover, neural entrainment is not restricted to the auditory domain. Recent research suggests that visual speech cues, such as lip movements and facial expressions, can also drive neu-

ral entrainment [Joon Kim et al., 2007, Siever, 2007]. This audiovisual entrainment allows the brain to integrate information from both the auditory and visual modalities, further enhancing speech comprehension and enabling us to decipher complex speech signals even in noisy or challenging listening environments.

1.2.2 Hemispheric specialization

Hemispheric specialization, also known as lateralization, refers to the phenomenon where certain cognitive functions and sensory processing are predominantly handled by one hemisphere of the brain [Toga and Thompson, 2003]. For most right-handed individuals and a large proportion of left-handed individuals, language processing, including speech perception and production, is primarily lateralized to the left hemisphere of the brain. This left hemisphere dominance for language is evident in the organization of the brain‘s language areas, such as Broca‘s area and Wernicke‘s area, which are typically located in the left frontal and temporal lobes, respectively [Morillon et al., 2010a]. Broca‘s area is involved in speech production and articulation, while Wernicke‘s area is crucial for language comprehension and the processing of grammatical structures. Connections between these areas and other language-related regions facilitate the flow of information required for language processing [Giraud and Poeppel, 2012]. In contrast, the right hemisphere plays a complementary role in language processing, particularly in aspects of language related to prosody, emotional and intonational content, and discourse comprehension [Güntürkün et al., 2020]. Additionally, the right hemisphere is involved in the processing of metaphorical language and the comprehension of ambiguous language cues. Regarding music processing, hemispheric specialization is more complex. While both hemispheres contribute to music processing, the right hemisphere is generally more involved in the perception of melody, timbre, and emotional aspects of music. The

right hemisphere is particularly crucial for processing pitch patterns and recognizing melodic contours [Yurgil et al., 2020, Koelsch, 2011]. On the other hand, the left hemisphere plays a larger role in the processing of rhythm, temporal aspects of music, and the analysis of harmonic structures. Language and music processing also interact in the brain, as evidenced by shared neural networks for syntax processing in language and musical structure analysis. The study by Albouy et al explores the brain‘s sensitivity to spectrotemporal modulation and its implications for hemispheric asymmetry in processing speech and melody [Albouy et al., 2020]. The findings of

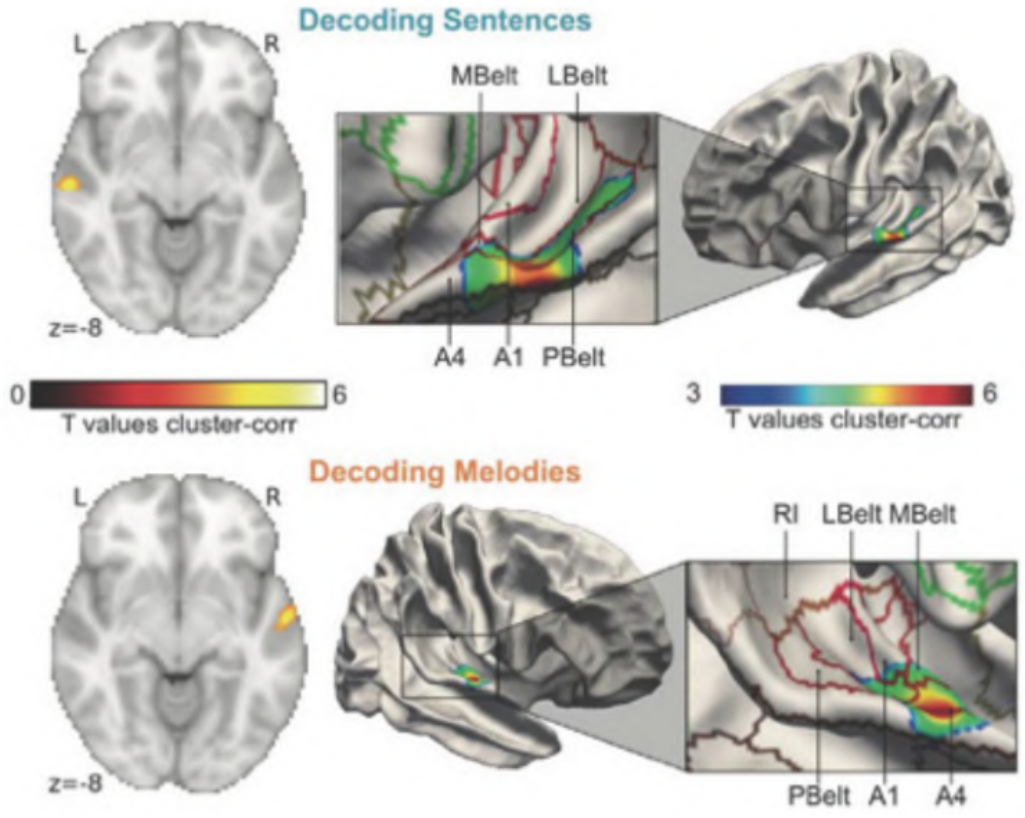

Figure 1.4: Brain asymmetry for speech and music is mediated by distinct sensitivity to spectrotemporal modulation. Functional MRI data reveals that the left auditory regions are responsible for neural decoding of speech, while the right auditory regions for melody processing. The effects of degradation on perception mirrored their impact on neural classification [Albouy et al., 2020].

the study revealed a clear hemispheric specialization in the auditory cortex for processing auditory information. Deterioration of temporal cues mainly affected speech component understanding but not melody comprehension, while degradation of spectral signals influenced melody discrimination but not speech comprehension [Albouy et al., 2020]. Speech content was primarily decoded in the left auditory cortex and was impaired by temporal deterioration, while melodic content was decoded predominantly in the right auditory cortex and was adversely affected by spectral degradation (see Fig. 1.4). These findings indicate that the left and right auditory cortices are connected to enhanced resolution in temporal and spectral modulation, respectively, showcasing their specialized roles in processing different aspects of auditory stimuli.

1.3 Structure to function

The functional metrics, as previously introduced in section 1.2, serve as invaluable tools in unraveling the intricacies of the brain‘s information processing mechanisms. These metrics, which provide insights into the dynamic neural responses during cognitive tasks, are often a direct outcome of the structural wiring of the brain. A prime example of this interplay between structure and function can be found in the phenomenon of contralateral dominance in functional responses within the primary auditory cortices during monaural condition [Langers et al., 2005]. This dominance is rooted in the structural organization of the auditory pathway, where auditory signals cross over, resulting in the preferential activation of contralateral brain regions in response to monaural stimuli [Langers et al., 2005, Ross et al., 2005]. Zooming out to the whole-brain level, these structural connections provide the scaffold that shapes various aspects of functional processing. There has been substantial evidence on the role of SC in information transfer between brain regions

[Honey et al., 2007], shaping network topology [Bullmore and Sporns, 2009], and mediating synchronization and coherence of neural activity [Stam et al., 2007]. At this macroscopic level structural connectivity in the brain refers to the physical wiring and anatomical connections between different brain regions. These connections play a crucial role in brain function, as they form the structural framework that allows for communication and information exchange among various neural networks. The brain‘s structural connectivity is primarily established during early development and continues to undergo modifications throughout life based on experience and learning. One of the key functions of structural connectivity is facilitating efficient information processing and integration across the brain [Mišić et al., 2015, Abeysuriya et al., 2018]. Nerve fibers, known as axons, form bundles called white matter tracts that connect different brain regions. These tracts serve as highways for transmitting electrical signals and information between neurons. The strength, density, and efficiency of these connections influence how efficiently information can travel through the brain, enabling the brain to perform complex cognitive tasks, sensory processing, and motor control. Moreover, structural connectivity underlies the formation and maintenance of functional networks in the brain. Regions that are structurally connected tend to form functional networks that work together to perform specific tasks or cognitive functions [Cabral et al., 2011, Sporns, 2010, van den Heuvel and Sporns, 2013, Sporns et al., 2004]. For example, the default mode network, responsible for self-referential thinking and daydreaming, is a functional network that emerges from structurally connected regions. Structural connectivity is also closely linked to brain plasticity and adaptability. Learning, memory, and skill acquisition are associated with changes in structural connectivity [Sporns, 2011]. New experiences and learning can lead to the formation of new connections or the strengthening of existing ones, allowing the brain to adapt and optimize its functioning based on the demands of the environ-

ment. There are several studies reported structural connectivity of the brain with electrophysiological [Finger et al., 2016, Scrascia et al., 2014, Filatova et al., 2018], fMRI [Cabral et al., 2011] and behavioural responses [Feng et al., 2021]. For example, the structural connectivity between the primary auditory cortex and the secondary auditory cortex is thought to play a crucial role in the processing of basic auditory features such as pitch, timbre, and harmony [Griffiths et al., 2000, Plakke and Romanski, 2014]. Similarly, the structural connectivity between the primary visual cortex and the secondary visual cortex is thought to play a crucial role in the processing of basic visual features such as color, shape, and movement [Bressler, Steven L and Nakamura, 1993]. On the other hand, more abstract and higher-level features of the environment, such as meaning, context, and emotion, require a more complex and dynamic interplay between different regions of the brain. These features are thought to be processed by distributed networks of brain regions that are connected through both structural and functional connections [van den Heuvel and Sporns, 2013, Mišić et al., 2018, Sporns, 2010]. However, as we move to more abstract and higher-order features, it becomes more difficult to assign them to specific regions of the brain and more likely to involve distributed networks of regions, which are connected through both structural and functional connections. These networks are thought to involve the dynamic interaction of different regions of the brain, which work together to process more complex and abstract information. For example, the processing of meaning in language requires the coordination of neural activity between regions involved in phonetic, lexical, and semantic processing, as well as regions involved in attention, working memory, and executive control [Morillon et al., 2010b, Kösem and van Wassenhove, 2017c]. Similarly, the processing of emotion in music requires the coordination of neural activity between regions involved in auditory processing, regions involved in the perception of pitch and rhythm, and regions involved in the processing of emotional

valence [Wang et al., 2023, Di and Biswal, 2019]. This lateralization is thought to be a result of the structural and functional properties of the brain, such as the patterns of connectivity between regions and the distribution of neural populations that are specialized for processing different features. Furthermore, disruptions in structural connectivity have been linked to various neurological and psychiatric disorders. Conditions like Alzheimer‘s disease, multiple sclerosis, and autism spectrum disorders often involve alterations in the brain‘s structural connections, which can lead to impairments in cognition, sensory processing, and motor functions [Fonseca et al., 2015, Scrascia et al., 2014]. In summary, structural connectivity provides the physical substrate for efficient communication between brain regions, supports the formation of functional networks, and underlies the brain‘s adaptability and learning capabilities. Understanding the complexities of structural connectivity and its relationship with brain function is essential for advancing our knowledge of the brain‘s organization and its implications for health and disease.

1.4 Scope of the thesis

The scope of this thesis is to comprehensively explore auditory processing by integrating concepts of oscillations, lateralization and structural connectivity of human brain. These elements encompass the foundation of cortical activity in the primary auditory cortices, the role of distinct oscillations and their lateralization, and the influence of structural connectivity on guiding functional responses. In the subsequent chapters, specific objectives will be pursued to achieve a coherent understanding of auditory cortical processing. These objectives include

- Investigating mechanistic basis of right hemispheric dominance of 40 Hz ASSR.
- Role of bilateral primary auditory cortices in mediating hemispheric special-

ization of melody and speech.

- Investigating structural-connectivity derived functional attributes in causal outflow from primary auditory cortices.

In the 2 chapter, we establish the presence of hierarchical cortical network during processing of a very basic auditory stimuli composed of pure tones, commonly known to generate auditory steady-state response. We successfully validate the presence of contralateral dominance in the primary auditory cortices during monaural stimulations. Furthermore, we find causal outflow from bilateral primary auditory cortices (PAC) are central to the right hemispheric dominance during processing of periodic tonal stimuli. In that chapter, we standardize tools such as source localization, Granger causality and laterality analysis that are required to characterize neural underpinnings of the auditory processing during different auditory environments. Building upon these analysis and findings, we hypothesize role of causal outflow from primary auditory cortices in mediating hemispheric specialization of melody and speech, two most important human auditory communication skills. In chapter 3, we aimed to investigate the frequency-specific outflow from the PAC during speech, melody and ASSR conditions. We employed electroencephalography (EEG) to record neural activity while 30 participants selectively attended to either the speech or melodic content of ecologically valid *a cappella* songs. We reconstruct source activity utilizing subject-specific anatomy of brain and investigate the laterality in the causal outflow from PAC. In the chapter 4, we explore the mechanistic basis of the hemispheric specialization of melody and speech. We record diffusion magnetic resonance imaging (dMRI) data, from the same participants recorded in study 3, to constrain the outflow from the PAC in a neuro-dynamic whole-brain connectome model. Building upon the findings of these studies to disambiguate between thalamo-cortical and cortico-cortical auditory inputs on corresponding network we undertook a Transcra-

nial Alternating Current Stimulation (tACS) study. By stimulating PAC by tACS we aim to causally entrain large-scale network and examine how these propagation leads to hemispheric lateralization. In a pilot study, we record EEG while 40 Hz sinusoidal alternating current is applied to a participant‘s right PAC. By delving into these interconnected aspects, this thesis aims to shed light on the intricate workings of auditory cortical processing and its implications for understanding how the brain perceives and processes auditory stimuli.

Chapter 2

Large-scale functional network undelie right hemispheric dominance of 40 Hz ASSR

The material presented in this chapter has been previously published as **Kumar N**, Jaiswal A, Roy D, Banerjee A. Effective networks mediate right hemispheric dominance of human 40 Hz auditory steady-state response. Neuropsychologia. 2023 Jun 6;184:108559. doi: 10.1016/j.neuropsychologia.2023.108559. PMID: 37040848.

2.1 Introduction

Auditory steady-state response (ASSR) is a phase-locked oscillatory response to periodic sound recorded from the scalp [Picton, 2013, Zhang et al., 2013]. ASSRs can be identified by the frequency-based analysis, exhibiting a sharp rise in spectral power and phase-locking across trials at the frequency of periodicity. In the literature, ASSRs have been reported widely to be elicited maximally at a stimulation fre-

quency of 40 Hz [Galambos et al., 1981, Hari et al., 1989, Pastor et al., 2002]. Moreover, ASSRs can be detected readily at a single participant level and do not show gender-specific differences among right-handed participants [McFadden et al., 2014, Melynyte et al., 2017]. Due to its robustness and reliability, 40 Hz ASSR is widely used for theoretical and clinical research, e.g., temporal auditory processing, screening hearing threshold, and measurement of consciousness during global anaesthesia [Farahani et al., 2020, Haghighi et al., 2018, Niepel et al., 2020], etc. Additionally, 40 Hz ASSR is also used as a biomarker in certain neuropsychological disorders like schizophrenia and autism [O'Donnell et al., 2013]. Speech and music on the other hand both elicit complex and broad-band responses within the auditory pathway. The Auditory Steady-State Response (ASSR) stands out as an ideal candidate due to its capacity to generate robust and high signal-to-noise ratio responses. Here we use ASSR to first establish auditory processing centers, mapping functional networks, and uncovering key attributes of auditory information processing.

In general, the processing of sensory stimuli requires coordinated interactions among specialised brain regions that are distributed across the hierarchal cortical networks [Bressler and Menon, 2010a, Fries, 2005]. Lithari and colleagues have reported the emergence of a frequency-specific large-scale network during the visual steady-state response, indicating synchronized activity across multiple regions of the brain in response to visual stimulation [Lithari et al., 2016]. Therefore, studying the pattern of information flow among specialised brain regions would allow us to understand the neural basis of ASSRs. There is converging evidence that neural generators for 40 Hz ASSRs predominantly lie in the right superior temporal gyri (STG) [Kim et al., 2019] and bilateral primary auditory cortices [Bohórquez and Özdamar, 2008, Pantev et al., 1996, Ross et al., 2005, Steinmann and Gutschalk, 2011] in addition to sub-cortical regions [Herdman et al., 2002, Poelmans et al., 2012, Steinmann and Gutschalk, 2011]. De-

spite the growing consensus on the regions involved in the activation of 40 Hz ASSRs, the interactions and information flow among the relevant nodes of ASSRs are yet to be fully investigated. Importantly, the patterns of information flow between relevant brain regions in the distributed auditory hierarchy are indicative of directed functional connectivity, which offers a refined picture of the communication channels and a critical role of the underlying drivers and followers involved in the generation of ASSRs [Bressler and Menon, 2010b, Lithari et al., 2016]. For example, a unidirectional information flow from one sensory node to a higher-order will reveal hierarchical processing. On the other hand, a bidirectional connectivity between cortical nodes would imply a parallel and simultaneously recurrent processing scheme. For instance, the flow of information between left and right auditory cortical nodes are mediated via strong cortico-thalamocortical feedback loops [Das et al., 2021]. Thus, an overall characterization of the direction of information flow in auditory pathways within and between two hemispheres will reveal that the functional organization between two hemispheres is governed by the symmetry/asymmetry of auditory stimulation during auditory tone processing tasks. Motivating our work from previous studies that suggest lateralization enables more efficient information transfer among specialised brain regions during language processing [Toga and Thompson, 2003], we explore ASSR lateralization at the cortical source space level and interactions among key cortical sources. We hypothesize that causal interactions between cortical sources will provide critical insights into underlying brain networks and their task-specific functional organization. Following studies demonstrating right hemispheric dominance of non-linguistic/tonal/musical auditory sounds [Toga and Thompson, 2003, Zatorre et al., 2002], we further hypothesize that the underlying effective brain network interactions [Friston, 2011] should also reflect the presence of hemispheric dominance. Furthermore, the directionality of effective connections will reflect the hierarchical aspects of underlying information processing.

Earlier studies have reported right hemispheric dominance in source activation during 40 Hz ASSRs. Existing evidence from structural and functional studies suggests that 70% of ascending auditory inputs from either ear cross at the brainstem level and 30 % remain on the same side [Hackett, 2015, Kaas and Hackett, 2000b, Langers et al., 2005]. Consequently, one would expect a contralateral dominance in primary auditory cortical (PAC) response during monaural stimulation conditions. Now, it's naturally intriguing how the information, particularly during the monaural right condition, that enters the left PAC is eventually redistributed to a specialised centre present in the right hemisphere. Transcortical communication through the corpus callosum (CC) has been suggested to compensate for this asymmetric input to achieve hemispheric specialization during the processing of distinct features of auditory stimuli [Aboitiz et al., 1992, Cammoun et al., 2015]. This can be very well experimentally validated by monaural stimulations. Hence, according to the principle of contralateral dominance, the monaural right would evoke a greater response in the left PAC than the monaural left condition [Andoh et al., 2015]. In the present work, we record human electroencephalography (EEG) during 40 Hz ASSRs during binaural and both monaural left and right stimulation conditions. We reconstruct trial-wise source activity employing subject-wise anatomical structure by co-registering EEG with individual subject Magnetic resonance imaging (MRI) data. We first confirm the presence of ASSR and its well-known right hemispheric dominance co-existing with contralateral dominance of early auditory processing. Subsequently, we characterize effective network interactions using spectral Granger's causality among sources of ASSRs.

2.2 Materials and methods

2.2.1 Participants

Twenty-one healthy, right-handed human volunteers (16 males, 5 females, age range 22-39 years old; mean $\pm$ SD = 28 $\pm$ 2.10) participated in this study. The right-handedness of participants was verified by the Edinburgh Handedness Questionnaire based upon a cut-off of 60-100. All the volunteers reported no medical history of audiological, neurological or psychiatric disorders. All of them had normal or corrected to normal visual acuity. Informed consent was given by all the volunteers in a format approved by the Institutional Human Ethics Committee (IHEC) of National Brain Research Centre that confirms the guidelines set by the Declaration at Helsinki. All participants were fluent in at least two languages, Hindi and English, but some were familiar with another language of Indian origin.

2.2.2 Experimental design

Stimuli consisted of sinusoidal tones of frequency 1 kHz and 25 ms duration, presented 40 times per second. Wherein, each tone of 25 ms had 2 ms fade in and faded out period (Fig. 2.1 A: Upper panel). Each trial comprised of 1s "On" block (auditory stimulation) period followed by 1s "Off" block (silent) period (Fig. 2.1A). A total of 100 trials were presented for each kind of auditory stimulation, i.e., monaural and binaural. In total, four experimental conditions, each lasting 200 s, were performed in the following order- 1) a baseline condition in which the volunteers were not given any tonal stimuli; 2) Binaural (in both ears); 3) Monaural left (only through left ear); 4) Monaural right (only through right ear). The time interval between each condition was set to 100 s (silent). Auditory stimuli were created and presented in Stim2 software (Compumedics, Inc., USA) at 85 dB sound pressure level.

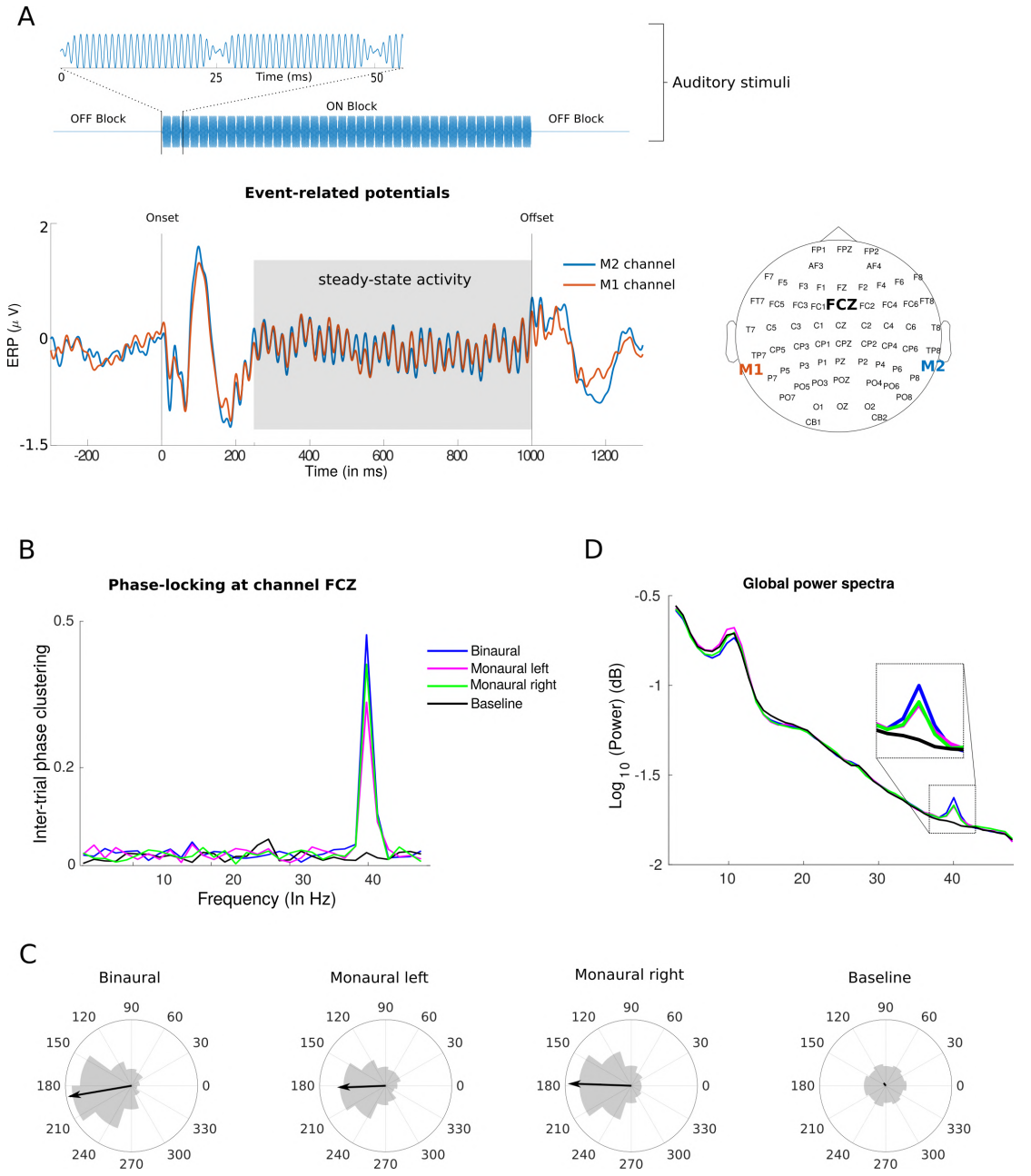

Figure 2.1: Steady-state response: (A) Stimuli (Upper panel): 25 ms of pure tone (1 kHz frequency), presented 40 times in a second during 1 s ON block interspersed by two OFF blocks (silent). Lower panel: Group-level ERPs of mastoid channels (M1 as orange and M2 as sky-blue) having oscillatory response in the time window of 250-1000 ms relative to the onset of periodic auditory stimuli. (B) ITPC of single channel (D) Group-level power spectrum showing sharp enhancement at 40 Hz during monaural left (magenta), monaural right (green), binaural stimuli (blue) relative to baseline (black) condition. (C) Phase-angle distribution at 40 Hz during auditory stimulation and baseline conditions. The arrow in the middle of each circle represents strength of ITPC.

The specific value of intensity was chosen to have reliable ASSR responses in all participants based on a prior pilot study in our group. Participants were instructed to stay still in a sitting position, fixate on a visual cross displayed on a computer screen and listen to the tones. Continuous scalp EEG was recorded when the volunteers were performing the experiment.

2.2.3 Data acquisition

EEG data were recorded using 64 Ag/AgCl sintered electrodes mounted in an elastic head cap according to the international 10-20 system. All recordings were done in a noise-proof isolated room using NeuroScan (SynAmps2) system (Compumedics Inc, USA) with a 1 kHz sampling rate. Abrasive electrolyte gel (EASYCAP) was used to make contact between EEG sensors and scalp surface, and impedance was kept below 5 $k\Omega$ in each sensor. The default EEG system-assigned reference electrode was placed at the vertex (Cz) and the ground electrode at the forehead (AFz). The electrode locations were obtained relative to three fiducials at the nasion and left and right preauricular points using a 3D digitizer (Polhemus Inc., Colchester, VT, USA).

2.2.4 Pre-processing of EEG signals

EEG data analysis was performed with Chronux (`http://chronux.org/`), EEGLAB [Delorme and Makeig, 2004], FieldTrip (`http://fieldtriptoolbox.org`) and custom MATLAB scripts (`www.mathworks.com`). EEG data was imported in MATLAB using EEGLAB from Neuroscan raw files. Continuous long-time EEG time series were bandpass filtered to retain frequencies between 3 and 48 Hz. Thereafter, eyeblinks and heartbeat artefacts were removed from EEG data using independent component analysis in-built in EEGLAB after careful visual inspection. The temporal

window of steady-state activity was identified from the grand mean event-related potentials (ERPs) of both mastoid channels [Coffey et al., 2016] (Fig. 2.1). Hence, baseline corrected epochs of 750 ms from "On" blocks were extracted from each trial, excluding the first 250 ms of the time series from the onset of auditory stimuli. Furthermore, simple threshold-based artefact rejection was applied to exclude the remaining noisy epochs. Hence, epochs having a voltage greater than $\pm 85\ \mu v$ were discarded. After artefact rejection, none of the epochs from monaural conditions of one participant survived the thresholding. Therefore, we removed the data of that participant from further analysis. Thereafter, we re-referenced the EEG signal to common mode average reference, followed by combining trials from every participant into a single pool for group analysis at the sensor-level. On average less than 5 trials were removed per subject. In total we have recorded 2000 trials from all participants per condition (100 trials X 20 participants). The surviving trials numbers were 1980 in binaural; 1975 for monaural left and 1980 trials for monaural right.

2.2.5 Identification of ASSRs at sensor-level

Inter-trial phase clustering

Inter-trial phase clustering (ITPC) was employed to ensure the presence of the phase-locked oscillatory response of 40 Hz. ITPC quantify the degree of non-uniformity or clustering in the distribution of oscillatory phase across trials at a particular frequency [Palva et al., 2005]. The value of ITPC range between zero and one, with one being perfect phase consistency across trials and zero being complete uniformity. Mathematically, ITPC is defined as

$$ITPC_f = \left|\frac{1}{n}\sum_{n=1}^{n} e^{i\theta}\right| \tag{2.1}$$

wherein, $\frac{1}{n}\Sigma_{n=1}^{n}$ represents an average of complex vector $e^{i\theta}$ across n trials; $e^{i\theta}$ is Euler's formula wherein θ is phase angle at frequency f derived from complex Fourier coefficients. We calculated the ITPC of all the channels for every conditions and selected a channel with maximum ITPC at 40 Hz (Fig. 2.1B). To assess the significance of phase clustering, the observed ITPC values were compared with a critical value $ITPC_{crit}$ computed at the significance level of $p = 0.01$ (Bonferroni corrected). The critical value corresponding to p-value was obtained as [Zar, 1999, Cohen, 2019]

$$ITPC_{crit} = \sqrt{-log(p) \times n^{-1}} \tag{2.2}$$

where n is the total number of trials. ITPC values higher than $ITPC_{crit}$ were considered statistically significant.

Power spectrum

The power spectrum was computed using Chronux function *mtspectrumc.m* scripts at each sensor, trial, and condition. First, power spectra were calculated in the frequency range of 3-48 Hz ($\sim 1\ Hz$ smoothing), and grand averaged for all channels and trials. Subsequently, t-statistic were calculated as test statistics between auditory stimulation and baseline conditions at the frequency of interest i.e., 40 Hz, followed by a statistical evaluation of observed t-statistic employing a permutation test. The procedure involves 1000 time shuffling of the trials among both conditions and measuring t-statistic in each permuted data sets. Thereafter, a histogram is plotted, comprising all 1000 t-statistic from permuted data creating a null distribution [Maris and Oostenveld, 2007]. Observed t-statistic were then thresholded to the 99^{th} quantile of the respective null distribution corresponding to $p = 0.01$.

Laterality analysis

Hemispheric asymmetry in brain responses was quantified using laterality index (LI), which is the difference between right hemisphere (RH) and left hemispheric (LH) responses normalized by the sum of responses in both hemispheres.

$$LI = \frac{RH - LH}{RH + LH} \tag{2.3}$$

The value of LI ranges between +1 and -1. Wherein, +1 represents complete right hemispheric dominance, -1 for complete left hemispheric dominance and 0 for a bilaterally symmetric response. Trial-wise median of 40 Hz spectral power and ITPC was calculated over right and left hemispheric sensors, excluding midline sagittal plane electrodes. Furthermore, to assess the statistical significance of LIs, the 95 % confidence interval (CI) was calculated as

$$CI = (\mu + t_{d.f.} \times S.E., \mu - t_{d.f.} \times S.E.) \tag{2.4}$$

where μ is the mean of data, t is the inverse of Student‘s t cumulative distribution function at corresponding $d.f.$ (degree of freedom), and $S.E.$ is the standard error of the mean. Moreover, to examine whether lateralization indices of different auditory conditions have equal means, we performed one-way ANOVA on the distribution of LI values of different stimulation conditions, followed by controlling for multiple comparisons employing the Tukey-Kramer post-hoc test.

2.2.6 Source localization of ASSRs

Evoked potentials

Early auditory potentials were reconstructed employing time domain exact low-resolution brain electromagnetic tomography (eLORETA) [Pascual-Marqui, 2007].

Similar to frequency domain eLORETA as described comprehensively below. We have utilised individual anatomy to reconstruct source waveforms while restricting the analysis to bilateral primary auditory cortices. Wherein, the respective coordinates of sources were obtained for both Heschl's gyri based on the Automated anatomical labelling (AAL) atlas [Rolls et al., 2015] (See figure 2.3 A; left panel). Sensor-level covariance matrices were computed for each condition from the 20 ms time series centred around N100 response. Remaining procedure kept same as frequency domain source analysis (See below) to obtain subject and trial wise source waveforms for each condition. Thereafter, laterality indices were computed for N100 amplitude between bilateral auditory cortices followed by statistical testing of asymmetry in individual condition and difference between each condition as per methods 2.2.5.

Frequency specific sources

Converging evidence suggests that utilising individual brain anatomy yields better source localization [Coffey et al., 2016]. Hence, source-level analysis was performed by co-registering EEG sensor locations to MRI-guided fiducial points. Exact low-resolution brain electromagnetic tomography (eLORETA) [Pascual-Marqui, 2007] was used to calculate the three-dimensional spatial distribution of source activity underlying 40 Hz ASSRs. Earlier research demonstrated that eLORETA yields a favourable performance when false positives were considered [Halder et al., 2019]. eLORETA employs distributed source modelling and estimates the current source density across brain volume by minimizing the surface Laplacian component during the construction of the spatial filter [Pascual-Marqui, 2007]. Additionally, eLORETA does not rely upon any assumption regarding the number of underlying sources while having excellent control over the suppression of false positives during the detection of sources [Halder et al., 2019]. Hence, source analysis employing eLORETA was per-

formed using the FieldTrip toolbox [Oostenveld et al., 2011] implemented in MATLAB and connectivity analysis was done by customized MATLAB scripts.

The ingredients to construct a frequency domain eLORETA spatial filter are the forward model and the cross-spectral matrix of sensor data. The forward model also called the volume conduction model for the head define how an electrical current propagates across brain and would be recorded at the sensor level. Therefore, geometrical properties of the head including surface description of brain, skull and scalp were derived from subject-specific T1-weighted anatomical MRI scan and used for forward modelling based on the boundary element method [Fuchs et al., 2001]. Subsequently, employing channel position leadfields for individual subjects were computed. Construction of leadfield requires description of locations known as grids on which the leadfields are calculated. Here, we first create $11,000$ template grids that were defined according to Automated anatomical labelling (AAL) atlas [Rolls et al., 2015]. Subsequently, these template grids were warped to individual MRI yielding 11,000 subject-specific grids arranged in normalized space. The leadfield matrix was computed at each grid in 3 orthogonal directions.

Moreover, we computed sensor-level cross-spectral matrices for each condition from the SSR time series ($250 : 1000$ ms), same as used for the sensor-level analysis (Fig. 2.1 A). Thus, we computed a spatial filter employing the subject-specific forward model and sensor-level cross-spectral matrix for each condition. A common spatial filter was computed from combined data i.e., trials from all four conditions were grouped into a single pool. Since, common filter employs cross-spectral matrices from all conditions hence, attenuating filter-specific variability during inverse modelling, i.e., the observed difference between different conditions is attributed only to the differences in conditions, not due to differences in the spatial filter. Subsequently, sensor-level cross-spectra were projected to the spatial filter obtaining the source power across trials, space and orientation. Since we do not have any prior

assumption about the orientation of the underlying source activity, the largest eigenvalue was selected as grid power from strongest dipole orientation that corresponds to the maximum variance of data. Consequently, subject and trial wise distribution of source power across brain volume was obtained for each condition. Thereafter, pairwise t-statistic was computed as test statistic for each grid between auditory stimulation and baseline condition. Since there was total $11,000$ grids hence would have required same number of statistical comparisons, therefore, to circumvent the multiple comparison problem we down-sampled the source powers from grid space to parcel space by taking median t-statistic of each parcel. Further, the prominent sources for each subject were selected after thresholding at the 95^{th} quantile from distribution of t-statistic of parcels and further tested for statistical significance by non-parametric statistic as described above for sensor-level 40 Hz spectral power (see section 2.2.5). Finally, for visualization purpose, all grids from significant parcels were visualized after rendering onto a cortical surface from the Colin27 brain template provided in the FieldTrip toolbox (`http://fieldtriptoolbox.org`).

2.2.7 Source activity reconstruction and connectivity analysis

The source-level Fourier coefficients were reconstructed by projecting the trial-wise sensor-level cross-spectral matrix to the spatial filter of significant parcels. These spectral coefficients were utilized to calculate global coherence, ITPC and Granger‘s causality among sources.

ITPC

We calculated ITPC from same areas based on the Fourier coefficients obtained from frequency domain eLORETA. Thereafter, laterality indices of ITPC were computed

between bilateral auditory cortices followed by statistical testing of asymmetry in individual condition and difference between each condition as per methods 2.2.5.

Global Coherence

Global coherence analysis was employed to identify the presence of a brain-wide large-scale functional network [Cimenser et al., 2011, Fonseca et al., 2015]. The global coherence can be calculated from the cross-spectral matrix using the leading eigenvalue method in two steps. First, cross-spectrum was computed as:

$$S_{ij}^{X}(f) = \frac{1}{n}\sum_{r=1}^{n} X_i^r(f) X_j^r(f)^* \tag{2.5}$$

where X_i^r and X_j^r are trial (r) and frequency (f) specific Fourier coefficients from the sources i and j, respectively and asterisk represents matrix transposition and complex conjugate calculated over n trials. Second, global coherence was computed as the ratio of the maximum eigenvalue and the sum of eigenvalues calculated from the cross-spectral matrices.

$$C_{Global}(f) = \frac{S_1(f)}{\sum_{r=1}^{k} S_r(f)} \tag{2.6}$$

where $C_{Global}(f)$ is the global coherence, $S_1(f)$ is the largest eigenvalue and the denominator $\Sigma_{r=1}^{k} S_r(f)$ represents the sum of eigenvalues of the cross-spectral matrix. The non-parametric statistical testing at $p < 0.01$ was performed to evaluate the significant differences in global coherences at 40 Hz during the auditory stimulation conditions. The differences in coherences between task and baseline condition were quantified using coherence Z-statistic [Maris and Oostenveld, 2007].

where $d.f.1$ and $d.f.2$ denote the degrees of freedom, $C_1(f)$ and $C_2(f)$ are coherence values during the first and the second conditions, respectively, at the frequency of interest (f = 40 Hz). The resulting Z-statistic was considered an observed test statistic, which was tested for significance after comparison with the null distribution as described above

$$Z = \frac{(tanh^{-1}(|C_1(f)|)) - (1/d.f._{.1} - 2) - (tanh^{-1}(|C_2(f)|)) - (1/d.f._{.2} - 2)}{\sqrt{(1/d.f._{.1} - 2) + (1/d.f._{.2} - 2)}} \quad (2.7)$$

where $d.f._{.1}$ and $d.f._{.2}$ denote the degrees of freedom $(2 * N * K)$, respectively in the first and the second condition while C_1 and C_2 are coherence values at the frequency of interest (f = 40 Hz). Resulting Z value was considered as an observed test statistic that was validated for significance by successful rejection of the null hypothesis. For creating a null distribution random partitions were done 1000 times by shuffling trials of two conditions and measuring coherence in each permuted data. Afterwards, a histogram is plotted comprising all 1000 coherence values from permuted data. Observed value is then compared with the 99^{th} and 1^{st} quantile of the respective permutation distribution to validate if it is smaller than 0.1 or larger than 99.9 (threshold values were set to 1%). If observed test statistic survive threshold testing, then it reflect that the probability of getting this result by chance is 0.01. Henceforth difference is considered as significant [Maris et al., 2007].

Directed sub-networks of ASSRs

After confirming the presence of a synchronized network, we calculated the multivariate Granger causality (GC) to establish the direction and strength of causal influence [Granger, 1969]. Subject-level nonparametric GC in the spectral domain

were calculated among sources [Granger, 1969, Dhamala et al., 2008]. This involved nonparametric spectral matrix factorization (using Wilson's algorithm) of the cross-spectral density to yield transfer function H and the noise covariance matrix Σ. Pairwise GC from Y to X at the frequency (f) can then be expressed as

$$G_{Y\to X}(f) = ln\frac{S_{xx}(f)}{S_{xx}(f) - (\Sigma_{yy} - \frac{\Sigma_{xy}^2}{\Sigma_{xx}^2}|H_{xy}|^2)} \tag{2.8}$$

where $S_{xx}(f)$ is the total spectral power (auto-spectrum) and the denominator represents intrinsic power (total power minus the causal contribution) of the "effect" signal [Geweke, 1982]. Please note that since ASSR being phase-locked to the external signal, can result in spurious coherence estimation among sources. However, the calculation of GC reflects "true" connectivity, since, if the information content is same between X and Y, the GC value would be nearly zero. Particularly, as per eq 2.8, Y should contain additional information that is useful in predicting the future values of X, over and above that can be predicted from the past values of X alone. Thereafter, measuring causality in both directions, one can locate the "source" and "effect" regions of the brain by comparing significant GC values in both directions. Since GC values follow unknown distribution, we adopt non-parametric statistical testing to assess significant GC spectral peaks among GC pairs [Brovelli et al., 2004]. First, 1000 permuted data sets were generated by independently shuffling trials from each source pair. Shuffling trial order in this way abolished task-specific information while keeping the data pool same. Thereafter, GC was computed, and the maximum GC value was selected over the frequency range from each permuted data set [Ding et al., 2006a]. Subsequently, a null distribution consisting of all GC values was constructed from the shuffled data set. GC peaks in unshuffled data were considered statistically significant when the observed GC value reached beyond the 99^{th} quan-

tile value ($p = 0.01$) of the null distribution. The multiple comparison problem was handled by Bonferroni corrections. We have also quantified the relative contribution of each source in the whole-brain causal network, as number of connections linked to each source. Mathematically, node degree was calculated as the number of edges connecting the source normalized by the maximum number causal connections each source could make i.e., $(N - 1) \times 2$. In our case, we found 6 significant sources, so any source could maximally make 10 causal connections. Additionally, since our objective included identifying the role of trans-cortical communication in manifestation of right hemispheric dominance during different stimulation conditions, we specifically focused on the inter-hemispheric flow. Here, to maximize the number of measurements, Granger causality was calculated again from all voxels in the left PAC to all voxels in right STG during different stimulation conditions. Subsequently, we evaluated the effect on interhemispheric flow during different stimulation conditions by a non-parametric Kruskal-Wallis test, followed by Tukey-Kramer post-test.

2.3 Results

2.3.1 Presence of ASSRs at sensor-level

In the time domain, evoked potential of mastoid channels showed steady-state activity in the time range of 250 - 1000 ms from the onset of periodic auditory stimuli (Fig. 2.1A: Lower panel). In the frequency domain, we evaluated the power spectrum and strength of inter-trial phase clustering (ITPC) during auditory stimulation and baseline conditions across the frequency range of $3 - 46\ Hz$. We found significant ITPC during all auditory stimulation conditions ($p < 0.01$) only at 40 Hz (Fig. 2.1B). Increase in the ITPC was a result of phase clustering around one region of polar space while the distribution of phase angles is uniform during the base-

line condition (Fig. 2.1C). Grand mean power spectra averaged over all electrodes and trials showed significant enhancement of spectral power at 40 Hz in binaural $[t(1970) = 4.19, p < 0.0001]$, monaural left $[t(1970) = 2.28, p < 0.0001]$ and monaural right condition $[t(1970) = 3.19, p < 0.0001]$ (Fig. 2.1D).

2.3.2 Hemispheric asymmetry

Sensor level

Laterality indices were calculated to quantify the degree of asymmetry during ASSRs across different stimulation conditions at sensor level and source level (from bilateral Heschl's gyri; Fig. 2.3 A). At sensor level hemispheric LI were calculated for both 40 Hz spectral power and ITPC. Wherein, mean LI values were greater than zero during every auditory stimulation condition suggesting right hemispheric dominance of ASSRs during binaural and both monaural conditions (Fig. 2.2 and Table 2.1). Particularly, for spectral power during the binaural condition, the group-mean hemispheric laterality index was $LI = 0.023$ and with 95% lower and upper confidence interval was 95% $CI = [0.010, 0.035]$. During the monaural left condition ($LI = 0.019, 95\%\ CI = [0.007, 0.032]$) and monaural right condition ($LI = 0.032, 95\%\ CI = [0.019, 0.045]$). One-way ANOVA among LI values across different stimulation conditions showed no significant difference in mean LI values across conditions ($F(2, 5910) = 1.01, p = 0.36$). The laterality indices calculated from ITPC values also followed similar pattern Fig. 2.2 B. Specifically, during the binaural condition, ($LI = 0.025, 95\%\ CI = [0.014, 0.036]$), monaural left condition ($LI = 0.037, 95\%\ CI = [0.025, 0.048]$) and the monaural right condition ($LI = 0.019, 95\%\ CI = [0.008, 0.030]$). Moreover, no main effect of auditory conditions was found on mean laterality indices ($F(2, 5910) = 2.51, p = 0.08$).

Source level

Source wave forms were low-pass filtered at 20 Hz to avoid distortion of ERP from high frequency activity. The source waveform analysis revealed a clear N100 response in both Heschl's gyri across all ASSR conditions (Fig. 2.3A). There were significant

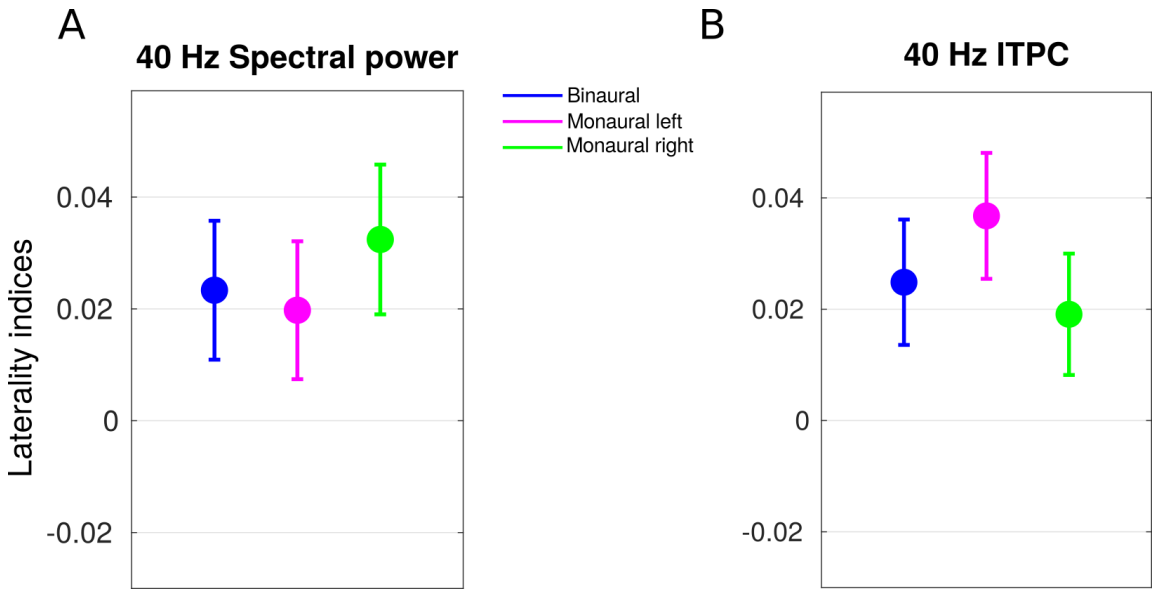

Figure 2.2: **Hemispheric asymmetry:** Group-level hemispheric laterality indices (LI) distribution for 40 Hz (A) spectral power and (B) ITPC during different stimulus conditions. The central node in each line represents mean of data while lower and upper boundary of the line represents the lower and upper limit of 95 % confidence interval, respectively.

amplitude differences observed between the left and right Heschl's gyri, consistent with previous studies. Asymmetry in the responses were quantified using LI analysis. Particularly, binaural condition showed bilateral response while both monaural conditions were clearly contralaterally dominant. Particularly, during binaural condition the group-mean laterality index was $LI = 0.020$ and with 95 % lower and upper confidence interval was $95\%\ CI = [-0.015, 0.055]$. During the monaural left condition ($LI = 0.088, 95\%\ CI = [0.061, 0.115]$) and monaural right condition ($LI = -0.037, 95\%\ CI = [-0.056, -0.017]$). One-way ANOVA

Table 2.1: Mean and 95 % confidence interval (CI) of laterality indices during different auditory conditions. (a) and (b) measured at sensor level. (c) and (d) measured at source level (Heschl's gyri). (C) N100 amplitudes were calculated from source waveforms derived from time domain eLORETA and (D) ITPC were calculated from Fourier transforms obtained from frequency domain eLORETA.

(a) Spectral power at 40 Hz from whole hemisphere

	Lower CI	Upper CI	Mean
Binaural	0.011	0.036	0.023
Monaural left	0.007	0.032	0.020
Monaural right	0.019	0.046	0.032

(b) ITPC at 40 Hz from whole hemisphere

	Lower CI	Upper CI	Mean
Binaural	0.014	0.036	0.025
Monaural left	0.025	0.048	0.037
Monaural right	0.008	0.030	0.019

(c) N100 amplitude of Heschl's gyri

	Lower CI	Upper CI	Mean
Binaural	-0.015	0.055	0.020
Monaural left	0.061	0.115	0.088
Monaural right	-0.056	-0.017	-0.037

(d) ITPC at 40 Hz of Heschl's gyri

	Lower CI	Upper CI	Mean
Binaural	0.018	0.066	0.042
Monaural left	0.046	0.097	0.071
Monaural right	-0.034	0.006	-0.014

among LI values across different stimulation conditions showed significant difference in mean LI values across conditions ($F(2, 57) = 22.03, p < 0.001$). Right hemispheric dominance was observed for binaural condition showing group-mean laterality index was $LI = 0.042$ and with 95% lower and upper confidence interval was 95% $CI = [0.018, 0.066]$. Though there was significant difference between monaural left and monaural right condition ($p < 0.001$), clear contralateral dominance was only present in monaural left condition i.e., ($LI = 0.071, 95\%\ CI = [0.046, 0.097]$). Monaural right response also not clearly left lateralised having mean $LI = -0.014$, and 95%($CI = [-0.034, 0.006]$). Overall, there was significant difference in mean LI values across conditions ($F(2, 57) = 15.12, p < 0.001$).

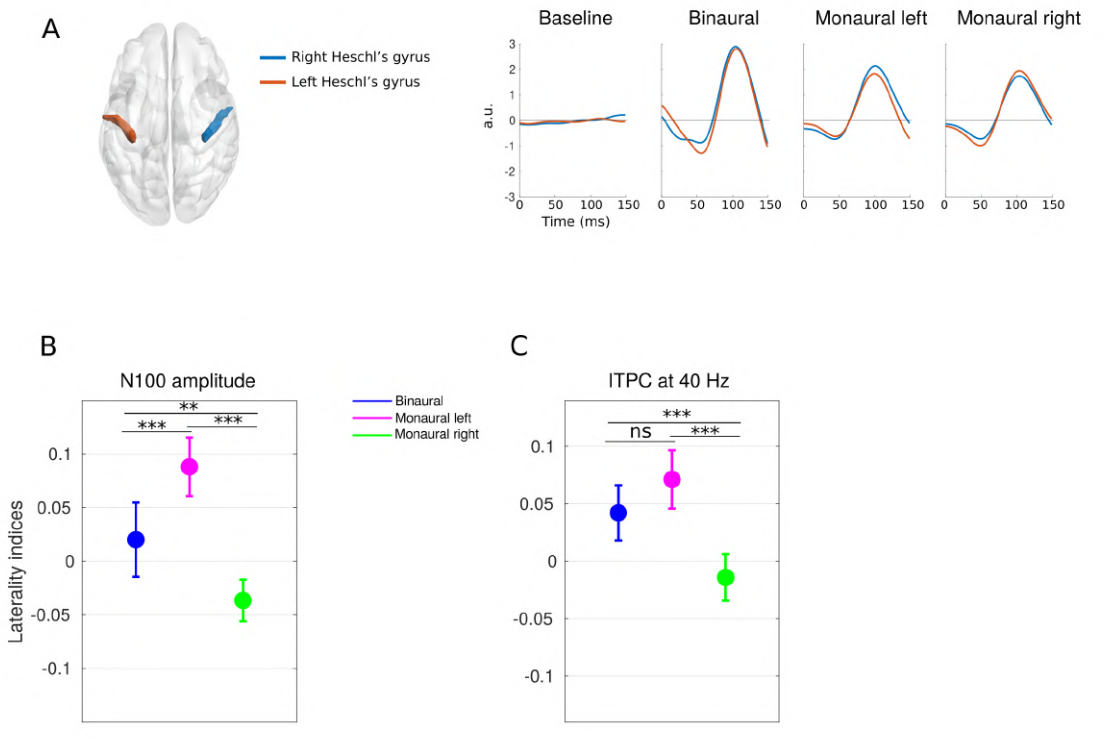

Figure 2.3: **Asymmetry at the primary auditory cortices:** A) Location of left and right Heschl's gyri (left panel) and Grand average source waveforms (Right panel). B and C Mean and 95 % confidence interval of laterality indices of (B) N100 amplitude and (C) ITPC from Heschl's gyri.

Overall, at source level LI were calculated for N100 response and ITPC from bilateral Heschl's gyri to validate the presence of contralaterality effect during monaural condition. In line with earlier studies, clear contralateral dominance in early auditory potentials was observed for monaural conditions. Particular pairwise p-values that define effect of auditory conditions on the laterality values obtained from Tukey-Kramer post-test are listed in Table 2.3.

Table 2.3: Pairwise p-values after multiple comparisons test Mean and 95 % confidence interval (CI) of laterality indices during different auditory conditions. (A) and (B) measured at sensor level. (C) and (D) measured at source level (Heschl's gyri). (C) N100 amplitudes were calculated from source waveforms derived from time domain eLORETA while (D) ITPC were calculated from Fourier transforms obtained from frequency domain eLORETA.

Group A	**Group B**	**A) Spectral Power**	**B) ITPC**	**C) N100**	**D) ITPC**
Binaural	Monaural left	0.919	0.300	0.002	0.164
Binaural	Monaural right	0.584	0.754	0.011	0.002
Monaural left	Monaural right	0.352	0.072	0.000	0.000

2.3.3 Source-level functional organization of 40 Hz ASSRs

Sources of ASSRs

Exact low-resolution brain electromagnetic tomography (eLORETA) was used to reconstruct whole-brain distribution of 40 Hz activity. The source activity was parcellated according to AAL atlas and tested for significance. The locations of significant sources during monaural left, monaural right and binaural conditions are shown in Fig. 2.4. Anatomical labels corresponding to significant source and their respective t-statistic are summarised in Table 2.4. In total, six sources were found significant at $p < 0.001$ during every stimulation condition. Interestingly, locations of sources

were same for binaural and both monaural conditions (see Table 2.4), namely, bilateral Heschl's gyri, bilateral precentral gyri, right superior temporal gyrus and right inferior frontal gyrus (triangular part). Hence, 4 sources were located in right hemisphere and 2 sources in left hemisphere for every stimulation condition. Though, the sources were same the source power of different regions differed across auditory stimulation conditions (Table 2.4 and Fig. 2.4).

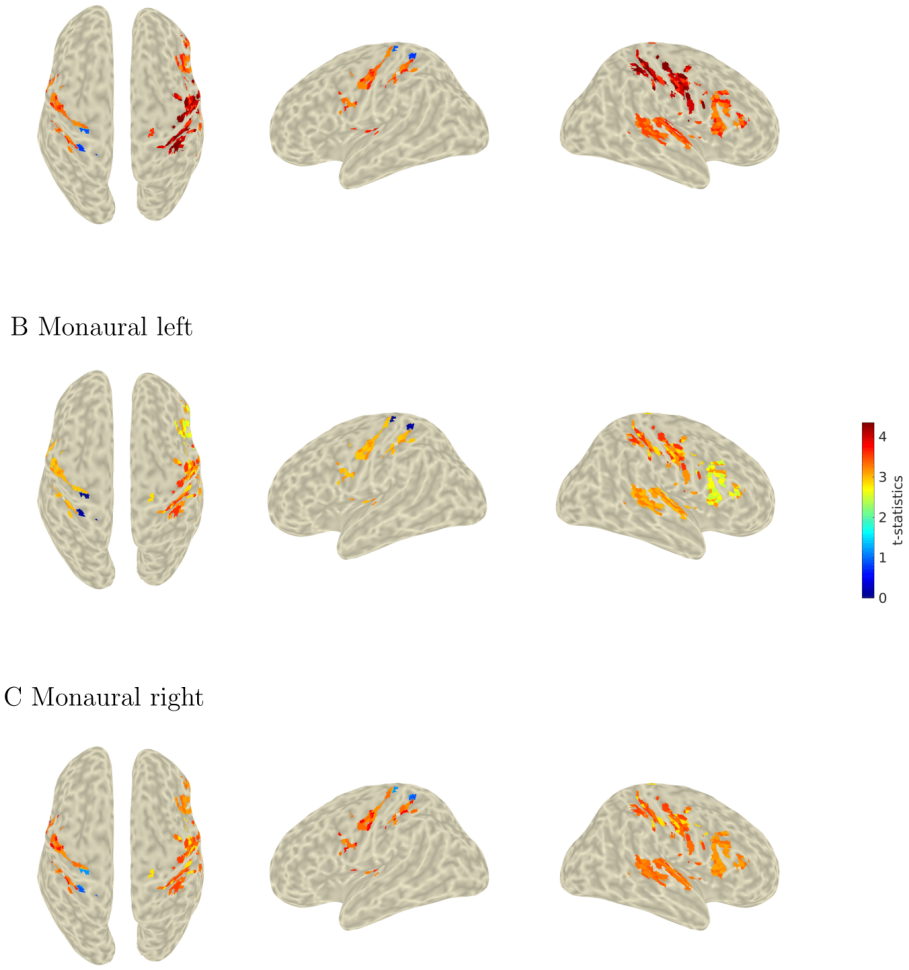

Figure 2.4: **Sources of 40 Hz ASSRs:** Source power rendered over cortical surface derived from Colin27 brain.

Table 2.4: Anatomical labels (according to AAL parcellation) of 40 Hz ASSRs sources along with their corresponding power (t-statistic between auditory stimulation and baseline condition).

Regions	**Binaural**	**Monaural left**	**Monaural right**
Right Heschl's gyrus	3.81	3.25	3.46
Left Heschl's gyrus	3.69	3.24	3.28
Right Superior temporal gyrus	3.52	3.12	3.31
Right Inferior frontal gyrus (triangular part)	3.39	2.70	3.17
Right Precentral gyrus	4.01	3.17	3.34
Left Precentral gyrus	3.35	3.01	3.34

Functional brain networks underlying ASSR

Global coherence measures the extent of coordinated neuronal activity over the whole brain [Cimenser et al., 2011, Kumar et al., 2016]. The enhancement in global coherences among ASSR sources was evaluated by nonparametric statistical testing [Maris and Oostenveld, 2007], employing Z-statistic as the test statistic. In line with our hypothesis, we observed a stimuli-specific enhancement of global coherence at 40 Hz, revealing a highly selective large-scale synchronization of neuronal assemblies at this frequency during binaural $[Z(20) = 1.35, p < 0.0001]$, monaural left $[Z(20) = 1.14, p < 0.0001]$, and monaural right $[Z(20) = 1.17, p < 0.0001]$ conditions (Fig. 2.5). The increase in whole-brain global coherence motivated for pairwise connectivity analysis employing Granger causality.

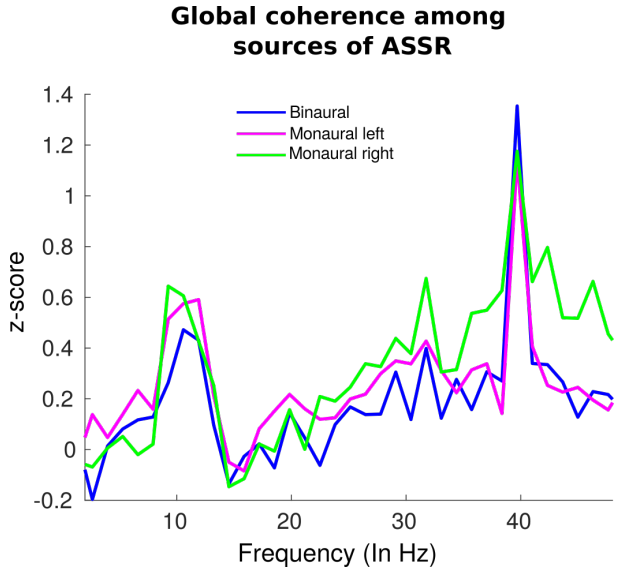

Figure 2.5: **Presence of large-scale network among ASSRs:** Enhancement in global coherence during auditory conditions was measured by z-statistic representing the normalized difference of coherence in task conditions relative the baseline condition.

Connectivity plots revealed the organization of directed network interaction during different auditory conditions (Fig. 2.6; Right panel). Interestingly, at least three GC interactions were common in all three conditions; namely, 1) Left HG to Right STG, 2) Right HG to Right STG and, 3) Right STG to Right IFG. Specifically, outflows from bilateral HG reaching to the right STG, consequently involving unidirectional interhemispheric flow from left HG to right STG. Presence of interhemispheric flow was in line with our hypothesis of involvement of trans-cortical flow during ASSR. During the monaural left and binaural conditions, there was bidirectional causal flow between right HG and right STG. During the binaural and monaural right condition, the right STG was bidirectionally connected to the right IFG. Node degree of ASSR sources (see Table 2.6) showed right STG was the most connected source among all ASSR sources having an average node degree of 0.43 followed by right HG (node degree = 0.17). Specifically, right STG was causally connected with bilateral HG and right IFG during every ASSR condition. Overall, three nodes from the right hemisphere (HG, STG and IFG) contribute to whole-brain causal network of ASSR while

left hemisphere had two nodes (HG, Precentral Gyrus). For visualization purpose, we did not plot GC flow from left HG to left PCG during the monaural left condition. Additionally, we found that the strength of inter-hemispheric flow was significantly different between at least two groups ($\chi(2, 8097) = 80.34, p < 0.0001$). Particularly, both binaural and monaural right were significantly different from monaural left conditions ($p < 0.0001$) however there was no difference between binaural and monaural right conditions ($p = 0.9$). The difference in distributions of inter-hemispheric flow was visualized by '*violin.m*' [Hoffmann, 2015]. The maximum interhemispheric flow was present during the binaural condition, followed by monaural right and least during the monaural left condition (Fig. 2.7).

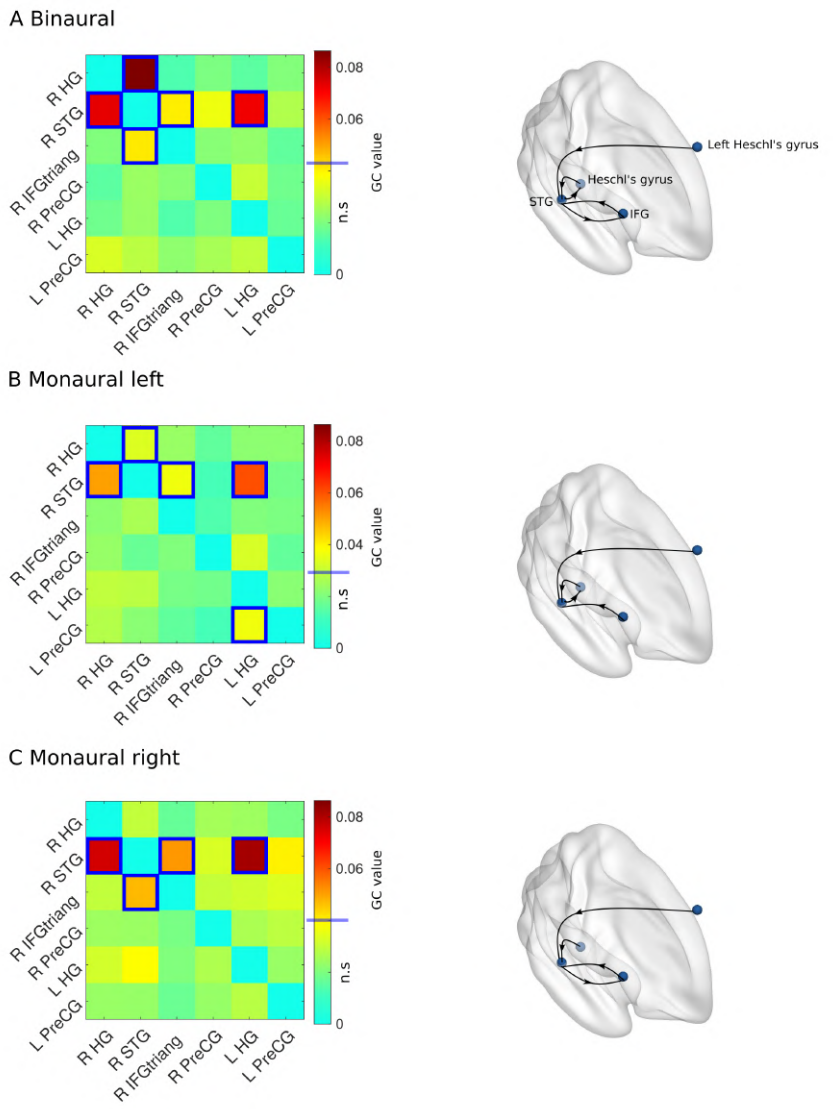

Figure 2.6: **Directionality among recruited sub-networks: Left panel:** heatmaps depicting pairwise GC values among ASSRs sources. 1st and 4th quadrant compose of GC pairs within right and left hemisphere, respectively. 2nd and 3rd quadrant depict respective interhemispheric GC flows. Significant GC values ($p > 0.01$) tested against surrogate data using a permutation-based non-parametric statistical test, were bordered by blue boxes. Schematic representation of frequency specific directed interactions that underlie 40 Hz ASSRs. Each black arrow represents a causal flow among brain regions denoted by blue nodes.

Table 2.5: Pairwise list of causally interacting sources pairs along with their respective causal strengths. Causal interactions among sources identified using Granger causality and significant causal interactions are illustrated in Fig. 2.6.

From	**To**	**GC value (10^{-2})**
Binaural		
R STG	R HG	8.6
R HG	R STG	7.3
L HG	R STG	7.2
R STG	R IFGtriang	4.1
R IFGtriang	R STG	4.1
Monaural left		
L HG	R STG	6.0
R HG	R STG	5.1
L HG	L PreCG	3.7
R IFGtriang	R STG	3.7
R STG	R HG	3.4
Monaural right		
L HG	R STG	8.2
R HG	R STG	7.6
R IFGtriang	R STG	5.1
R STG	R IFGtriang	4.7

Table 2.6: Node degree of ASSRs sources in the whole-brain network of ASSRs during different auditory stimulation conditions. Fourth column show the average of node degree calculated as mean of node degree in all 3 conditions.

Source Name	**Binaural**	**Monaural left**	**Monaural right**	**Average**
Right Superior temporal gyrus	0.50	0.40	0.40	0.43
Right Heschl‘s gyrus	0.20	0.20	0.10	0.17
Right Inferior frontal gyrus	0.20	0.10	0.20	0.17
Left Heschl‘s gyrus	0.10	0.20	0.10	0.13
Left Precentral gyrus	0.00	0.10	0.00	0.03
Right Precentral gyrus	0.00	0.00	0.00	0.00

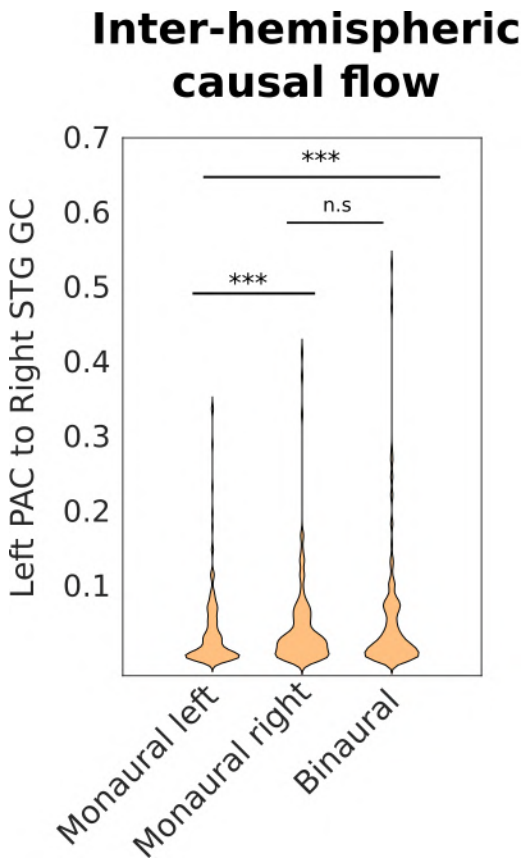

Figure 2.7: **Interhemispheric causal flow:** Variability in the GC strengths from left primary auditory cortex to the right STG during different auditory conditions.

2.4 Discussion

Our study attempted to reveal the directed interactions that unfold during the entrainment from periodic auditory stimuli of tonal nature in brain dynamics. We validated the presence of right hemispheric dominance of 40 Hz ASSR using spectral analysis and phase-locked components of the ASSR as estimated via Inter-trial phase clustering (ITPC). The main results of hemispheric lateralizations were same in both measures as non-phase locked component in ASSRs is very less, reported by our recent study [Singhal et al., 2023]. Hence, spectral power is mostly attributed to the phase-locked component of ASSR. The stimuli-driven sources of neuronal oscillations were present across the hierarchy of cortical auditory pathways Heschl's gyrus

(HG), superior temporal gyrus (STG), precentral gyri, inferior frontal areas corroborating with the previous fMRI, PET and EEG/MEG studies [Farahani et al., 2020, Poelmans et al., 2012, Reyes et al., 2004, Steinmann and Gutschalk, 2011]. Furthermore, we explored the information flow organization in these structures using effective connectivity analysis. We found that the right STG serves as an integrative area, receiving inputs from both primary auditory cortices, wherein information from the left primary auditory cortex is received via trans-cortical pathways, the organizational symmetry of which was dependent on the ears being stimulated. Furthermore, our directional network analysis suggests bidirectional interactions between right STG and frontal regions may provide efficient information exchange required for a comprehensive mapping of the auditory environment that ultimately manifests as right hemispheric dominance. The present findings may provide not only a network-level basis for right hemispheric dominance during 40 Hz ASSRs but also a clue about how the variability in the strength inter-hemispheric flow is dependent on the ear being stimulated. For instance, due to the pre-existing contralateral dominance, right PAC receives least auditory input during monaural right condition, and thereby require greater inter-hemispheric flow to compensate for the asymmetric input.

2.4.1 Sources of ASSR

A significant oscillatory response was seen in bilateral HG during every condition. HG residing in the primary auditory cortex is known to be the first cortical structure that receives auditory inputs (Hackett, 2015). Both monaural conditions showed contralateral dominance in early evoked potentials (See 2.3). Contralateral dominance of primary auditory areas during monaural stimulations is a well-established phenomenon reported in several fMRI, PET and EEG/MEG studies and attributed to the crossing of ascending anatomical fibres at the brainstem

level [Hackett, 2015, Kaas and Hackett, 2000a, Langers et al., 2005]. In line with these findings, the observed contralateral dominance of N100 and ITPC measures at primary auditory cortices during monaural conditions (see Fig. 2.3 and Table S1). Essentially, both measures are associated with distinct aspect of auditory processing. For instance, The N100 measure, which is an early auditory potential, showed clear asymmetry and varied among different auditory conditions (see Table S1 and S2). On the other hand, an increase in the ITPC is associated with late auditory potentials that are right hemispheric dominant for 40 Hz ASSR. In addition to the classic auditory pathway, we also report activation beyond the primary auditory cortex, for instance, bilateral pre-central gyri, which is in line with earlier findings on reconstructed 40 Hz ASSRs sources with equivalent dipole modelling [Farahani et al., 2020]. Interestingly, significant activation in the right inferior frontal gyrus (triangular part) (rIFG) was also found during every condition of ASSR. Right IFG, an analogue of Broca‘s area in the right hemisphere has been suggested to process sound length and attending to pitch/rhythms [Plakke and Romanski, 2014, Wang et al., 2015]. Though most sources of 40 Hz ASSR are well established, the enhancement of global coherence among sources in the present study reveals inter-areal brain synchronization among sources, a prerequisite of communication among neuronal assemblies [Bressler and Menon, 2010b, Fries, 2005]. Further analysis of directed information flow among sources provides a much clearer understanding of the role of observed sources.

2.4.2 Interhemispheric transfer

During every stimulation condition, there were causal flows originating from both primary auditory cortices reaching the right STG, consequently requiring an interhemispheric causal flow from the left PAC (Fig. 2.6). There are anatomical fibres

that support this information flow. In general, interhemispheric transfer of information is achieved via the corpus callosum [Andoh et al., 2015]. The corpus callosum provides a functionally relevant scaffold for mediating proper communication across both hemispheres. Although the inter-hemispheric flow was present during every auditory stimulation condition, there was differences in strength of interhemispheric flow during different conditions (Fig. 2.7). The observed differences in the strength of interhemispheric pathway during different task conditions suggest its differential functional requirements. Due to existing afferent structural constraints, irrespective of the ear being stimulated both PAC receives some amount of acoustic information in tandem with the manifestation of contralateral dominance during monaural conditions [Langers et al., 2005]. The right hemispheric specialization to process rhythmic features of acoustic input would require transfer of information from left PAC to specialised centres present in the right hemispheres. Hence, the monaural right condition would naturally require higher inter-hemispheric flow to compensate for the early asymmetric inputs. Alternatively, during the monaural left condition, wherein the information is already dominant in left hemisphere (Fig. 2.3) would show least involvement of inter-hemispheric flow. The strength of inter-hemispheric flow was maximum during the binaural condition (Fig. 2.7). In general, binaural condition requires more trans-cortical communication to integrate incoming bilateral acoustic inputs in addition to the transfer of primary information from PAC to the secondary auditory cortex. The complexity in dissociation of these two kinds of information prevents a straightforward explanation of inter-hemispheric flow during binaural conditions.

2.4.3 Integrative nature of STG

After initial processing in bilateral HG, information related to ASSR is feedforwarded to the right superior temporal gyrus (rSTG). Several studies of ASSRs have reported prominent activations in rSTG [Langers et al., 2005, Mäkelä and Hari, 1987]. We observed rSTG showing maximum inward causal information flow in the whole network (See Fig. 2.6 and Table 2). This type of causal information flow from primary sensory areas to intermediate areas of the auditory pathway suggests the integrative nature of rSTG mediating acoustic-pattern analysis. Ross and colleagues proposed that the right auditory cortex process temporal regularities associated with pitch processing of incoming sound [Ross et al., 2005]. In the context of the earlier view, rSTG can be considered as a specialised region for detecting regularities in acoustic input and subsequently sending information to higher-order frontal cortices. Also, our analyses revealed that rSTG is bidirectionally connected to the right inferior frontal gyrus (BA45). STG to frontal gyrus causal flow can be considered a bottom-up process, while causal influence from frontal to right STG can be seen as a top-down modulation or relevant for predicting incoming sensory inputs. Right IFG (rIFG) areas are known to be associated with identifying features like sound length and attending to pitch/rhythms plausibly utilising periodic cues received from STG [Plakke and Romanski, 2014]. Activity in rIFG along with activation in bilateral primary auditory cortex was also reported by Reyes and colleagues using PET imaging in response to 40 Hz amplitude modulated (AM) tone [Reyes et al., 2005]. Several studies have reported anatomical projections from STG to the frontal cortex [Hackett, 2011, Kaas and Hackett, 2000b, Plakke and Romanski, 2014]. Wang and colleagues identified a functional network comprising the frontal cortex and superior temporal regions that are sensitive to tone repetition patterns, which is associated with human‘s unique ability for language processing [Wang et al., 2015]. Here we

show, this fronto-temporal network that is central to processing of periodic structure of auditory stimuli, is mediated by bidirectional interactions between rSTG and right frontal regions.

2.4.4 Right hemispheric dominance

The present findings could give us a possible basis for right hemispheric dominance during 40 Hz ASSRs, as observed in several past studies by exploring the directed information flow among cortical sources. We argue that the right hemispheric lateralization of 40 Hz can be attributed to the right STG and its bidirectional interaction with the right frontal region Fig. 2.6. Furthermore, the activation pattern was similar in every condition, suggesting it as a central network for processing of periodic auditory stimuli and facilitator of brain-wide entrainment of cortical rhythms. This is in line with the previous finding that suggested tonal or melodic stimuli are predominantly processed in the right hemisphere while speech and language stimuli showed left hemisphere dominance [Albouy et al., 2020, Zatorre and Belin, 2001, Ross et al., 2005, Zatorre and Gandour, 2008] thus, following the same reverberating theme of right hemispheric dominance in music processing.

2.5 Methodological considerations

We have employed distributed source modelling based on individual-subject anatomy to account for variability in participant head size. Our source analysis was not limited to cortical regions, but we did not detect any significant activations in the subcortical areas of the brain. However, it should not be assumed that subcortical sources do not play a role in the whole-brain processing of the ASSR. There are substantial studies about the role of thalamocortical circuits in mediating both auditory-cortices and generation of ASSR [Lee, 2013, Steinmann and Gutschalk, 2011]. How-

ever, in our study, the detectability of thalamus and other sub-cortical regions were limited by several methodological factors. In principle, sub-cortical regions of the brain are prone to signal cancellation due to their deep location and irregular cell architecture, causing cortical activity to dominate over sub-cortical activity [Attal et al., 2007, Fahimi Hnazaee et al., 2020]. Consequently, poor signal-to-noise ratio for deeper sources [Halder et al., 2019], particularly in estimating the 40 Hz ASSR as higher frequency phases are more susceptible to distortion during propagation to the scalp. Emerging studies suggest the possibility of detecting sub-cortical sources by limiting the source analysis to pre-defined areas or by defining the region of interest larger than its actual volume [Coffey et al., 2016, Farahani et al., 2021]. However, in our study, both of these approaches would be counter-intuitive as we did not have prior assumptions about the locations of source-level network dynamics. The influence of sub-cortical activity on whole-brain network auditory processing could be potentially delineated in a future EEG-fMRI study where source network locations can be identified over long-time scales from BOLD activity and source-level EEG time series reconstructed from a spatial-filter that is better receptive to thalamic signals.

2.6 Conclusion

Comprehensive source-level network analysis provides a plausible explanation of hemispheric asymmetry of 40 Hz ASSRs during binaural and both monaural conditions. Right hemispheric dominance emerges due to bidirectional flow between the right STG and right frontal area (see Summary Fig. 2.8). Inter-hemispheric flow compensates for pre-existing contralateral dominance in early sensory processing to yield right hemispheric specialization of tonal processes. Overall, while the source locations and direction of information flow were similar across both monaural and

binaural conditions, their differential strength of activation underlies the processing of different auditory environments. In the present study, we have established the tools and methods to uncover the presence of a hierarchical information flow in the auditory network and found that causal outflow from primary auditory cortices serves as central role in mediating right hemispheric dominance. This study serves as a foundation and therefore we could move ahead with our main objective to understand mechanistic basis of hemispheric specialization of melody and speech.

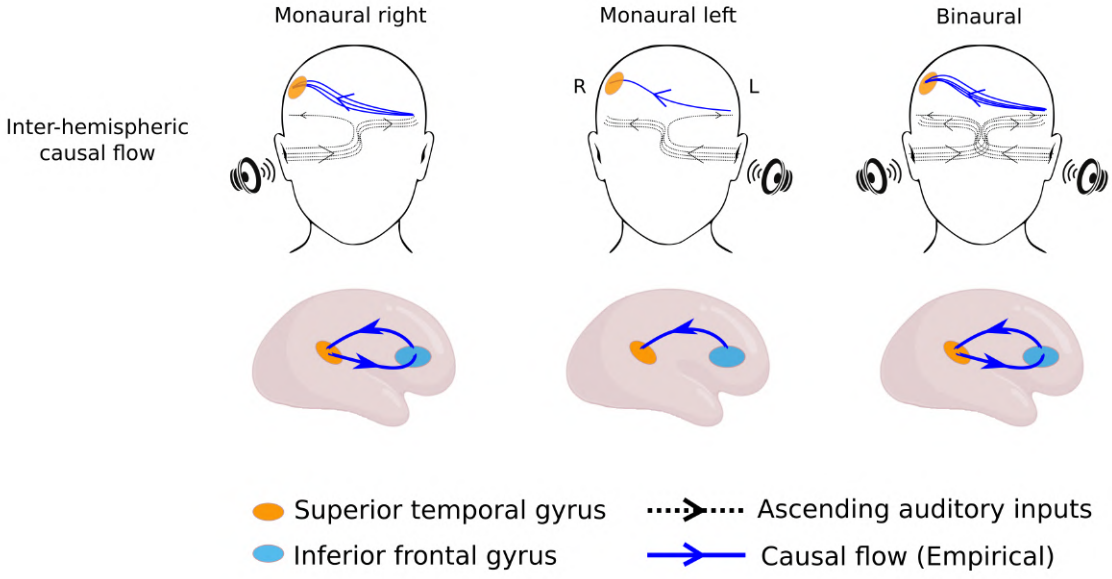

Figure 2.8: **Schematic representation of effective networks during ASSR:** Mechanisitc basis of right hemispheric dominance during 40 Hz ASSR. Upper panel: The figure highlights compensatory inter-hemispheric flow against contralateral dominanace in primary auditory cortices during monaural conditions. Lower panel: bidirectional flow between the right STG and right frontal area

Chapter 3

Role of primary auditory cortices in mediating hemispheric specialization of melody and speech

3.1 Introduction

The presence of dichotomy or dualism is the one the most fundamental attribute of the auditory system. It is well-known that the left hemisphere specializes in speech processing, while the music is predominantly processed in the right hemisphere [Zatorre, 2022]. At the lower sensory level, converging evidence suggests that the left primary auditory cortex is specifically attuned to rapid temporal changes associated with language processing, while the right primary auditory cortex is dominant in processing spectral changes associated with music processing (Albouy et al., 2020; Zatorre and Belin, 2001). However, the causal link of pri-

mary auditory cortices on the hemispheric specialization remained unresolved. The auditory system is hierarchically organized, with information flowing from lower-level sensory regions to higher-order processing centers [Kaas and Hackett, 2000b, Kaas and Hackett, 2000b]. The primary auditory cortices (PAC) are the first cortical structure to receive ascending auditory inputs exhibiting a rich repertoire of oscillatory activity [Gourévitch et al., 2020, Hackett, 2011]. These oscillations in distinct frequency bands are involved in encoding pitch, temporal envelope, and spectral content, as well as transforming them into perceptual experiences and subsequent communication within the auditory system. The PAC is interconnected with specialized higher-order cortical regions, such as the superior temporal gyrus, superior parietal lobule, and prefrontal cortex, enabling the transmission of oscillatory information across multiple frequency bands. This integration of motor, syntactic, and working memory information constructs a coherent representation of the auditory scene [Kösem and van Wassenhove, 2017b, Plakke and Romanski, 2014]. In our previous work in chapter 2, we show frequency-specific outflow from the PAC are central to the right hemispheric dominance of auditory steady-state response (ASSR) [Kumar et al., 2023]. Therefore, the oscillatory activity in PAC and subsequent propagation dynamics are required to be specific to the nature of the auditory stimuli. Particularly, communication dynamics across different regions enable the binding of disparate features, the segmentation of auditory streams, and the formation of hierarchical representations.

Speech and music, being two fundamental forms of human auditory communication, require specialized processing in the brain [Hickok and Poeppel, 2007, Zatorre, 2022]. The distinctive characteristics and processing requirements of speech and music necessitate the specific transmission of oscillatory information from the PAC to higher-order regions. Speech processing involves the encoding of fast temporal changes of auditory stimuli, while music comprises rapid spectral changes containing com-

plex melodic, rhythmic, and harmonic structures. Consequently, the perception of speech and music is determined by the organization of oscillatory activity in the PAC, as well as the subsequent propagation dynamics for processing auditory information in each domain. Understanding how this oscillatory information is transmitted to higher-order regions is crucial for comprehensive mapping of the complex dynamics underlying auditory perception and hemispheric specialization. Phase synchronization and coherence coupling mechanisms have been proposed as plausible mechanisms for information transfer and communication between brain regions [Fries, 2005]. These mechanisms involve the synchronization of oscillatory activity in higher-order regions with the PAC, promoting coordinated processing of auditory information [Bauer et al., 2020, Berger et al., 2019]. The synchronization ensures temporally aligned oscillatory phases required for the integration of auditory information across different frequency bands, enabling the perception of rhythmic patterns and extraction of temporal cues.

From a theoretical perspective, *causal complementarity* and *input asymmetry* can explain the findings such as increased left hemispheric dominance of language processing is associated with increased right hemispheric dominance of face processing [Brederoo et al., 2020] and motor processing [Gotts et al., 2013]. Unequal involvement of inter-hemispheric communication for different functions via integrative mechanisms [Gotts et al., 2013] have been proposed as key players from the vantage point of brain network mechanisms. This work takes the help of the fact that bihemispheric human auditory processing network exhibit pleiotropy - left hemispheric language processing and right hemispheric melody processing [Albouy et al., 2020], to understand how input asymmetries affects intrinsic structural network that facilitates the propagation of neuroelectric signals coordinate dynamically over time.

In the present study, we aimed to investigate to investigate the frequency-specific outflow from the PAC during speech, melody and ASSR conditions. We employed

electroencephalography (EEG) to record neural activity while participants selectively attended to either the speech or melodic content of ecologically valid *a cappella* songs. We reconstruct source activity utilizing subject-specific anatomy of brain and investigate the laterality in outflow from PAC. Understanding the precise mechanisms underlying the transmission and integration of oscillatory activity in speech and melody processing contributes to our comprehensive mapping of the complex dynamics involved in auditory perception.

3.2 Methods

3.2.1 Participants

Thirty healthy participants (14 males, 16 females, age range 22-34 years old; mean $\pm SD = 27 \pm 3.14$) participated in this study. All participants were right-handed, as confirmed by the Edinburgh Handedness Questionnaire with a cut-off score of 60-100, and reported no history of audiological, neurological or psychiatric disorders. All had normal or corrected-to-normal visual acuity. Informed consent was obtained from all participants in a format approved by the Institutional Human Ethics Committee (IHEC) of National Brain Research Centre, in accordance with the guidelines set by the Declaration of Helsinki. All participants were fluent in at least two languages, Hindi and English, with some having knowledge of another language of Indian origin.

3.2.2 Experimental procedure

3.2.3 Auditory stimuli

We have used two types of auditory stimuli 1.) amplitude modulated tone and 2.) *a cappella* songs. To generate Auditory steady-state response participants were

presented with hundred trials of auditory stimuli comprising pure sine waves of frequency 500 Hz amplitude modulated at 40 Hz. The total duration of the auditory experiment was 200 s, wherein each trial constituted 1 s of auditory stimulation with 1-s interstimulus silence interval. The second set of auditory stimuli consisted of 100 a cappella songs prepared by Albouy and colleagues, and have been used and described in more detail in their earlier reports [Albouy et al., 2020]. Particularly, the a cappella songs composed of 10 tones, each with an identical rhythm, and ten English sentences composed of 10 syllables each. Sentences were modified to adjust with the rhythm of the melodies. All melodic and sentence materials were combined in all possible combinations to form 100 a cappella songs. The resulting set of 100 songs had a mean duration of 4.1 seconds.

3.2.4 Paradigm and experimental setup

The EEG session consisted of 3 blocks. First, the participants underwent 5 minutes of EEG recording in a resting state while fixating one a cross displayed at the center of screen. Second, after being verbally instructed about the task the participants were presented with pairs of a cappella songs via earphones and were instructed to compare them. To ensure that participants focused their attention on speech or melody during the presentation of a cappella song, they were engaged in a match-to-sample task (See Fig. 3.1). The trial started with a visual cue indicating the relevant domain (sentence or melody) for 1200 milliseconds. Subsequently, the first song was presented, followed by a 1000 millisecond interstimulus interval (ISI), and then the second song was presented. Throughout the entire duration of the songs and ISI, a fixation cross was presented at the center of the screen. Following the presentation of the second song, participants were presented with a question on the screen, requiring them to assess whether the two speech contents were identical or different,

irrespective of the melody to which they were sung. In the case of melody trials, this process was reversed, with the judgment based solely on the melody, independent of the sentence content. Participants were required to respond by selecting the right arrow key on the keyboard when the domain was the same and the left arrow key for different. The response window lasted for 2000 milliseconds, and participants received no feedback. The total duration of a trial was approximately 12 seconds, and the total duration of the experimental block was 20 minutes. There were four types of combinations included: (1) both speech and melody were different in the song pair, (2) sentence was the same but the melody was different, (3) sentence was different and the melody was the same, and (4) both sentence and melody were the same. Each combination had 24 trials, resulting in a total of 96 trials presented. The sentence/melody questions and same/different responses were pseudo-randomly presented, with each stimulus type uniformly distributed over the entire experiment. Auditory stimuli were played binaurally via sound tubes at an overall intensity of approximately 60 dB SPL. Presentation software (Neurobehavioral Systems, Berkeley, CA, USA) was used to control stimulus presentation and record participants responses. Continuous electroencephalography (EEG) was recorded in a noise attenuated isolated room using a BrainVision Recorder acquisition system, which included an actiCHamp module with 63 active channels placed according to the International 10-20 electrode placement system. SuperVisc electrolyte gel (EASYCAP) was used to establish contact between the EEG sensors and the scalp. Continuous EEG data were acquired at a sampling rate of 1 kHz, and the impedance of each sensor was kept below 10 $k\Omega$. The reference electrode was positioned at the vertex (Cz), and the forehead (AFz) electrode was selected as the ground. The electrode locations were obtained with respect to three fiducials at the nasion and left and right preauricular points using a 3D digitizer (Polhemus Inc., Colchester, VT, USA).

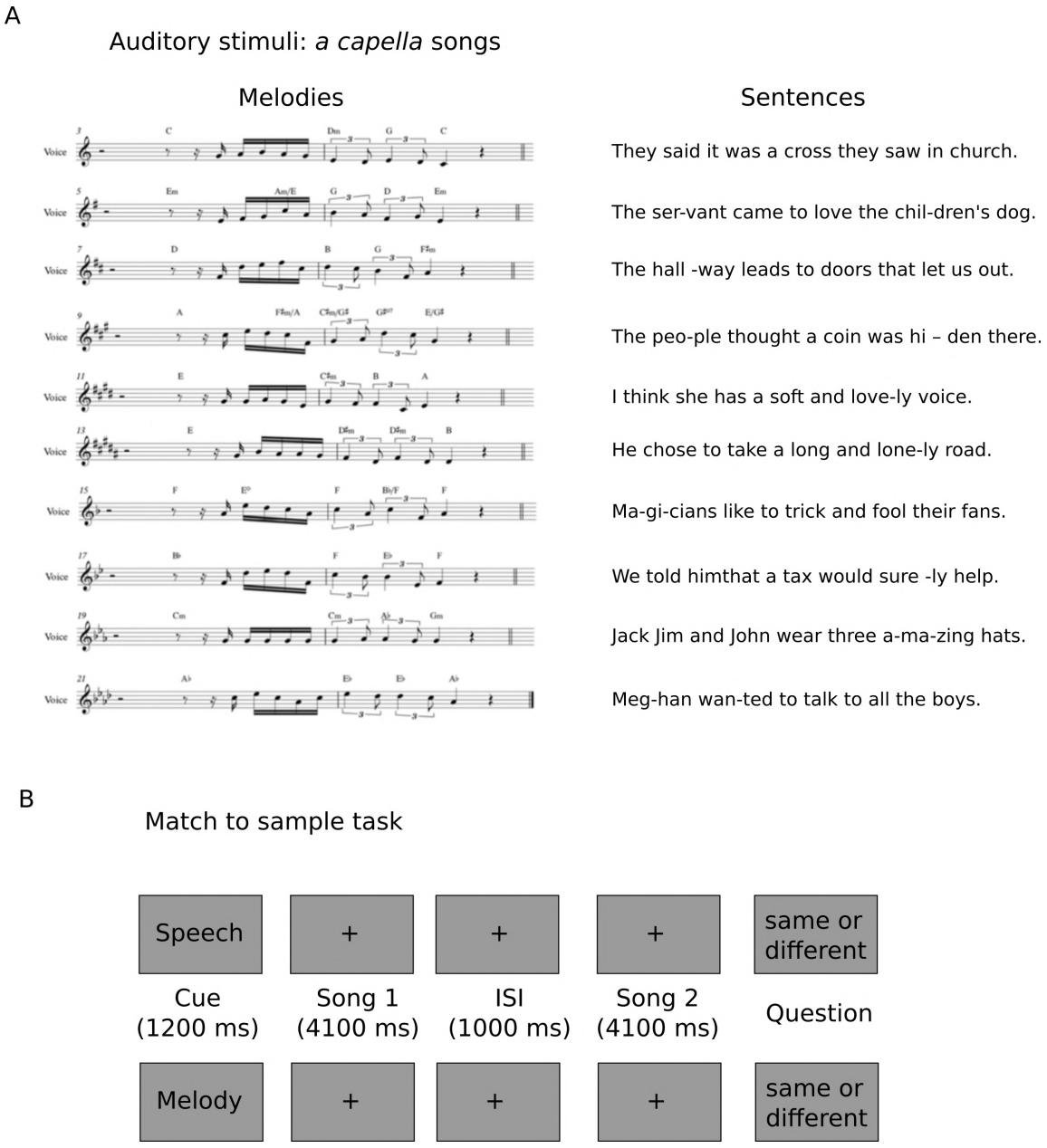

Figure 3.1: **Task design:** A.) Auditory stimuli. Ten original melodies (Left panel) and ten English sentences (Right panel). The English sentences were modified to match the melodies' rhythm, and subsequently, the melodic and sentence components were combined together to create *a cappella* songs [Albouy et al., 2020]. B.) A pair of *a cappella* song were presented in two conditions. 1.) speech and 2.) melody. They grey boxes represent visual screen.

3.2.5 EEG Preprocessing

Initial EEG data analysis was performed with EEGLAB (Delorme and Makeig, 2004), FieldTrip (`http://fieldtriptoolbox.org`) and custom MATLAB scripts (`www.mathworks.com`). Firstly, using EEGLAB continuous EEG data from each auditory block and resting state were bandpass filtered between 2-48 Hz and independent component analysis was employed to eliminate eyeblinks, muscular, and heartbeat artifacts. The ASSR block trials were epoched from the entire 1 second from the onset of stimuli, while for the a cappella song block, first hit trials were identified and segregated into two groups for speech and melody trials and epoched in 4 seconds from the onset of song. In addition, non-overlapping 1 second and 4 second with 50 % overlapping time segments from the resting state data were epoched to be utilized as the baseline condition for the ASSR and song blocks, respectively. After detrending the trials, threshold-based artifact rejection was applied at $\pm 80\ \mu V$. Following the preprocessing steps, an average of 97 trials from the ASSR block, 81 trials (out of 96) from the speech block, and 69 trials (out of 96) from the melody block were retained. The preprocessed EEG data were then re-referenced to a common average reference and downsampled to 250 Hz for further processing.

3.2.6 Source-level analysis

To estimate frequency-specific oscillatory sources, we utilized exact low-resolution brain electromagnetic tomography (eLORETA) as described in chapter 2. First for forward modelling, MRI data from each participant (see 4.2 in Chapter 4 for MRI data aquistion) was segmented into three tissue types, and meshes were created with 3000, 2000, and 1000 vertices for brain, skull, and scalp, respectively. The boundary element method (BEM) was employed to generate the realistic volume conduction model using the OpenMEEG package [Fuchs et al., 2001, Gramfort et al., 2010].

Subsequently, the EEG channels were aligned with the BEM model based on 3 fiducials present in both Polhemus data and MRI. Thereafter, leadfields were created for 3 orthogonal directions using the sensor positions and the volume conduction model. The location of vertices within the leadfield was defined based upon the participant-specific structural data parcellated according to Desikan-Killiany atlas in freesurfer [Desikan et al., 2006], with an average resolution of 4 mm. Subsequently, the cross-spectral for each frequency band ($2 - 48\ Hz$) were computed from the preprocessed sensor level data over the entire time window for each condition for ASSR, speech, melody, and baseline conditions. Frequency-specific spatial filters were computed from combination of the forward model and cross-spectral matrix for each condition. Separate spatial filters were constructed for ASSR, speech, and melody conditions, with 1-second and 4-second rest trials serving as baseline conditions, respectively. To reduce dimensionality, principal component analysis was performed on the spatial filters of vertices belonging to individual parcels, resulting in the spatial filters of 68 regions of interest. The trial-wise sensor-level cross-spectra were then projected to the spatial filter, obtaining subject and trial-wise distribution of source power across the brain volume for each condition. Next, pairwise t-statistics were computed between auditory stimulation and respective baseline conditions. Prominent sources for each subject were selected by thresholding at the 95^{th} quantile from the distribution of t-statistics of parcels. Hence, we obtained frequency-specific sources during 40 Hz ASSR, speech and melody conditions. Since spectral response during speech and melody are broadband spectral power were averaged in different frequency bands for delta, theta, alpha, beta and gamma.

3.2.7 Granger causality analysis

From the source we obtained the reconstructed Fourier coefficients of entire frequency range. Thereafter, subject-wise multivariate Granger causality (GC) was calculated in the spectral domain to determine the **causal outflow from PAC to whole-brain** as described in chapter 2, eq. 2.8. The resutling GC spectra of speech and melody condition were divided into respective frequency bands, i.e., delta ($2-4\ Hz$), theta ($4-8\ Hz$), alpha ($8-13\ Hz$), beta ($13-30\ Hz$), and gamma ($30-48\ Hz$) bands. Significant frequency bands were identified from non-parametric statistical testing [Brovelli et al., 2004]. First, 1000 permuted data sets were generated by independently shuffling trials between resting condition and auditory conditions. Thereafter, GC was computed, and the maximum GC value was selected over the frequency range from each permuted data set [Ding et al., 2006b]. Subsequently, a null distribution consisting of all GC values was constructed from the shuffled data set. GC bands in unshuffled data were considered statistically significant when the observed GC value reached beyond the 99th quantile value ($p = 0.01$) of the null distribution. The multiple comparison problem was handled by Bonferroni corrections. Since, the key hypothesis of the manuscript was to investigate the input to the auditory network which is inevitably gated by left and right PAC, we restricted our analysis of GC to only the causal outflows from bilateral PAC to other nodes of the auditory network.

3.2.8 Laterality analysis

To evaluate the extent of asymmetry in outflow from the primary auditory cortex (PAC) during auditory conditions, we employed computing the Laterality Indices (LI)(see 2.2.5). By adding the Granger causality (GC) outflow from both the right and left PAC, we obtained a spatial distribution of the GC outflow. The LI was then

calculated as the difference between the GC outflow in the right region and the left region, divided by the sum of the outflows from both regions.

3.3 Results

In this empirical study, EEG data were collected from a group of 30 participants during three auditory conditions, melody, speech, and 40 Hz ASSR. The laterality of frequency-specific Granger causality outflow from bilateral primary auditory cortices was estimated.

3.3.1 Target regions of PAC

Frequency-specific source activities were reconstructed using eLORETA at Desikan Kiliany regions for each subject during speech, melody, ASSR and resting conditions. Multivariate Granger causality analysis revealed significant ($p < 0.01$) outflow from bilateral primary auditory cortices at distinct frequency ranges including delta, theta, beta and gamma during both speech and melody conditions (Figure 3.2 and Table 3.1). The significant sources for ASSR were observed specifically at 40 Hz, whereas speech and melody conditions exhibited distinct frequency bands with some sources showing responses at multiple frequency bands. The spatially averaged frequency-spectrum of outflow was similar in speech and melody condition (Figure 3.2; Right panel). The distribution of significant sources across different frequency bands and conditions is summarized in Table 3.1. Overall, the regions that show activations included superior temporal, middle temporal lobe, precentral, Broca‘s areas (pars opercularis and pars triangularis), superior frontal, supramarginal and Insula. Moreover, activations in Lateral orbitofrontal and parahippocampal were exclusive to ASSR. Notably, the left pars opercularis showed significant activation across all frequency bands during speech conditions, indicating its involvement in

left hemisphere dominance during language processing. On the other hand, the right pars triangularis exhibited significant activation across all frequency bands specifically during melody conditions, suggesting its role in right hemispheric dominance during melody processing (Figure 3.2).

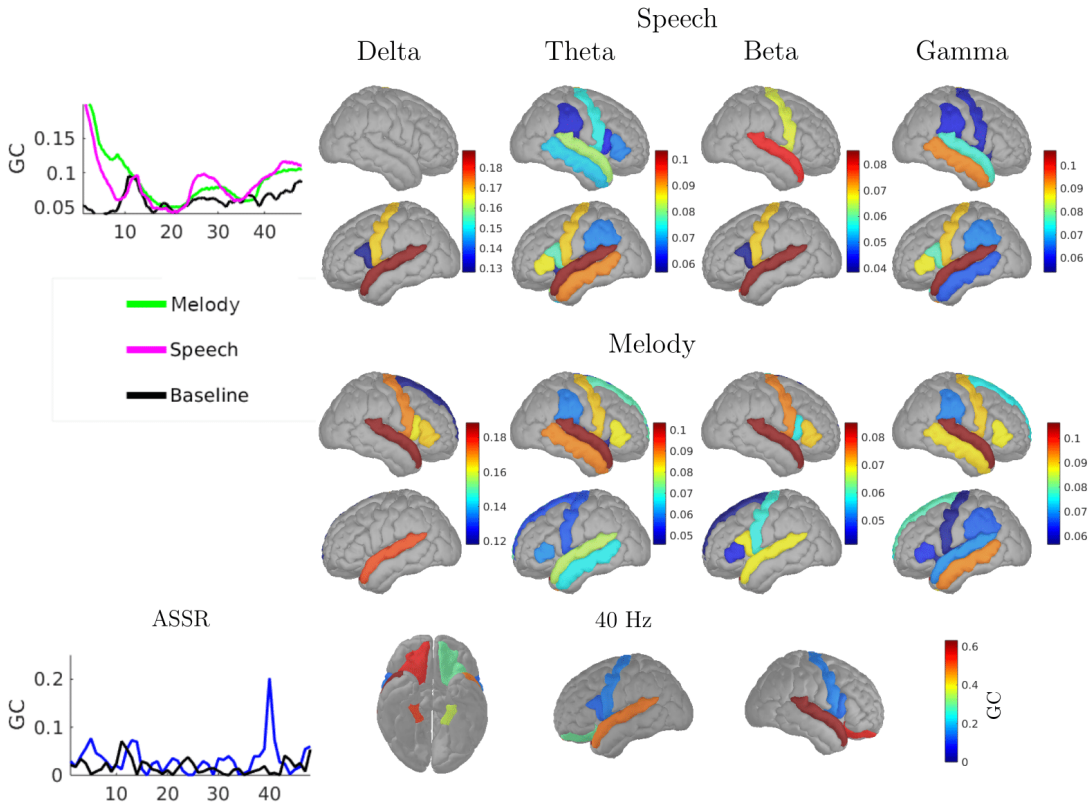

Figure 3.2: **Sources of 40 Hz ASSRs:** Source power rendered over cortical surface derived from Colin27 brain.

3.3.2 Asymmetry in functional responses

The laterality indices revealed varying degrees of hemispheric dominance across different brain regions and auditory conditions. The comprehensive list of regions, along with their corresponding 95 % confidence intervals and means are provided in Table 3.2. From the perspective of hemispheric specialization during

Table 3.1: Frequency-specific target regions of bilateral primary auditory cortices during different auditory conditions and their Granger causality strength.

Region	Speech				Melody				ASSR
	Delta	Theta	Beta	Gamma	Delta	Theta	Beta	Gamma	40 Hz
L Superior temporal	0.189	0.103	0.085	0.106	0.203	0.121	0.068	0.072	–
L Precentral	0.176	0.090	0.072	0.093	–	–	0.059	0.063	0.203
L Pars opercularis	0.148	0.081	0.044	0.084	–	–	0.067	–	0.187
L Middle temporal	–	0.094	–	0.073	–	0.114	–	0.092	–
L Pars triangularis	–	0.088	–	0.091	–	0.109	0.046	0.068	–
L Supramarginal	–	0.072	–	0.075	–	–	–	0.069	–
L Insula	–	0.062	–	–	–	–	–	0.061	–
L Superior frontal	–	–	–	–	–	0.107	0.042	0.079	–
R Superior temporal	–	0.085	0.080	0.083	0.211	0.147	0.082	0.102	0.218
R Precentral	–	0.089	0.069	0.068	0.201	0.134	0.073	0.089	0.197
R Pars opercularis	–	0.070	–	–	0.196	–	0.058	–	0.187
R Pars triangularis	–	0.076	–	–	0.198	0.132	0.069	0.087	–
R Middle temporal	–	0.067	–	0.097	–	0.138	–	0.088	–
R Supramarginal	–	0.064	–	0.069	–	0.116	–	0.070	–
R Insula	–	–	–	0.065	–	0.107	–	–	–
R Superior frontal	–	–	–	0.170	–	0.125	0.073	0.076	–
R Lateral orbitofrontal cortex	–	–	–	–	–	–	–	–	0.209
R Parahippocampal	–	–	–	–	–	–	–	–	0.205

speech, melody and ASSR, certain regions exhibited complete lateralization, indicating that both the upper and lower confidence intervals lie on the same side of zero (Figure 3.3). Particularly, during ASSR the right hemispheric dominance was present in superior temporal gyrus (STG) with mean laterality index was LI = 0.13 and with 95 % lower and upper confidence interval was 95% $CI = [0.08, 0.18]$; lateral orbitofrontal ($LI = 0.31, 95\%\ CI = [0.17, 0.44]$) and parahippocampal ($LI = 0.19, 95\%\ CI = [0.05, 0.32]$). For the speech condition during beta frequency range, the left hemispheric dominance was present in STG ($LI = -0.03, 95\%\ CI = [-0.04, -0.02]$), precentral (PrC) ($LI = -0.03, 95\%\ CI = [-0.05, -0.01]$), pars opercularis ($LI = -0.07, 95\%\ CI = [-0.10, -0.05]$) and in gamma range STG ($LI = -0.13, 95\%\ CI = [-0.15, -0.10]$), PrC ($LI = -0.16, 95\%\ CI = [-0.24, -0.08]$), pars opercularis ($LI = -0.22, 95\%\ CI = [-0.31, -0.13]$). For the melody condition during beta frequency, the right hemispheric dominance was present in STG ($LI = 0.10, 95\%\ CI = [0.06, 0.14]$), PrC ($LI = 0.11, 95\%\ CI = [0.03, 0.18]$), pars triangularis ($LI = 0.20, 95\%\ CI = [0.05, 0.35]$) and during gamma range, STG ($LI = 0.17, 95\%\ CI = [0.12, 0.22]$), PrC ($LI = 0.17, 95\%\ CI = [0.04, 0.31]$), pars triangularis ($LI = 0.12, 95\%\ CI = [0.03, 0.22]$).

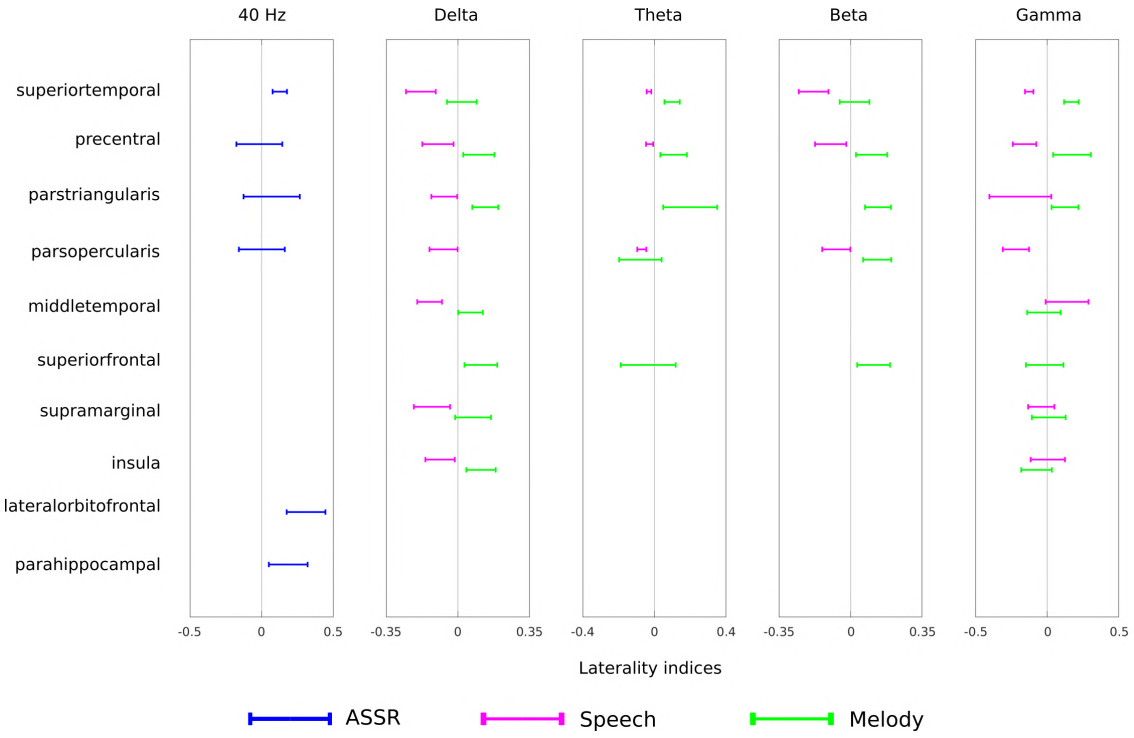

Figure 3.3: **Frequncy-specific asymmetry:** Laterality indices during speech (magenta), melody (green) and ASSR (blue) conditions. The error bars denote 95 % confidence interval of mean.

Table 3.2: 95 % Confidence Intervals of laterality indices during speech, melody, and ASSR conditions in distinct frequency range.

Speech

Regions	Delta			Theta			Beta			Gamma		
	Mean	Lower CI	Upper CI	Mean	Lower CI	Upper CI	Mean	Lower CI	Upper CI	Mean	Lower CI	Upper CI
Superior temporal	-0.181	-0.253	-0.108	-0.030	-0.043	-0.018	-0.181	-0.253	-0.108	-0.125	-0.154	-0.096
Precentral	-0.097	-0.174	-0.021	-0.027	-0.047	-0.006	-0.097	-0.174	-0.021	-0.159	-0.240	-0.077
Pars triangularis	-0.066	-0.130	-0.003	–	–	–	–	–	–	-0.187	-0.403	0.029
Pars opercularis	-0.071	-0.139	-0.002	-0.071	-0.096	-0.045	-0.071	-0.139	-0.002	-0.218	-0.309	-0.126
Middle temporal	-0.138	-0.198	-0.078	–	–	–	–	–	–	0.139	-0.010	0.289
Superior frontal	–	–	–	–	–	–	–	–	–	–	–	–
Supramarginal	-0.126	-0.214	-0.038	–	–	–	–	–	–	-0.041	-0.133	0.051
Insula	-0.087	-0.158	-0.015	–	–	–	–	–	–	0.004	-0.116	0.125

Melody

	Mean	Lower CI	Upper CI	Mean	Lower CI	Upper CI	Mean	Lower CI	Upper CI	Mean	Lower CI	Upper CI
Superior temporal	0.019	-0.053	0.092	0.099	0.057	0.142	0.019	-0.053	0.092	0.170	0.119	0.221
Precentral	0.103	0.026	0.179	0.107	0.033	0.181	0.103	0.026	0.179	0.173	0.041	0.306
Pars triangularis	0.134	0.070	0.197	0.200	0.049	0.351	0.134	0.070	0.197	0.124	0.030	0.217
Pars opercularis	–	–	–	-0.079	-0.197	0.040	0.129	0.061	0.198	–	–	–
Middle temporal	0.062	0.002	0.122	–	–	–	–	–	–	-0.023	-0.139	0.094
Superior frontal	0.112	0.032	0.192	-0.035	-0.188	0.118	0.112	0.032	0.192	-0.018	-0.148	0.113
Supramarginal	0.074	-0.014	0.162	–	–	–	–	–	–	0.011	-0.106	0.128
Insula	0.113	0.042	0.185	–	–	–	–	–	–	-0.073	-0.181	0.034

40 Hz ASSR

Regions	Mean	Lower CI	Upper CI
Superior temporal	0.127	0.077	0.177
Precentral	-0.016	-0.177	0.144
Pars triangularis	0.070	-0.126	0.266
Pars opercularis	0.001	-0.159	0.160
Lateral orbitofrontal cortex	0.309	0.174	0.444
Parahippocampal	0.185	0.050	0.320

3.4 Discussion

The present study investigate task induced electrophysiological response during speech, melody, and ASSR conditions. Particularly, with a specific focus on the role of the primary auditory cortices (PAC) and their outflow in governing hemispheric specialization. This study establish a causal link between PAC dynamics and hemispheric specializations. Firstly, we reconstruct the subject-wise source activity and compute Granger causality outflow from bilateral PAC in distinct frequency bands. The findings reveal a common frequency-specific outflow from PAC in both speech and melody conditions, reaching to distinct regions reflecting domain-specific organization of the auditory system. Furthermore, the laterality analysis of causal inflow in target regions complies with well-established hemispheric dominance of left hemisphere for speech, right hemisphere for melody, and right hemisphere for ASSR, suggesting role of PAC in respective hemispheric specializations.

3.4.1 Hierarchical and domain-specific organization of the auditory system

The primary auditory cortices (PAC), located in the temporal lobes, serve as the initial cortical hub receiving ascending auditory inputs, primarily from the thalamus, and exhibit oscillatory responses to complex sounds within a frequency range of approximately 1 to 100 Hz [Gourévitch et al., 2020]. Different frequency bands have been associated with different types of processing, with gamma activity often linked to higher-level processing, such as attention and perception, while lower-frequency activity may be more involved in basic sensory processing. Moreover, the PAC is involved in the transformation of acoustic features (such as frequency information) into percepts (such as pitch height and pitch chroma) for melody [Koelsch, 2011]. However, the specific patterns of activity can vary depending on the characteris-

tics of the stimulus and the context in which it is presented. Albeit, dominant in contralateral PAC, ascending auditory inputs are represented in both PAC. Auditory information thereafter is propagated to specialized regions across the brain volume. The subsequent propagation from PAC is dependent on the content of the auditory stimuli. Processing in later regions can be observed by oscillatory response in specialized regions. Higher-order auditory regions, such as the secondary auditory cortex and the superior temporal gyrus (STG), are thought to be specialized for processing higher-frequency information, such as the formants of speech and the timbre of musical instruments. These regions are thought to play a critical role in the analysis of the spectral and temporal properties of sounds, and they are activated by the complexity and variability of sounds. Albouy and colleagues demonstrated the sensitivity of the left PAC to speech features and the right PAC to melody features [Albouy et al., 2020]. On the other hand, there is substantial evidence of left hemispheric specialization for speech and right hemispheric specialization for music [Zatorre and Belin, 2001, Zatorre et al., 2002]. In our study, we provide causal evidence for the contribution of PAC in the hemispheric specialization of speech and melody. The information flow from sensory cortex to frontal cortex represents a bottom-up process [Ding et al., 2021]. This contributes to our understanding of the hierarchical organization of auditory processing, as it reveals the flow of oscillatory information from lower-level sensory regions to higher-order cognitive regions. Although the oscillatory patterns observed during speech and melody conditions are similar, characterized by frequency-specific outflows from the bilateral PAC, the specific regions involved in receiving these oscillations differ between speech and melody conditions. This suggests that the observed oscillatory patterns do not encode generic processing of acoustic signal dynamics but instead capture specific linguistic or musical features. Our experimental paradigm ensures the selective attention of participants to the speech or melody aspects of

ecologically valid auditory stimuli (a cappella songs), thereby eliminating confounding effects of signal properties. The involvement of distinct regions in processing these acoustic environments indicates specialized and domain-specific organization within the auditory system [Angulo-Perkins and Concha, 2019, Peretz et al., 2015, Scott and McGettigan, 2013, Xie et al., 2018]. Furthermore, the presence of homologous areas in the opposite hemisphere, such as the superior temporal gyrus (STG), motor cortex, and Broca's area, suggests a bilateral representation and processing of auditory stimuli. Homologous areas share an evolutionary history and tend to perform similar functions, necessitating communication to coordinate their respective functions [Agcaoglu et al., 2018, Karolis et al., 2019, Wan et al., 2022]. This parallel processing mechanism enables the brain to handle the complementary nature of speech and music, two most important auditory communication skills. By distributing the cognitive load, the brain enables simultaneous processing when speech and melody are presented together, as in the case of ecologically valid a cappella songs [Angulo-Perkins and Concha, 2019]. The identified target regions of the primary auditory cortices (PACs) in our study during both speech and melody conditions are consistent with previous literature and widely recognized as auditory-related regions [Giraud and Poeppel, 2012, Hickok and Poeppel, 2007, Morillon et al., 2010a]. The regions in the left hemisphere are known for processing various linguistic aspects, including phonological analysis, syntactic structure, semantic processing, and articulation. Conversely, the right hemisphere is implicated in processing non-linguistic aspects of auditory stimuli, such as melodic and tonal structures, pitch variations, temporal patterns, and rhythmic patterns in melody [Zatorre and Belin, 2001, Zatorre and Gandour, 2008]. There are reports suggesting the frontal and parietal regions of the brain, such as the inferior frontal gyrus (IFG) and the intraparietal sulcus (IPS), are involved in the entrainment of external rhythms. These regions are thought to play a critical role in the integration of auditory and motor infor-

mation, and they are activated by the synchronization of movement with a regular beat[Koelsch, 2011]. It is important to note that these regions are not completely independent and they can interact with each other in a hierarchical way. The processing of different frequency ranges may also be influenced by other factors such as attention, cognitive states, and task demands. Additionally, frequency-specific lateralization may also vary among individuals, depending on factors such as handedness, age, and musical experience. Additionally, the ability of a single region to receive input at multiple frequencies highlights the brain's capacity to decode and integrate distinct aspects of oscillatory activity for coherent representation of auditory percept. This multi-scale hierarchy integrates motor, syntactic, and working memory information, contributing to the construction of a comprehensive auditory scene.

Chapter 4

Causal outflow from primary auditory cortices in dual time-scales underlie hemispheric specialization of melody and speech

4.1 Introduction

In the chapter 2 and 3 we established the role and propagation dynamics from bilateral primary auditory cortices in mediating hemispheric specialization. However, the nature and mechanistic basis of these oscillatory based information transfer is yet to be understood. Understanding how this oscillatory information is transmitted to higher-order regions is crucial for comprehensive mapping of the complex dynamics underlying auditory perception and hemispheric specialization. Im-

portantly, the efficacy of information transfer and coupling mechanisms between brain regions is naturally contingent upon the underlying structural connectivity, which provides the structural framework for the precise routing of oscillatory activity [Avena-Koenigsberger et al., 2017, Sporns, 2011]. Structural connectivity refers to the physical macroscopic connections between different brain regions, primarily mediated by white matter tracts. There has been substantial evidence on the role of SC in information transfer between brain regions [Honey et al., 2007], shaping network topology [Bullmore and Sporns, 2009, Cabral et al., 2011], and mediating synchronization and coherence of neural activity [Stam et al., 2007]. The white matter strength, which represents the integrity and density of the fiber tracts connecting different brain regions, influences the efficiency and magnitude of information transfer. In addition, the fiber lengths determine the time constants of information propagation [Cabral et al., 2011]. However, how a static network subserves the different functional requirements of strengths of coupling and temporal delays during speech and melody remain an open question? The brain accomplishes this by precisely manipulating the timing and coordination of neural signals through two key factors: conduction velocities and a scaling factor applied to fiber thickness. Conduction velocities, which denote the speed at which neural impulses travel along nerve fibers, play a pivotal role in governing the temporal aspects of neural communication. Varied conduction velocities facilitate the emergence of distinct time delays, thereby shaping the arrival and integration of neural information across disparate regions. This temporal coding ensures the precise synchronization necessary for intricate processing tasks. Additionally, the brain utilizes the scaling factor applied to fiber thickness as a means of regulating synchronization strength. By modulating these factors, the brain can finely adjust the degree of coordination between neural signals. Despite the underlying static structural connectivity within the brain, modulation by conduction velocities and synchronization strength enables

the generation of functionally relevant diverse range of time delays and strengths of information propagation. This understanding enhances our comprehension of the brain‘s intricate adaptability for specific cognitive demands and environmental stimuli such as speech and melody. Transmission delays in neural communication among functional brain network nodes has been identified as a key variable that facilitates the entry and exit to synchronized oscillatory states of the brain [Ghosh et al., 2008, Petkoski et al., 2018]. While several studies have argued that the transmission delays are of structural origin specifically introduced via myelin degradation along axons [Ghosh et al., 2008, Petkoski et al., 2018, Pathak et al., 2022], empirical evidences point out towards the existence of functionally tuned synaptic delays [Stange-Marten et al., 2017]. Concurrently, synaptic scaling weights can be measured from diffusion weighted imaging (dWI) data [Schirner et al., 2015] and guide the whole-brain synchrony captured by phase coherence in functional magnetic resonance imaging (fMRI) and magnetoencephalography (MEG) signals [Cabral et al., 2011, Pathak et al., 2022]. While the weights become a property of an individual‘s brain structure, task-specific input asymmetries such as speech or melody can be mapped to the conduction velocities with which communication is orchestrated among the auditory network nodes.

Here, we hypothesized that hemispheric lateralization of speech and melody emerge as spatial modes of a collective behavior exhibited by a large-scale auditory network. Current work takes the help of the fact that bi-hemispheric human auditory processing network exhibit pleiotropy - left hemispheric language processing and right hemispheric melody processing [Albouy et al., 2020], to understand how input asymmetries affects intrinsic structural network that facilitates the propagation of neuroelectric signals coordinate dynamically over time. Using empirical EEG recordings obtained in chapter 3 and dynamic modelling of whole brain connectome in the present work, we establish that lateralized functional processing in brain networks can be

captured as spatial modes arising from complex non-linear interactions between input asymmetries and brain structural properties [Pang et al., 2023, Roberts et al., 2019]. In the present study, we aimed to investigate to investigate the frequency-specific outflow from the PAC during speech, melody and ASSR conditions. In previous chapter 3, we employed electroencephalography (EEG) to record neural activity and reconstruct source activity utilizing subject-specific anatomy of brain and investigate the laterality in outflow from PAC. In the present study, to find the mechanist basis of the lateralization, we computed theoretical lateralization indices by integrating diffusion weighted magnetic resonance imaging (DWI) data from the same participants, to constrain the outflow from the PAC in a neural dynamic model. The model used coupled Kuramoto oscillator framework [Kuramoto, 1984] to capture the phase dynamics of an individual source node [Petkoski et al., 2018, Pathak et al., 2022] and coupled through connection matrix generated from DWI data [Schirner et al., 2015]. We argue that the transmission delays for the purpose of this study are set at the gatekeeper node - PAC, based on the input, in a context dependent manner differentially for speech vs melody processing and hence can be estimated by model inversion techniques for task contexts and for different frequency bands - a novel approach to estimate time-scales of neural control. Further, subject-specific estimates of these delays allowed comparative analysis between empirical and theoretical LI, paving the way for individualized predictions required to establish the robustness of the analysis [Seghier and Price, 2018] (see methods 4.2). The frequency-specific tuning of such transmission delays was validated by additional ASSR recordings. Together, understanding the precise participant-specific mechanisms underlying the transmission and integration of oscillatory activity during speech and melody processing contributes to the comprehensive mapping of the ecologically complex auditory signals to lateralized brain responses. We demonstrate that parametric modulation of conduction speeds that effectively control the transmission delays - a key metric

for understanding information processing and control of any biological network, acts as the switch for selection of the spatial mode indexing lateralization of speech and melody. These results provide novel insights into the intricate dynamics of auditory processing and underscore the significant role of structural connectivity in shaping frequency-specific neural responses. Understanding the precise mechanisms underlying the transmission and integration of oscillatory activity in speech and melody processing contributes to our comprehensive mapping of the complex dynamics involved in auditory perception.

4.2 Methods

4.2.1 Participants and Experimental procedure

We have recorded diffusion weighted MRI data (DWI) from the same participants who volunteered in the previous study 3. Informed consent was obtained from all participants in a format approved by the Institutional Human Ethics Committee (IHEC) of National Brain Research Centre, in accordance with the guidelines set by the Declaration of Helsinki

4.2.2 MRI-DWI acquisition and analyses

The T1-weighted structural MRI images were acquired on a Philips Achieva 3.0 T MRI scanner with the following parameters: $TR = 8.4\ ms,\ FOV = 250 \times 230 \times 170$, flip angle = 8°, 170 sagittal slices, and voxel size of $1 \times 1 \times 1\ mm$. The preprocessing of MRI images and volumetric parcellation for individual subjects were performed using Freesurfer, based on the Desikan- Kilinay atlas (`http://surfer.nmr.mgh.harvard.edu/`). Diffusion weighted Imaging data was acquired through a single-shot echo planar imaging in 3.0 T Philips Achieva Scanner. The DWI sequence was performed

with $TR = 8800\ ms$, $TE = 75\ ms, FOV = 210 \times 210 \times 128\ mm$, flip angle = 9°, matrix size = 104×104, slice thickness = $2\ mm$, no gap, 64 axial slices, and voxel size of $2 \times 2 \times 2\ mm$. The diffusion was measured along 32 non-collinear directions using a b-value of $1000 s/mm^2$, with a $b = 0$ included as the first volume of the acquisition.

4.2.3 Image processing

The processing of diffusion data and T1 MRI data to construct structural connectome was performed in FSL and ANTS based MRtrix (`http://mrtrix.org/`), BrainSuite (`https://brainsuite.org/`), and FreeSurfer. Structural connectivity estimation was performed employing the BATMAN pipeline implemented in MRtrix software (See method pipleline in Figure 4.1). Particularly, probabilistic tractography was performed based on the Constrained Spherical Deconvolution (CSD) algorithm [Tournier et al., 2004, Tournier et al., 2007]. The CSD algorithm evidently outperforms the diffusion tensor model (DTI) in regions containing crossing fibers, which DTI cannot capture due to its ellipsoid approach to fiber orientation estimation. The initial preprocessing of diffusion-weighted images included denoising to estimate the spatially varying noise maps [Veraart et al., 2016a, Veraart et al., 2016b], unringing to remove Gibbs ringing artifacts was performed in MRtrix [Kellner et al., 2016] and bias field correction of diffusion images [Tustison et al., 2010]. Then MRI images are preprocessed for co-registration with diffusion data. Therefore, firstly, skull-stripping of MR images was performed by the Cortical Surface Extraction Tool [Sandor and Leahy, 1997, Shattuck et al., 2001], followed by correction of gain variation by the Bias Field Corrector (BFC) software [Shattuck et al., 2001], part of the BrainSuite. Particularly, it is used to correct image intensity non-uniformities in magnetic resonance images, which can cause confounding effects in tissue classification. BFC estimates a correction field based on a series of

local estimates of the tissue gain variation and corrects for the non-uniformity field by dividing the original image by the estimated tri-cubic B-spline. Thereafter, BrainSuite Diffusion Pipeline (BDP) was used to correct motion and geometric distortions of diffusion images inherent to Echo-Planar Imaging sequences [Bhushan et al., 2012], co-registration of diffusion and anatomical images, and obtaining b-values and b-vectors to be used for further estimation of response functions [Haldar and Leahy, 2013, Shattuck and Leahy, 2002]. Subsequently, to determine the diffusion orientation within each voxel, a response function was derived using Dhollanders algorithm from representative tissue types of the brain i.e., white matter, gray matter, and cerebrospinal fluid [Dhollander and Connelly, 2016]. Thereafter, Fiber Orientation Distributions (FOD) were estimated using the CSD algorithm. Intensity normalization was performed to correct for global intensity differences, and a whole-brain tractography was generated using probabilistic tractography in tandem with biologically plausible Anatomically Constrained Tractography algorithm to generate 20 million tracts seeded in gray matter [Smith et al., 2012]. The tractogram was then coregistered onto individual MRI, and a subset of one hundred thousand tracts was filtered out to reduce CSD-based inherent bias in overestimation of longer tracks by Spherical-deconvolution Informed Filtering of Tracts (SIFT) algorithm [Smith et al., 2013]. Finally, the connectome was parcellated by mapping the tracts onto MRI data, defined according to the Desikan Kiliany atlas [Desikan et al., 2006] that was segmented in FreeSurfer (`https://surfer.nmr.mgh.harvard.edu/`). The resulting 68 x 68 parcellated whole-brain structural connectivity (SC) weights and fiber lengths matrices were representative of the number of streamlines and mean streamline length between each node pair, respectively (See Fig. 4.1). The SC matrix and fiber length matrix were both symmetric matrices and values at the diagonals of structural connectivity and fiber length matrix representing self-connectivity and length with self, respectively, were set at zero.

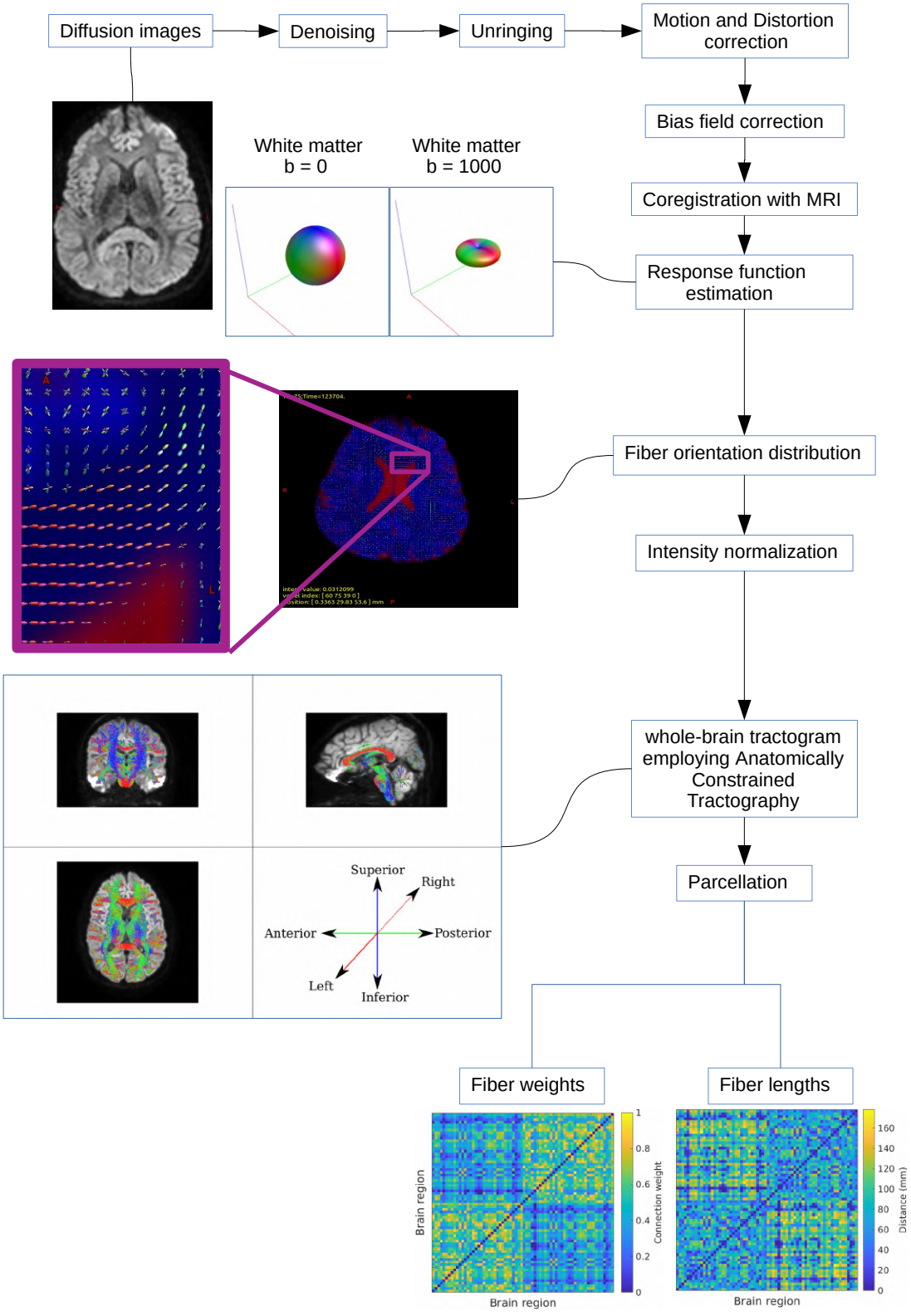
Diffusion images
Denoising
Unringing
Motion and Distortion correction
Bias field correction
Coregistration with MRI
Response function estimation
White matter b = 0
White matter b = 1000
Fiber orientation distribution
Intensity normalization
whole-brain tractogram employing Anatomically Constrained Tractography
Parcellation
Superior
Right
Anterior
Posterior
Left
Inferior
Fiber weights
Fiber lengths
Brain region
Brain region
Connection weight
Brain region
Distance (mm)

Figure 4.1: **Pipeline to obtain structural connectivity matrices:** DWI data is preprocessed and response function are obtained. At b-value of zero meaning no diffusion gradient, a sphere denotes isotropic diffusion. At $b = 1000\ s/mm^2$ the response function become flat due to anisotropic water diffusion of whiter matter. Subsequently, FODs overlaid on each tissue type color coded cerebrospinal fluid is depicted as red and white matter is shown in blue, zooming in, red signalizes that the primary orientation is left-to-right, green means posterior-to-anterior (y-axis), and blue represents orientations in the inferior-to-superior direction (z-axis). Thereafter, streamlines are generated followed by parcellating the streamlines to obtain the number of streamlines as fiber weights and mean streamline length as fiber legths connecting pair of regions.

4.2.4 Network model of neural activity

We aimed to model the propagation of oscillatory activity from primary auditory cortices to specialized regions of the brain during ASSR, speech and melody processing using a simplified computational model, retaining the essence of key physiological parameters. The propagation of oscillation can be conceptualized as unidirectional interactions originating in PAC to form a functional neural network. Such networks communicate via phase-based synchronization. We employ the Kuramoto model to simulate these series of synchronizations [Kuramoto, 1984]. Kuramoto model is a phase-based model mediated by synchronization among coupled oscillators. Hence, a network of 68 coupled oscillators was simulated, each oscillator representative of a brain parcel also comprising bilateral primary auditory cortices (PAC). Each other oscillators had intrinsic noise η, which was randomly drawn from a distribution with a mean of zero and a standard deviation of one reflecting the natural variability of oscillatory dynamics in the brain. The remaining two oscillators situated in the primary auditory cortices and have fixed intrinsic frequencies that correspond to their oscillatory responses. This framework allowed the unidirectional propagation of entertainment from PAC to the specific nodes and consequent enhancement of spectral power of those nodes at the frequency of PAC stimulation (Figure 4.2;right panel).

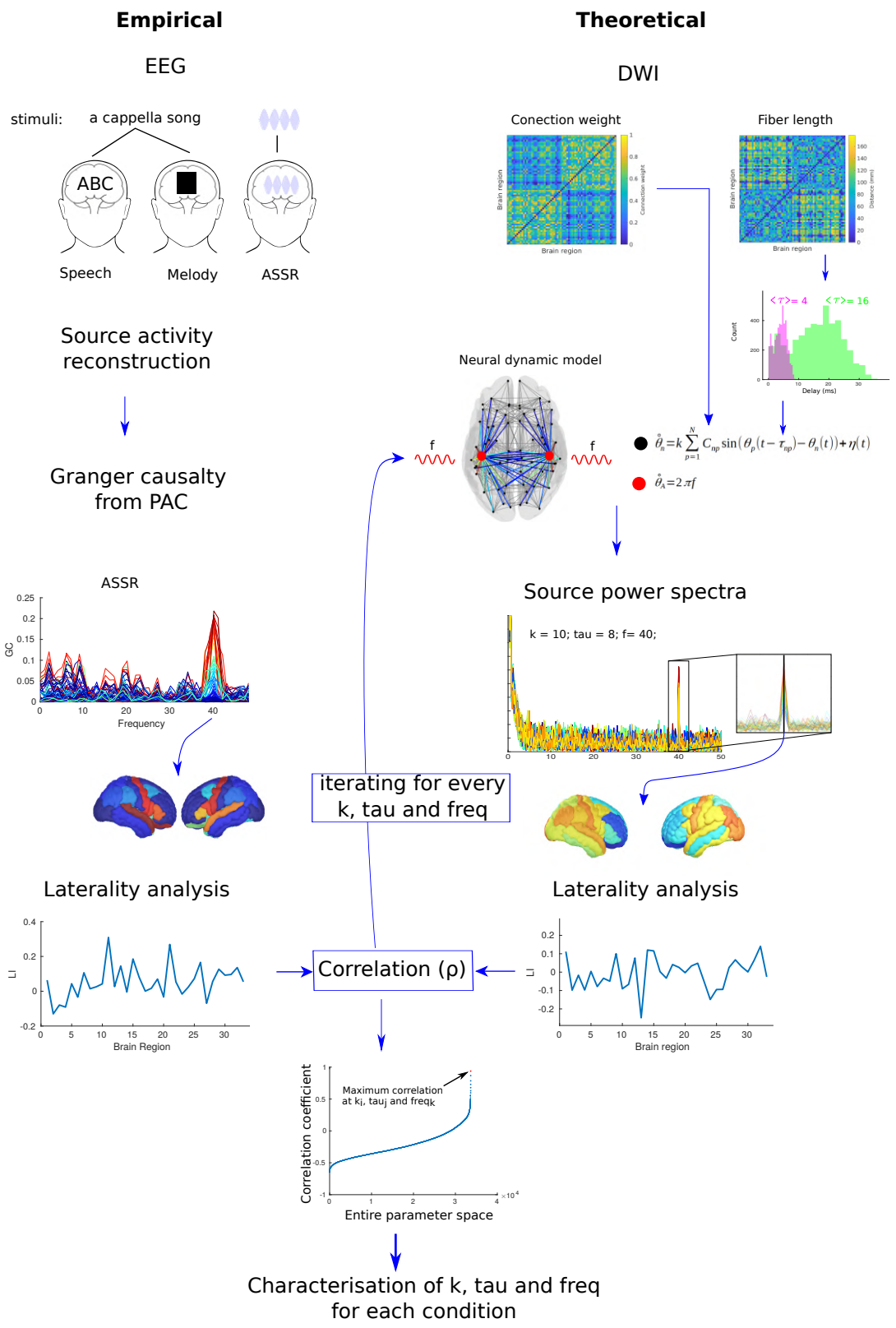
Empirical
Theoretical
EEG
DWI
stimuli:
a cappella song
ABC
Speech
Melody
ASSR
Conection weight
Fiber length
Source activity reconstruction
Granger causalty from PAC
Neural dynamic model
f
f
Source power spectra
k = 10; tau = 8; f= 40;
ASSR
GC
Frequency
iterating for every k, tau and freq
Laterality analysis
Laterality analysis
LI
Brain Region
Correlation (ρ)
LI
Brain region
Maximum correlation at ki, tauj and freqk
Correlation coefficient
Entire parameter space
Characterisation of k, tau and freq for each condition

Figure 4.2: **Overview of the methodology:** The figure illustrates the pipeline of study, incorporating both empirical and theoretical analyses. The left panel depicts the empirical analysis, highlighting the experimental setup and data processing steps involved in recording neural activity using electroencephalography (EEG) while participants selectively attended to speech or melody stimuli. For visualization purpose, after source localization only ASSR analysis was represented. The right panel represents the theoretical analysis, showcasing the averaged structural connectivity (SC) network that was derived from diffusion magnetic resonance imaging (MRI) data. This network served as a constraint for a neural dynamic model to simulate the frequency-specific outflow from the primary auditory cortices.

Notably, these functional interactions are not supposed to be instantaneous and are contingent on the structural connectivity. Hence, we constrained the synchronization of entrained activity by integrating structural connectivity in the Kuramoto model. To make the model bio-physiologically realistic, information about structural connectivity was incorporated in the model by having the coupling between oscillators determined by strength of anatomical connections (fibre thickness in dWI, see section "Image processing and structural connectivity). The time scale separation for processing of "fast speech and "slow melody could be achieved by a propagation time-delay (τ) in the model such that the current phase $\theta(t)$ is dependent on its interaction with the past phase $\theta(t-\tau)$. Inadvertently, τ can be conceptualized to be emerging from a joint contribution of the functional processing in the auditory network and the constraints posed by myelination, although the former is the only quantity that can change in a participant and in a session specific way. Thus, the dynamics of each oscillator θ_n are governed by the following equation:

$$\dot{\theta}_n = k \sum_{p=1}^{N} C_{np} \sin\left(\theta_p(t-\tau_{np}) - \theta_n(t)\right) + \eta, \tag{4.1}$$

$$\forall_n = 1, 2, \ldots, (N-2), \quad p \in [1, N], p \neq n$$

The coupling strength matrix C_{np} was normalized between 0 and 1 such that the

maximum strength among connections was 1 and k is the global mean coupling strength used to scale all the coupling strengths; represents transmission delay for the propagation of information between two nodes, given the length of the fiber. Thus, $\tau_{np} = \frac{D_{np}}{v}$, where for a bio-physiologically realistic communication speed (v) is $5-20\ ms$ in the adult primate brain (Ghosh et al., 2008), mean tau ($< \tau >$) ranged from 3.4 to 17. Thus, C_{np} and τ_{np} respectively represent the coupling strength and time delay between node n and p. Therefore, the dynamics of phase (θ) at any node will be a function of its anatomical strength and distance with other nodes and propagation speed (v), which is set by the nature of functional processing. While equation 4.1 the value of iterates from 1 to 68 including auditory nodes. This implies that phase dynamics of non-AC will depend on phase dynamics of all other nodes including bilateral auditory cortices (auditory nodes) are defined as,

$$\dot{\theta}_A = \omega_A \tag{4.2}$$

where $\omega_A = 2\pi * f_A$ frequency of AC (f_A) nodes.

Participant-wise model fitting

The subject-by-subject laterality indices obtained from the empirical Granger-causality estimation, were fitted with the LI‘s computed from analyzing synthetic neural time-series generated by the network model (equations 4.1, 4.2). The system of differential equations (equations 4.1, 4.2) was numerically integrated using the Euler integration method for 250000-time points with a step size (dt) of 0.0001 representative of 25 seconds duration. We took the sine of (θ) obtained at each node which represents a simulation of neural time series at EEG source level. Subsequently, we calculated the power spectral density from 68 nodes. For each combination of frequency (f), global coupling (k), and time delay (τ) model simulation,

simulated lateralization indices were calculated from power spectral density obtained from each 68 parcels (equation 2.3). We ran an optimization algorithm to obtain a set (k_{opt}, τ_{opt} and f_{opt}), at which the Pearson correlation between simulated and empirical LI reaches a global maximum. Hence, a model inversion was achieved for the following ranges of each parameter,$f_{opt} \in [1, 48]$; $\tau_{opt} \in [3.417]$;$k_{opt} \in [1, 20]$. The frequency window of interest was guided by the observation window of current study, the range of and has been shown earlier to represent biophysically relevant [Ghosh et al., 2008, Cabral et al., 2011].

We hypothesize, to process a specific auditory task, phase-based communication in an oscillatory network can be achieved by adjusting the combination of these free parameters (k_{opt}, τ_{opt} and f_{opt}). While the fitting was constrained by maximizing Pearson correlation between empirical LI and model generated LI, frequency-specificity of these optimal parameters model need to be studied to ensure that the simulated neural responses align with the observed empirical frequency-specific enhancements in Granger causality (GC) outflow from the bilateral primary auditory cortices (PAC). Hence, the model inversion was carried out independently for the major frequency bands, delta ($2-4Hz$), theta ($4-8Hz$), alpha ($8-13Hz$), beta ($13-30Hz$), and gamma ($30-48Hz$) for speech and music stimuli and also specifically at 40Hz for ASSR condition. It was required to ensure the frequency specificity of the model i.e., the significant distribution f_{opt} across subjects should fall into the corresponding frequency range. For instance, the confidence interval of f_{opt} to predict empirical theta lateralization should fall into the theta range. Hence, to establish a valid comparison between empirical EEG frequency and that can establish the frequency selectivity of the model we also correlated across a range of probable model frequencies ($f_{simrange}$) and estimated the of 95 % confidence bound of resultant predicted f_{opt}. Since, the outflow from PAC during speech and melody existed in the broadband frequency range rather than a single frequency unlike the model simulation, making the com-

parative assessments between model and empirical results are not straightforward since the model inversion process can lead to spurious non-unique values of frequencies and other parameters. Hence, 40 Hz ASSR condition where the signal displays a salient entraining frequency becomes a further validation ground to assess whether the model can be frequency-selective. Outflow from bilateral PAC was shown earlier to be present only at 40 Hz [Kumar et al., 2023] during 40Hz ASSRs. Hence, for the purpose of current study, demonstration of maximum proximity of model generated LI to empirical LI concomitant with matching of model estimated frequency and ASSR frequency gives us the confidence about the model estimation process when a complex range of frequencies are present in signal, e.g., during speech and music processing. Furthermore, there could be different number of target regions in each frequency bands across different conditions. Hence, for practical reasons and to standardize the comparative analysis across conditions, empirical distribution of LI values across the entire brain volume (34 values) are correlated. Thus, the combination of k_{opt}, τ_{opt} and f_{opt} that yielded maximum correlation with empirical LI was selected for each subject. Note that the k_{opt}, τ_{opt} and are valid only if the f_{opt} lies within the same range of empirical frequency band.

Furthermore, to confirm the accuracy of the model in utilizing structural connectivity (SC) to guide predictions, a control condition was implemented. In this condition, the weights and fiber lengths of the SC matrices for each subject were shuffled and used for the connectome model simulation. Specifically, the weights and fiber lengths of the SC matrices were randomly reassigned while maintaining the same number of connections and nodes. Comparative analyses were then performed between the shuffled and empirical 40 Hz ASSR condition, focusing on the assessment of the frequency specificity of the model. In particular, the model‘s ability to accurately predict the frequency-specific responses, hence at 40 Hz, was examined. The presence of frequency-specific enhancement (f_{opt}) in the shuffled and unshuffled conditions was

compared, with particular emphasis on the distribution of frequencies in each condition. By contrasting the shuffled and unshuffled conditions, this assessment aimed to determine the extent to which the model's predictions were reliant on the intact organization of the structural connections in the brain. Notably, the fact that each task state such as processing speech / melody requires idiosyncratic distribution of these free parameters given the specific nature of information processing. Additionally, these neurophysiologically relevant free parameters would not be identical in every subject owing to the inter-subject variability [Seghier and Price, 2018]. Subject-specific prediction enables not only contribute to the robustness of the analysis but also enables attributing the functional variability to the differences in individual structural connectivity. Nevertheless, another attribute of population studies is the existence of central tendency in the distribution of free parameter across subjects. Hence, assessing the normality of k_{opt} and τ_{opt} across subjects was required in this framework to evaluate the suitability of assuming a normal distribution for these parameters. A normal distribution indicates a predictable and stable pattern of parameter values, which is desirable for interpreting and generalizing the results of our model. Hence, we assessed the extent of prediction for individual regions and its inter-subject variability since the empirical source analysis revealed that only specific regions exhibited frequency-specific enhancement in Granger causality (GC) outflow from the bilateral PAC. We employed a linear regression analysis, wherein the empirical LI values of individual regions across subjects were regressed against the corresponding simulated LI values. The goodness of fit was evaluated by assessing the coefficient of determination (R-squared) and the significance of the regression coefficients. The LI values of a particular region were selected from the spatial distribution of LI that yielded maximum correlation f_{opt}, k_{opt} and τ_{opt}. Finally, we examined the global coupling (k_{opt}) and mean delay (τ_{opt}) between the speech and music conditions across all frequencies via paired t-test. This analysis allowed us to

explore whether the brain exhibited distinct functional mechanisms to process auditory signals of various spatiotemporal complexities, e.g. speech, music and rhythmic tonal sounds.

4.3 Results

In the empirical study in chapter 3, EEG data were collected from a group of 30 participants during three auditory conditions, melody, speech, and 40 Hz ASSR. The laterality indices (LI) of frequency-specific Granger causality outflow from bilateral primary auditory cortices were estimated for each task conditions. In the current theoretical study, we present the computational modelling results, where bilateral primary auditory cortices were stimulated in-silico, at frequencies ranging from 1 to 48 Hz. The entrainment propagated throughout the entire brain constructed via coupling brain areas (using Desikan-Kiliany parcellation) with strengths derived from diffusion MRI derived structural connectivity (see Methods, as well as [Schirner et al., 2015]). Model parameters - a range of realistic conduction velocities that influences the effective time-scales of processing information (time delays in the oscillator model,τ), global coupling values (k) among the nodes, were predicted using from best fits of empirical LIs using model generated LIs. Parameters estimated from the model inversion were subsequently used for inferring about the underlying neural mechanisms of functional hemispheric lateralization.

4.3.1 Estimation of transmission delays, synaptic scaling and neurally mapped input frequencies

We employed the Kuramoto phase oscillator network (Kuramoto, 1984) coupled by heterogeneous coupling derived from diffusion weighted images to model neural oscil-

lations observed in the whole-brain connectome (see Methods 4.2 for details). Since our interest is only in the causal outflow from PAC, the input node was only PAC for the simulations (see Methods for details, equations 4.1, 4.2). Subsequently, the steady-state oscillatory responses in each node of this network stems from the inflow of communication from PAC. Hence, the laterality indices (LI) can be computed using the power spectral density at each parcel. By maximizing the correlations between the simulated and empirical LI's we can undertake a model inversion to estimate transmission delays (τ_{opt}), global coupling (k_{opt}) and neurally mapped input frequencies (f_{opt}). Subsequently, the following issues were addressed. First, we take the auditory steady state responses tuned sharply at a specific entraining input frequency to validate if the network model can predict the LI's, tuned at the known frequency, while, readjusting transmission delays and global coupling (Figure 4.3). Second, after establishing the validity of the auditory network model, we investigate the complex multi-frequency EEG response for speech and melody processing and estimate the transmission delays and global coupling while ensuring frequency selectivity in band specific (delta, theta, beta and gamma) responses and maximizing the LIs (Figure 4.3). The estimated parameters can then be used to understand the mechanisms of processing speech and melody by a commonly shared structural auditory network.

4.3.2 Validation of auditory network model using ASSR

Since, ASSR is a sharp frequency tuned response, the proposed auditory network model parameters when fitted with a constraining factor of maximizing LI 4.2, should be able to detect the frequency of tuned neural oscillations around 40 Hz. Using a realistic parameter search space $f_{opt} \in [1, 48]$; $\tau_{opt} \in [3.417]$;$k_{opt} \in [1, 20]$; frequency-selectivity of the simulated auditory network was estimated by first constructing a

null distribution with 95% confidence bounds for f_{opt}. The control null distribution was created by shuffling the SC matrices, such that each connection weight is essentially a random rational number between 0 and 1, and using this randomized SC to generate neural time series that was used to fit the empirical 40 Hz ASSR. No frequency-specificity was observed from the resultant synthetic data, f_{opt} was distributed in the whole $f_{simrange}$. The maximum correlation ranged between 0.4 to 0.7 across all participants, thus delimiting the correlation value of 0.7 as a threshold correlation that can be generated for randomly connected network (Figure 4.3; upper right panel). In contrast, when using the unshuffled SC matrices, the empirical 40 Hz ASSR showed frequency specificity, with a 95% confidence interval of $[39.4, 40.9]$ Hz and maximum correlation values ranging from 0.79 to 0.96 (both > 0.7), thus, confirming the model's ability to predict empirical responses. The 95% confidence intervals for k and τ were $[2.5, 3.5]$ Hz and $[1.5, 2.2]$ Hz respectively. The distributions of both k_{opt} and τ_{opt} followed a normal distribution, assessed using Lilliefors test with k-stat values of 0.24 ($p < 0.001$) and 0.16 ($p = 0.043$) and τ, respectively (Figure 4.3; upper right panel).

4.3.3 Mechanisms underlying lateralization of causal outflow in beta and gamma frequencies during speech and melody processing

During speech and melody conditions, no frequency-specificity could be predicted by the auditory network model in the delta and theta frequency bands (Figure 4.3; bottom panels). In the delta range, the 95% confidence intervals of f_{opt} for speech and melody were [17.6, 29.8] Hz and [15.7, 26.9] Hz, respectively, indicating no frequency-specific prediction. Similarly, in the theta range, the 95% confidence intervals for speech and melody were [19.2, 30.8] Hz and [16.0, 28.1] Hz, respectively. Therefore,

the k_{opt} and τ_{opt} values for these frequency ranges are not considered reliable.

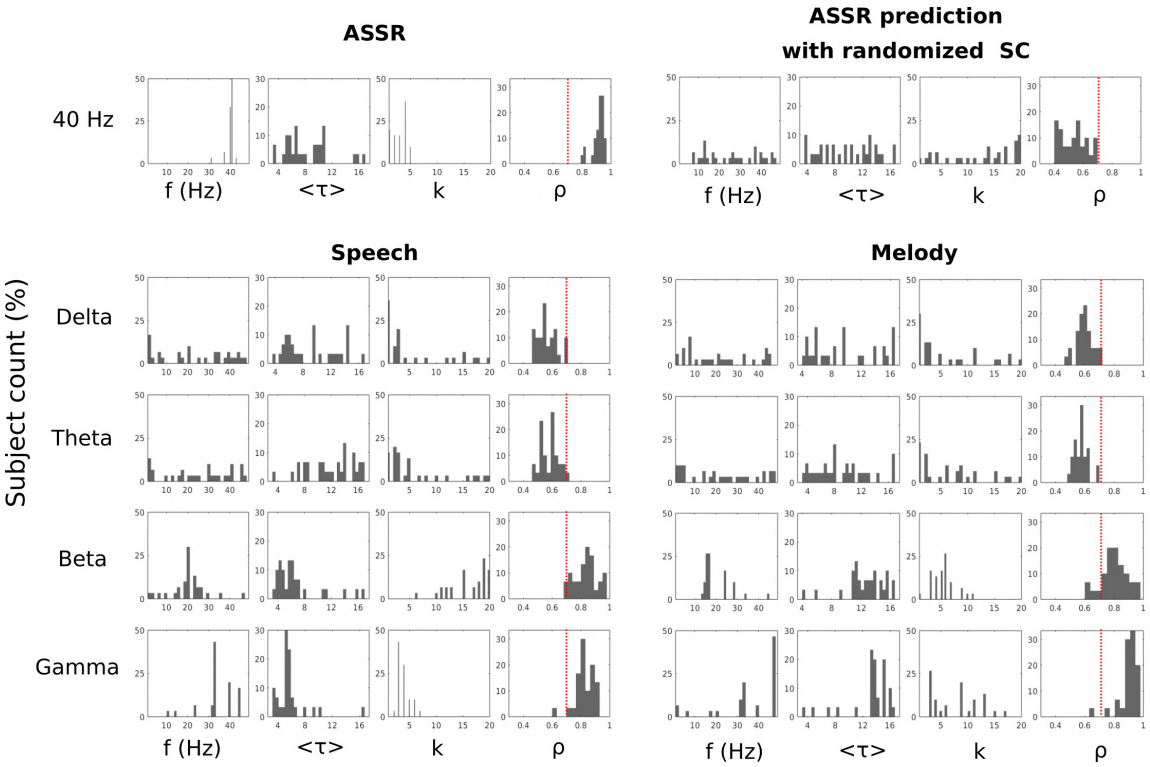

Figure 4.3: **Prediction accuracy of frequency simulation (f (Hz)), global coupling (k), and global delay (τ):** Distributions of prediction accuracy of free parameters ASSR, ASSR with shuffled SC, speech, and melody conditions. The x-axis represents the different simulation parameters, while the y-axis represents the prediction accuracy. The first column in each condition demonstrates the effectiveness of the frequency simulation in accurately predicting the neural responses. The last panel shows the correlation coefficients of respective predictions.

On the contrary, frequency-specificity was observed in beta and gamma frequency bands. For speech, the 95% confidence interval of f_{opt} in beta was [17.2, 23.7] Hz, and for melody, it was [17.6, 22.8] Hz. In gamma, for speech, the 95% confidence interval of f_{opt} was [31.0, 41.7] Hz, and for melody, it was [31.1, 37.4] Hz. These CIs indicated that the model correctly captured the frequency-specificity activity of empirical data within the beta and gamma bands. The values of k_{opt} and τ_{opt} also showed normal distributions for these frequency bands, indicating a smooth and gradual transition in the model‘s behavior required for a consistent and reliable model performance.

The complete list of 95% confidence intervals for frequency, k_{opt} and τ_{opt}, as well as the results of the normality tests, are present in Table 4.1.

Individual-specific prediction of functional lateralization in auditory processing networks

To assess the prediction of lateralization, we conducted linear regression analyses in the beta and gamma frequency ranges to evaluate the extent of prediction for individual regions found significant in the empirical data. Most regions significantly predicted lateralization in the empirical data, with the exception of the supramarginal gyrus during speech condition in the gamma band. Figure 4.4b shows the respective prediction score for the individual brain region. Overall, the prediction score for the ASSR condition was greater than the speech and melody condition. When both the upper and lower confidence intervals of a region‘s laterality index (LI) for both the simulated and empirical data fell on the same side of zero, we considered the model to successfully predict the side of lateralization for that region. Consistent with the empirical conditions, several regions exhibited lateralization. Particularly, during the ASSR condition, right hemispheric dominance was predicted by the superior temporal gyrus (STG), parahippocampal cortex, and lateral orbitofrontal cortex (Figure 4.4a). During speech and melody conditions, the STG predicted left hemispheric dominance during speech and right hemispheric dominance during both beta and gamma frequencies. The precentral gyrus predicted the side of lateralization during speech beta and gamma, and in melody during beta frequencies. Additionally, the pars opercularis predicted left hemispheric dominance during speech gamma conditions.

Table 4.1: Assessing the validity of free parameters (Frequency, k and tau) after model inversion using 95% Confidence Interval and Normality Test.

	95% Confidence Interval						Normality Test			
	Frequency		k		τ		k		τ	
	Lo CI	Up CI	Lo CI	Up CI	Lo CI	Up CI	k stat	p value	k stat	p value
Control ASSR	21.6	31.1	10.6	15.4	1.8	2.6	0.16	0.042	0.13	0.195
ASSR	39.4	40.9	2.5	3.5	1.5	2.2	0.24	> 0.001	0.16	0.043
Speech delta	17.6	29.8	3.2	7.7	1.7	2.4	0.32	> 0.001	0.15	0.091
Melody delta	15.7	26.9	3.8	8.4	1.8	2.6	0.26	> 0.001	0.15	0.093
Speech theta	19.2	30.8	3.8	8.4	2.4	3.1	0.27	> 0.001	0.12	0.339
Melody theta	16.0	28.1	4.6	8.9	1.7	2.4	0.19	> 0.001	0.12	0.339
Speech beta	17.2	23.7	14.8	17.5	1.1	1.8	0.19	0.006	0.28	> 0.001
Melody beta	17.6	22.8	4.7	6.3	2.6	3.1	0.18	0.015	0.18	0.010
Speech gamma	31.0	41.7	6.2	9.4	2.7	3.3	0.24	> 0.001	0.29	> 0.001
Melody gamma	31.1	37.4	3.5	4.3	1.0	1.5	0.18	0.014	0.37	> 0.001

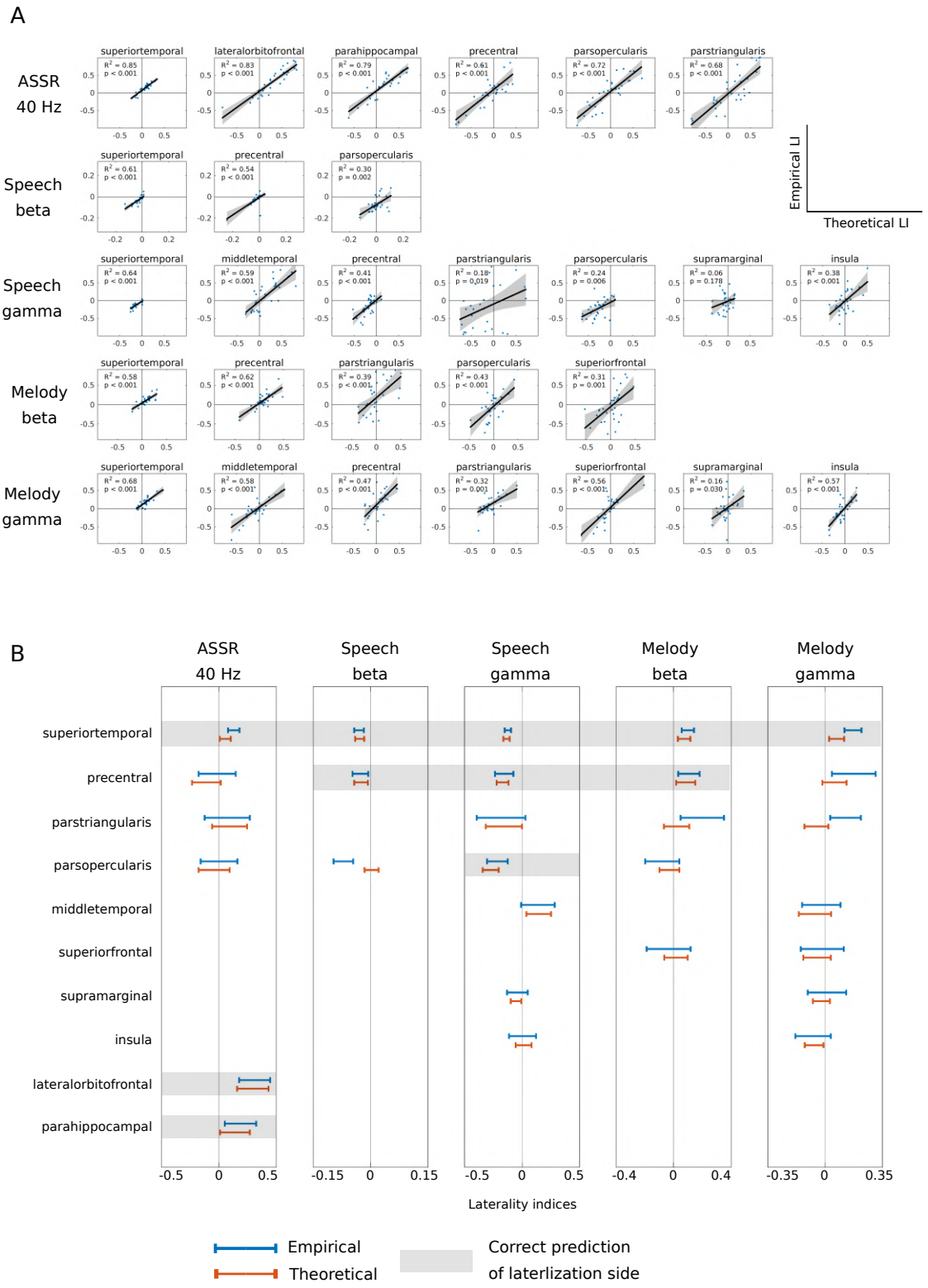
A
ASSR 40 Hz
Speech beta
Speech gamma
Melody beta
Melody gamma
Empirical LI
Theoretical LI
B
ASSR 40 Hz
Speech beta
Speech gamma
Melody beta
Melody gamma
superiortemporal
precentral
parstriangularis
parsopercularis
middletemporal
superiorfrontal
supramarginal
insula
lateralorbitofrontal
parahippocampal
Laterality indices
Empirical
Theoretical
Correct prediction of laterlization side

Figure 4.4: **Lateralization prediction accuracy of individual regions:** (A) Linear Fitting of Empirical and Theoretical LIs, scatter plot shows the linear fitting of empirical LI (Y-axis) against theoretical LI (X-axis). Each dot represents the LI of one subject. The analysis focuses on beta and gamma frequencies for speech and melody conditions, as well as 40 Hz for the ASSR condition. (B) Confidence Intervals for Lateralization Indices (LI), the confidence intervals for the LI during empirical (blue) and theoretical (orange) analyses. The shaded background indicates cases where both empirical and theoretical LIs fall on either side of zero, indicating accurate prediction of the lateralization direction.

LI prediction from auditory network model follows the auditory processing hierarchy

Interestingly, we observed a systematic decrease in R-squared values for individual regions along a specific axis of information flow. When arranging the regions in a specific order, namely superior temporal gyrus (STG), middle temporal gyrus (MTG), insula, precentral gyrus, Broca‘s area, and supramarginal gyrus, for both speech and melody conditions, we found that the degree of prediction exhibited a consistent linear decrease in the gamma frequency band (Figure 4.5 b). This pattern was observed in both the speech condition $[R^2 = 0.93, p = 0.001]$ and the melody condition $[R^2 = 0.93, p = 0.001]$. Note that, similar analysis in the beta frequency band was not feasible due to the limited number of regions. However, in the beta range the highest prediction accuracy was present in STG for speech and PrC for melody condition.

The paired t-tests showed the presence of overall differences in neural processing characteristics between speech and melody stimuli Fig. 4.5. The findings revealed a significant difference in the k parameter [t = 3.05, p = 0.003], indicating distinct global coupling between the two conditions. Moreover, there was a significant difference in the tau parameter [t = 11.32, $p < 0.0001$], suggesting variations in temporal delays during the processing of speech and melody stimuli. These analyses shed light on the global neural dynamics and temporal characteristics associated with different auditory stimuli.

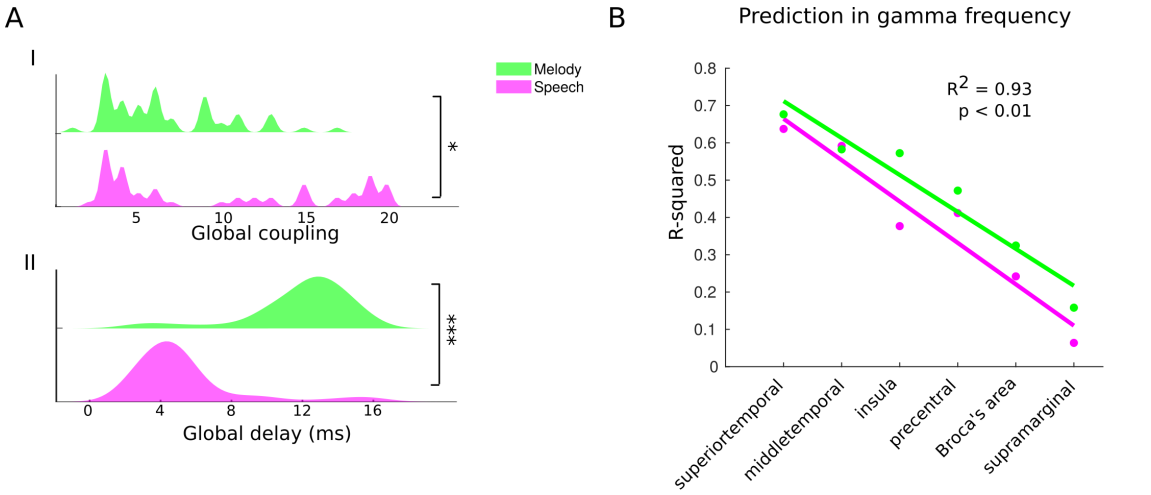

Figure 4.5: A) Distribution of global coupling and global delay for beta and gamma frequencies in speech and melody conditions. The distributions are visualized using kernel smoothing with a bandwidth of 0.3 to enhancing the clarity of the patterns. B) Decrease in prediction accuracy along the auditory hierarchy in gamma range in the speech and melody conditions.

4.4 Discussion

The present study introduces a novel approach of modeling the task induced electrophysiological response during speech, melody, and ASSR conditions. Particularly, with a specific focus on the role of the primary auditory cortices (PAC) and their outflow in governing hemispheric specialization. Our study combines empirical analysis (in chapter 2) and neural modeling to establish a causal link between PAC dynamics and hemispheric specializations. One notable aspect of current study is the individualized parametrization structure to function mapping. By integrating individual diffusion magnetic resonance imaging (DWI) data into our neural model, we ensure subject-specific variability of the structural constraints underlie the inter-subject variability of neural dynamics [Seghier and Price, 2018]. Firstly, in the empirical study, we reconstruct the subject-wise source activity and compute Granger causality from bilateral PAC in distinct frequency bands. Our findings reveal a common frequency-specific outflow from PAC in both speech and melody conditions, reach-

ing to distinct regions reflecting domain-specific organization of the auditory system. Furthermore, the laterality analysis of causal outflow complies with well-established hemispheric dominance of left hemisphere for speech, right hemisphere for melody, and right hemisphere for ASSR, suggesting role of PAC in hemispheric specializations. To further understand the characteristics of this outflow and lateralization, we utilize a structurally-guided frequency-specific neural model. We validate the frequency-specificity of the model and characterize the neurophysiologically relevant conduction velocity and global coupling characteristics of each auditory condition. Importantly, we found dichotomy in the temporal scales of information transfer from bilateral PAC, attributing to the differences in the physical properties of the auditory signal.

4.4.1 Role of Structural Constraints in Lateralized Network Dynamics

The physical structure of the brain, including the patterns of connectivity between brain regions, plays a crucial role in shaping the processing of information [Honey et al., 2007, Sporns, 2010]. The structural properties of the brain provide the foundation for the brain‘s ability to process basic features of the environment. However, it is important to note that brain structure is static while functions are not. While basic features of auditory processing can be explained solely based on the network properties of structural connectivity, more abstract and higher-level features of the environment, such as meaning, context, and emotion require a more complex and dynamic interplay between different regions of the brain [Bauer et al., 2020, Berger et al., 2019, Di and Biswal, 2019]. Our findings revealed that the model incorporating structural connectivity (SC) and oscillatory interactions achieved the highest prediction accuracy in the 40 Hz ASSR

condition. This observation suggests that the neural processes associated with the ASSR are primarily rooted in the basic stages of cortical processing and do not necessitate any non-linear or higher-level processing mechanisms. The linear decrease in prediction accuracy across hierarchical brain regions further support this inference. Furthermore, high prediction in motor regions in beta range could be attributed to the "hard-wiring" of auditory-motor interaction as reported earlier [Morillon et al., 2010b]. These findings hint that the higher-level processing or other factors beyond phase-based interactions contribute to propagation of delta and theta oscillations [Pandey et al., 2022]. On the other hand, the processing of meaning in language requires the coordination of neural activity between regions involved in phonetic, lexical, and semantic processing, as well as regions involved in attention, working memory, and executive control [Kazanina and Tavano, 2023]. Similarly, the processing of emotion in melody requires the coordination of neural activity between regions involved in auditory processing, pitch perception, and emotional valence [Gnanateja et al., 2022, Wang et al., 2023, Yurgil et al., 2020]. These distinct functional requirements are supported by the structural connectivity between these regions. The brain accomplishes this by precisely manipulating the timing and coordination of neural signals through two key factors: conduction velocities and a scaling factor applied to fiber thickness. Conduction velocities, which denote the speed at which neural impulses travel along nerve fibers, play a pivotal role in governing the temporal aspects of neural communication. Varied conduction velocities facilitate the emergence of distinct time delays, thereby shaping the arrival and integration of neural information across disparate regions [Cariani and Baker, 2022]. This temporal coding ensures the precise synchronization necessary for intricate processing tasks [Ibrahim et al., 2021, Petkoski et al., 2018]. Additionally, the brain utilizes the scaling factor defined here as global coupling, applied to fiber thickness as a means of regulating synchronization strength. By modulating this factor, the brain can

finely adjust the degree of coordination between neural signals. Hence, despite the underlying static structural connectivity within the brain, modulation by conduction velocities and synchronization strength enables the generation of a diverse range of time delays and strengths of information propagation.

4.4.2 Stimuli-dependent shifts in communication delays

Our study revealed distinct temporal scales for auditory processing. The observed differences in conduction velocities between speech and melody stimuli in our study align with previous findings that speech exhibits rapid temporal changes and melody shows fast spectral changes [Zatorre and Belin, 2001]. Our simulation model suggests that these differences in conduction velocities contribute to the functional lateralization observed in speech and melody processing. The faster conduction velocities in the left hemisphere, specialized for speech, enable the precise analysis of temporal changes associated with speech processing, while the slower conduction velocities meaning greater time window allows to capture fine spectral resolution of melody in the right hemisphere. The role of dichotomous or distinct categories within a system could be the causes of development of separation of cognitive processes or functional specialization observed in dichotomies. More over as suggested earlier, brain‘s parallel processing mechanism allows it to effectively handle the complementary aspects of speech and melody, which are two crucial forms of auditory communication. By distributing the cognitive load, the brain enables simultaneous processing when speech and melody are combined, as seen in ecologically valid a cappella songs.

The concept of stimuli-dependent shifts in communication delays for dynamic processing correspond to the the adaptability of the human brain. When observing a distinct distribution of the delays in response to a range of similar stimuli, such as speech and melody, we uncover evidence of a distinct and separate organization of

neural processing for these auditory categories. This phenomenon exemplifies categorical segregation, where the brain selectively assigns stimuli to different processing categories, and it underlines the capacity for a transition from one state to another, marking the brain‘s agility in switching from one information-processing mode or category to another. This dynamic process involves temporal discrimination, allowing for the rapid adjustment of neural communication delays based on the unique properties of incoming sensory information. It suggests the presence of distinct neural networks optimized for speech and music processing, where sensory encoding and feature extraction, as well as neural processing speed, are tailored to efficiently capture the intricacies of each stimulus type, highlighting the brain's versatility in temporal organization and information processing.

In summary, we highlight the dichotomy or dualistic nature of the auditory system at distinct levels. In the case of acoustic signals, a cappella songs, the auditory system utilizes two divergent but related (temporal and spectral) cues embedded in a common signal to dissociate perceptual experiences in the form of speech and melody, highlighting the dichotomy of auditory system. In our empirical study, we show the presence of common oscillatory outflow in homologues regions situated in another hemisphere hints at "spatial" dichotomy. The common oscillatory signatures observed in the brain may represent a common underlying neural process gives rise to distinct hemispheric dominance. Furthermore, the variations in conduction velocities result in different temporal processing characteristics, enabling the specialized processing of speech and melody in their respective hemispheres. We suggest the divergent nature of temporal processing arising from same anatomical structure exhibits "temporal" dichotomy.

Chapter 5

Transcranial Alternating Current Stimulation (tACS) induced neural oscillations in auditory networks

5.1 Introduction

In continuation of our earlier studies exploring the role of primary auditory cortex (PAC) and its associated neural oscillations in auditory processing and cortical hemispheric specialization, we now delve deeper into the causal relationship between PAC dynamics and the cortical asymmetry. Building upon the findings of our previous work in cahpters 2, 3 and 4 which revealed a frequency-specific outflow from the PAC contributing to the right hemispheric dominance of auditory steady-state response (ASSR), the present work aim to disambiguate between thalamo-cortical and cortico-cortical auditory inputs on corresponding network. While our previous study provided valuable insights into the frequency-specific outflow from the PAC, leaving the empirical causal link between PAC dynamics and hemispheric specialization unanswered. Importantly, auditory information begins with its initiation in

lower-level brainstem structures. As this information progresses through the auditory system, due to the structural pathway crossing, further ascending auditory stimuli are represented in contralateral pathway (As discussed in chapter 1). Subsequently, this acoustic information ascends to the primary auditory cortices (PAC), the initial cerebral cortex processing hub for auditory stimuli. Within the PAC, intricate functional processing unfolds. The central question here is that whether the information about the right hemispheric cortical dominance is already present in ascending auditory inputs or it is determined by the PAC. This determination may relies on the PAC‘s functional processing. Therefore, to experimentally and causally answer this hypothesis, we turn to Transcranial Alternating Current Stimulation (tACS), an innovative non-invasive brain stimulation technique, as the next step in our research endeavor. The rationale behind employing tACS lies in its unique capability to modulate neural oscillations in targeted brain regions by applying weak electrical currents through scalp electrodes [Helfrich et al., 2014, Hanslmayr et al., 2019]. By modulating specific oscillatory frequencies in the PAC, by-passing the initial auditory processing in the lower auditory pathway, we aim to causally modulate the neural dynamics and examine their direct impact on the lateralization. Importantly, post-tACS stimulation, the auditory information continues its trajectory, reaching higher cortical regions known for their involvement in advanced auditory tasks, such as generation of the 40 Hz Auditory Steady-State Response (ASSR). The crux of this approach lies in observing whether right hemispheric dominance continues to manifest conspicuously within these higher cortical regions after direct PAC stimulation via tACS. The presence of right cortical dominance would suggest that the functional processing within the PAC, influenced directly by tACS, plays a decisive role in determining hemispheric specialization, thereby decoupling it from the structural pathways that originated in the lower brainstem. This approach could be extended into the study of intricate interplay between PAC oscillations and higher-

order brain regions involved in language and melody processing (see cahpters 3 and 4). By studying how tACS-induced PAC entrainment influences functional connectivity within auditory networks, we can gain a comprehensive understanding of the neural interactions that support complex auditory perception. This stimulation technique operates on the principle of frequency-specificity, wherein the applied alternating current matches the target neural oscillation frequency, effectively "entraining" or synchronizing the activity of neural populations at that specific frequency [Helfrich et al., 2014, Hanslmayr et al., 2019]. The rhythmic electrical stimulation influences the excitability of underlying neurons, promoting resonance with the applied frequency and reinforcing the natural oscillatory patterns of the brain. As a result, tACS can enhance or suppress neural oscillations in a controlled and temporally precise manner, thereby modulating cognitive functions and perceptual processes. It can modulate spike timing and information processing by altering firing rates and spike timing in susceptible networks. The effectiveness of tACS depends on the interaction of endogenous and exogenous oscillations, with different mechanisms like resonance and imposed patterns playing a role. The results of our tACS study are anticipated to provide valuable insights into the continuum of our previous work, substantiating the role of PAC as the seed of cortical processing and elucidating how specialization begins at this fundamental level. Additionally, by examining the effects of PAC entrainment on functional connectivity, we aim to shed light on the network dynamics that underlie auditory perception and contribute to the distinct perceptual responses to speech and melody. In this study, we present the design and implementation of our tACS experiment, where participants are exposed to tACS applied to the PAC. We hypothesize that tACS-induced entrainment of specific oscillatory frequencies will lead to changes in neural activity within the PAC, consequently involving functional connectivity within auditory networks.

The comprehensive analysis of transcranial alternating current stimulation (tACS)

electroencephalography (EEG) data is a multifaceted endeavor. It entails optimized preprocessing steps aimed at refining the data quality, as well as addressing tACS-induced non-physiological components and artifacts [Noury et al., 2016]. Given the intricacies involved, it becomes essential to establish a specific experimental setup and paradigm design that can effectively capture and isolate the relevant neural responses. In order to ensure the accurate recording and subsequent analysis of EEG data influenced by tACS, it is imperative to begin with a pilot study. This preliminary investigation serves the purpose of standardizing both the recording and analysis protocols. By conducting a pilot study, we could refine the experimental procedures, and establish a reliable foundation for subsequent data collection and analysis. In alignment with these considerations, we undertook the recording of a basic tACS-EEG pilot study. The primary objective of this pilot study was to fine-tune the methodology, validate the experimental design, and assess the feasibility of recording EEG data under the influence of tACS. By conducting this initial pilot, we aimed to streamline the procedures for subsequent investigations, ensuring robust and accurate data collection and analysis.

5.2 Participants

One, right-handed participant, with a age of 32 years participated in the study after providing written informed consent. The participant had no history of neurological or psychiatric disorders and were medication-free at the time of the experiments.

5.3 Experimental Setup and Data Collection

The EEG configuration was consistent with the details outlined in chapter 3. Utilizing a BrainVision Recorder acquisition system, an actiCHamp module equipped

with 63 active channels was employed, following the standardized International 10-20 electrode placement system. To establish optimal contact between the EEG sensors and the scalp, SuperVisc electrolyte gel (EASYCAP) was applied. Continuous EEG data were captured at a sampling rate of 5 kHz, chosen to enhance the correction of tACS-induced artifacts. The impedance of each sensor was depicted in Figure 5.3. The reference electrode was positioned at the vertex (Cz), while the ground electrode was situated on the forehead (AFz).

5.4 Electrical stimulation

Transcranial electrical stimulation was administered using rubber electrodes measuring 5×5 cm^2 from nurostym, Neuro Device Group, Poland. These electrodes were affixed to the midline of the scalp, specifically centered over electrode positions Cz (anode) and T8 (cathode), beneath the EEG cap (Figure 5.3). T8 was identified as possible electrode to stimulate right primary auditory cortices. The impedance of the tACS electrodes was maintained below 10 $k\Omega$, by the application of Ten20 conductive paste. A sinusoidally alternating current of 1000 μA, was delivered at 40 Hz, utilizing a battery-driven stimulator. During sham and stimulation condition the current was ramped up over 10 seconds to 1000 μA, but discontinued during the sham condition. Participant were unaware about whether he received sham or stimulation. The sham condition preceded electrical stimulation to avoid carry-over effects of tACS. The experimental setup involved two blocks of sessions: a sham block and a tACS block (See Fig. 5.2). Each of these blocks was preceded and followed by a period of 2 minute of resting state recording. There was a 2-minute gap between the sham and tACS blocks. The main stimulation period consisted of 20 minutes of tACS stimulation, which was surrounded by 2 minutes of pre-stimulation recording and followed by 2 minutes of post-stimulation recording (See Fig. 5.2). Throughout

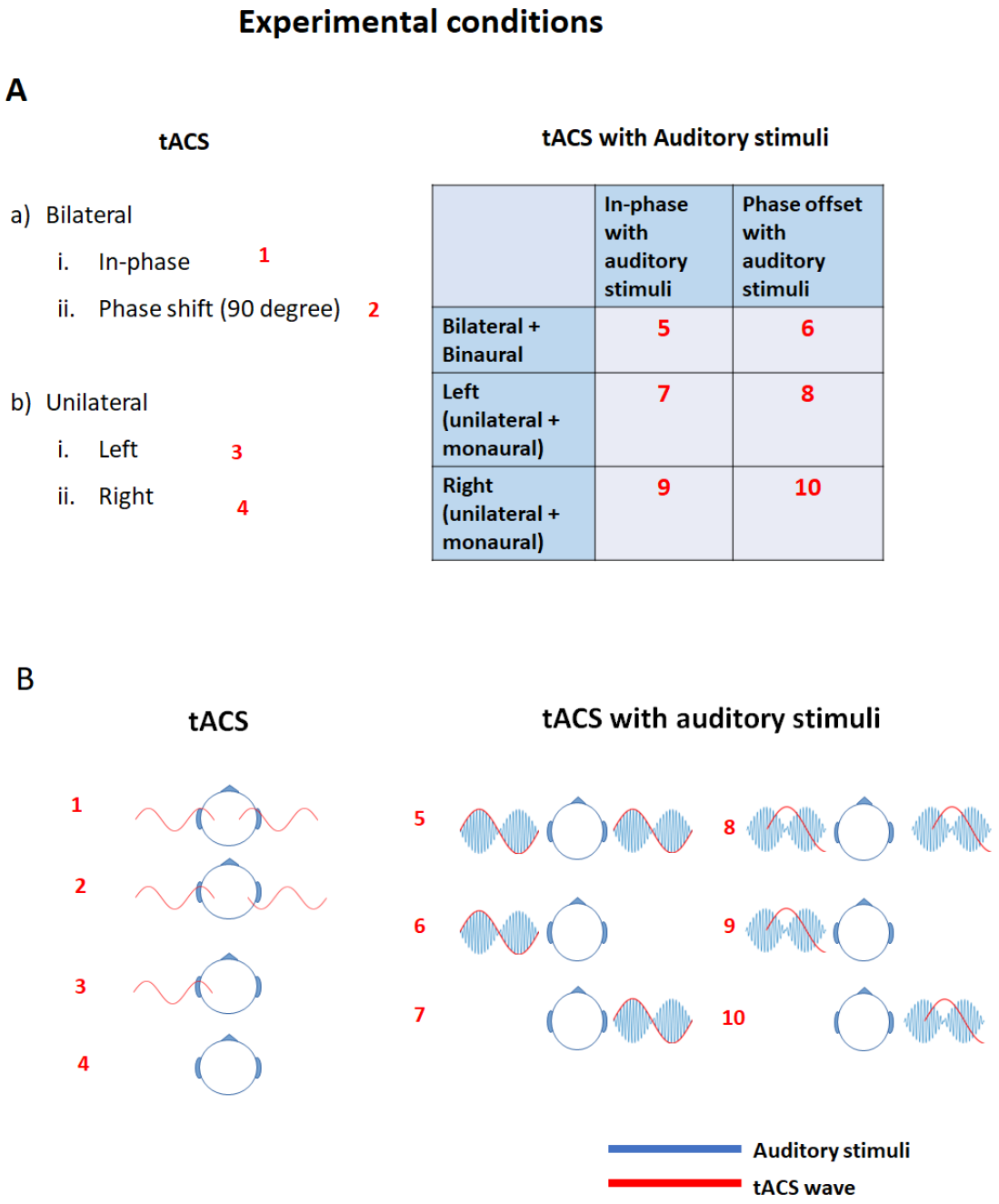

Figure 5.1: **Paradigm design:** Possible experimental conditions to charecterize the effect of tACS stimulations on auditory networks. The number in red color mark the number of experimental condition. This inculde only tACS stimulation of AC (left panel) and with auditory stimuli (Right panel), during binaural, monaural left and monaural right conditions. During auditory stimuli conditions the tACS stimulation could also be applied with 90° relative phase difference with the auditory stimulation to investigate the combined efffect of tACS application and auditory stimuli.

the administered stimulation was tolerable and did not induce visual sensations or uncomfortable skin perceptions.

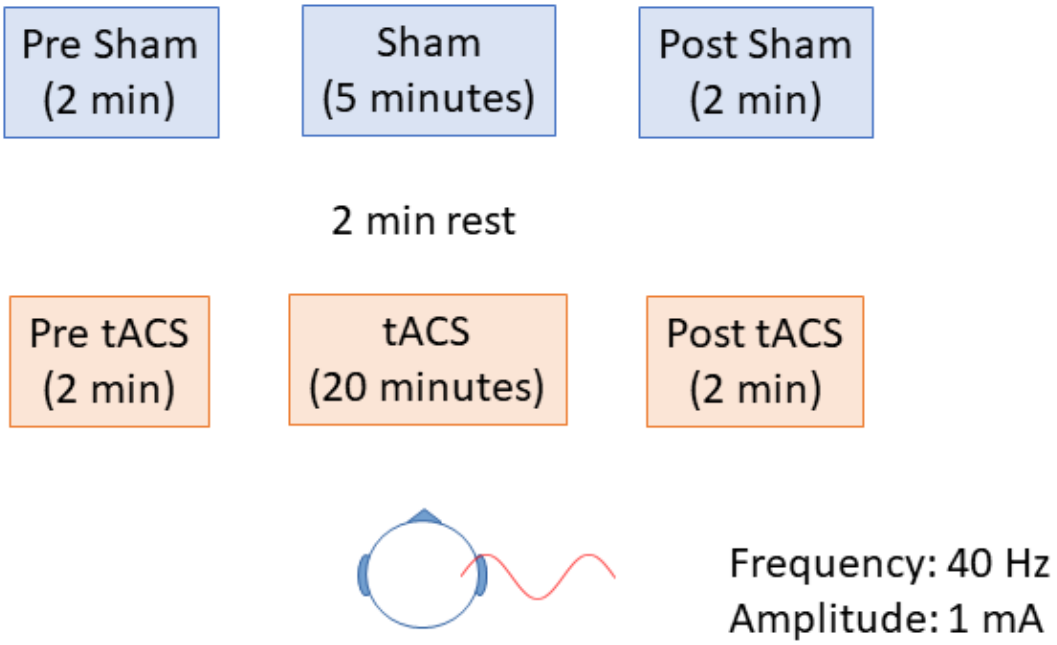

Figure 5.2: Experimental design to test the presence of entrainment, a prerequisite of the main experiment. The first block consisted of sham conditions (blue color) to prevent carryover effects of tACS. Subsequently, the tACS stimulation after a break of 2 minutes rest condition. Continous EEG was recorded in both expermintal conditions

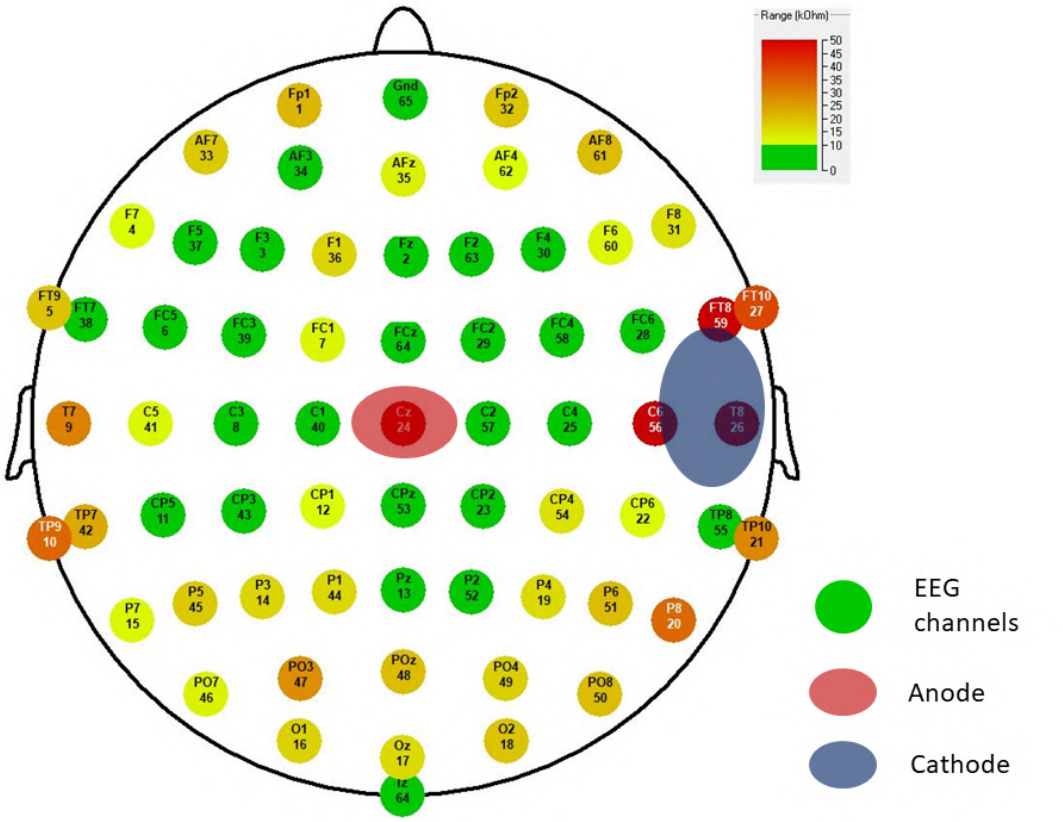

Figure 5.3: Illustration of the location of tACS electrodes. EEG channels are represented as circles while their color represent impdences before the EEG recording. Cathode represented as blue placed below T8 EEG channel to stimulate right auditory cortex. Anode represented as red placed over Cz channel. EEG channels were placed according to 10-20 locations.

5.5 tACS induced artifact rejection

The EEG data was imported into MATLAB using the built-in function of EEGLAB and underwent detrending. Across the pre-sham, sham, post-sham, pre-tACS, and post-tACS intervals, the recorded voltage remained within the range of approximately ± 10 μv. However, during tACS application, the observed voltage amplitude exhibited values in the range of approximately 20,000 microvolts (see Fig. 5.4). This significant increase in voltage amplitude was attributed to substantial artifacts induced by the tACS application at the 40 Hz stimulation frequency

[Kasten and Herrmann, 2019]. Power spectral density (PSD) analysis revealed a pronounced peak at 40 Hz, along with a broadband rise near this frequency (see Fig. 5.5). Notably, the amplitude of these artifacts exceeded that of physiological oscillations, presenting a challenge as the study was focused on investigating the effects at 40 Hz.

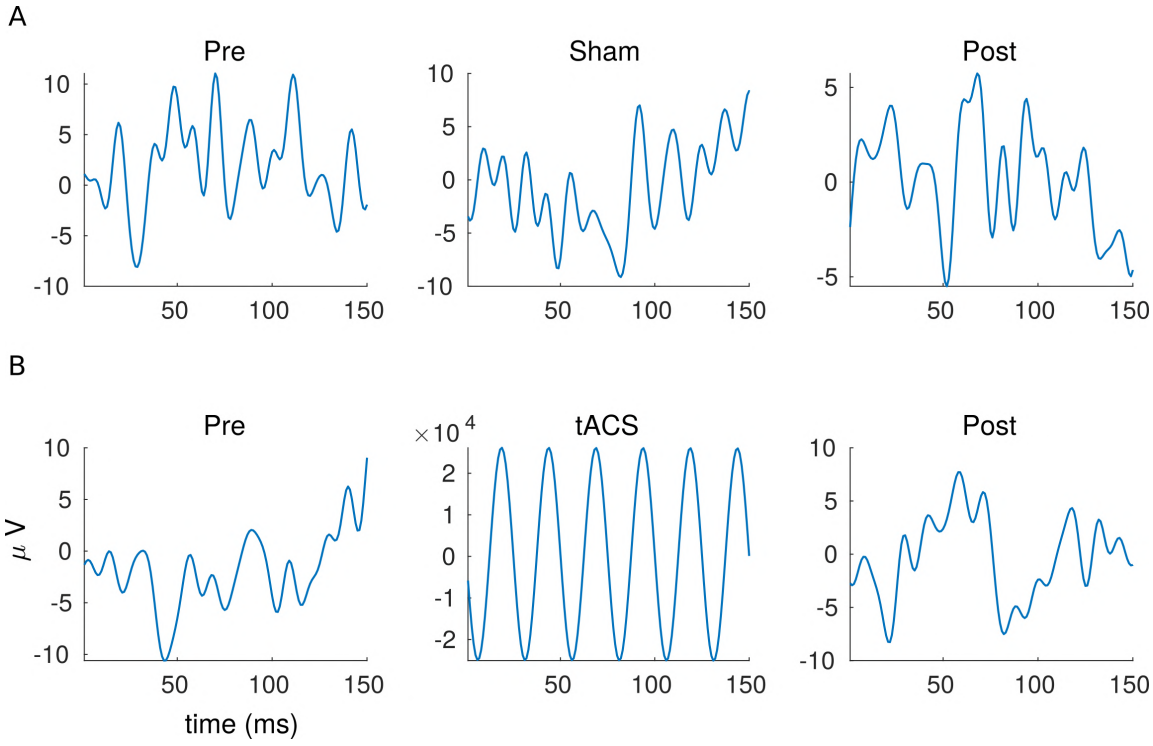

Figure 5.4: EEG voltage potential magnitude scale during A) Sham and B) tACS conditions. The figure highlight the presence of tACS induced massive sinusoidal artifact greater than ideal EEG sinal in several order of magnitude

Addressing these challenges proved complex. A conventional notch filter operating at the stimulation frequency could not effectively remove the artifact. The wide bandwidth of the notch filter inadvertently resulted in the removal of essential EEG information. The complexity of the artifact's waveform was evident, as illustrated in Figure 5.5. Moreover, the absolute amplitude of the artifacts across individual electrodes remained uncertain, with variations stemming from factors such as varying

electrode impedance due to factors like drying, blood circulation, and muscle movements [von Conta et al., 2022, Noury et al., 2016]. These impedance changes influence the stimulator's output voltage, altering the current delivered and thereby modulating the artifact. Furthermore, these non-linear artifacts exhibited non-stationary characteristics, further complicating their removal and analysis.

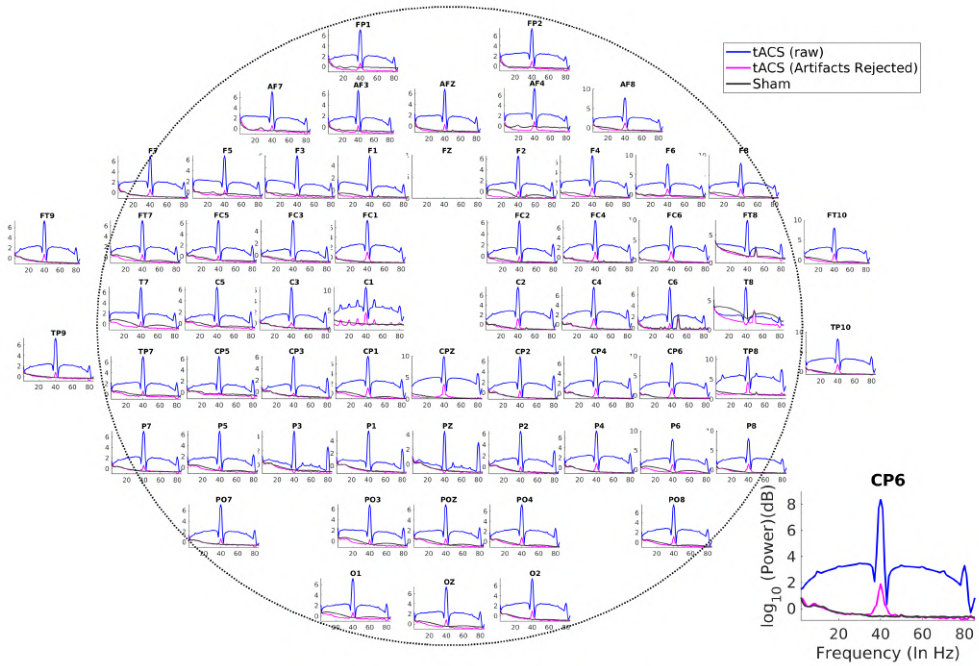

Figure 5.5: Power spectral density of each EEG channel during tACS (before artifact rejection) by blue line, Sham by black line and tACS condition after artifact rejection by SMA and PCA method represented by magenta line

5.5.1 Superposition of Moving Averages

We employed a method called the Superposition of Moving Averages (SMA), which draws inspiration from techniques often used in simultaneous EEG-fMRI studies [Kohli and Casson, 2015]. This concept is depicted in Figure 5.6. To elaborate, we initially divided the EEG time series (represented as X(i, t)) into distinct non-overlapping segments. The length of each segment was chosen to match the natural

cycle of the tACS stimulation frequency. Then, for each segment (y(i, n)), along with its neighboring segments (a total of M), we performed a central averaging process. This resulted in what we call a local artifact template (A(i, n)), which was specific to both the point in time window and the EEG channel. The artifact template derived through this process encapsulates the typical pattern of the tACS-induced artifact present in the EEG signal. Following this, we subtracted this artifact template from the original data (Figure 5.6). Once this subtraction was completed, we reconstructed the signal by reversing the segmentation process. This final result provided us with the core EEG data captured during the tACS stimulation period. An interesting aspect of this technique is its adaptability to different numbers of EEG channels. Since the artifact template is unique to each EEG channel, the SMA method can be applied effectively to EEG data collected using varying numbers of channels. By successfully eliminating artifacts while preserving channel-specific information, the SMA technique proved to be a valuable asset for analyzing tACS EEG data.

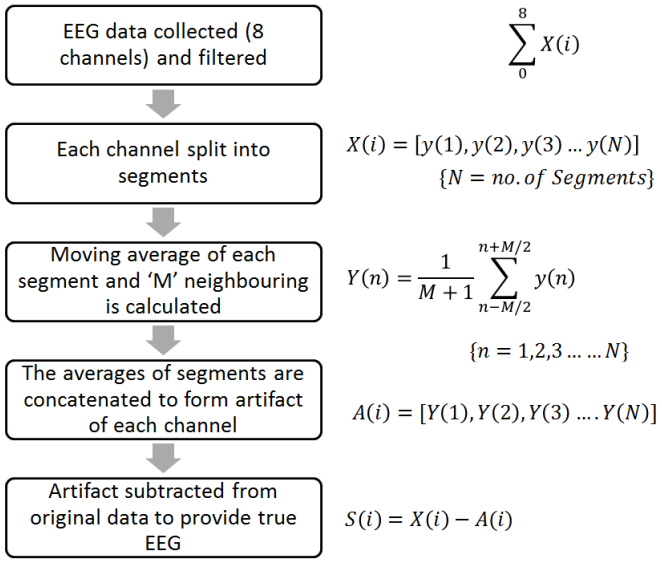

Figure 5.6: Pipeline of Superposition of Moving Averages (SMA) method for tACS-EEG artifact rejection. Each channel's data is segmented independently prior to the calculation of a moving average, which is then subtracted from the initial data recorded for that channel. Taken from [Kohli and Casson, 2015].

5.5.2 Principal Component Analysis

To mitigate the impact of residual artifacts on the EEG data, we employed Principal Component Analysis (PCA) as a corrective approach. PCA is a mathematical technique used for transforming data into a new coordinate system, enabling the identification of patterns in the data by capturing its main sources of variance. In our context, PCA was employed to separate the underlying neural signal from the noisy artifacts present due to the tACS stimulation. The procedure involved computing PCA on the EEG data, which effectively identified the linear combinations of EEG channels that explained the most variance in the data. By identifying and removing the principal components that corresponded to the tACS-induced artifacts, we were able to retain the components that represented the neural activity. This approach is particularly effective when artifacts and neural activity exhibit different spatial patterns and frequency characteristics. After removing the noisy components, the EEG data was reconstructed using the remaining principal components. Thereafter, the reconstructed EEG data was downsampled to a sampling rate of 250 Hz.

5.6 Results

As a result of applying SMA and PCA, we observed a significant reduction in the amplitude of voltage fluctuations caused by the tACS artifacts. Specifically, these two method not only removed the non-physiological 40 Hz frequency but also broad-band noise associated with it (see Figure 5.5) resulting the voltage fluctuations bounded within the range of plus-minus 30 microvolts (see Figure 5.7). This reduction in artifact amplitude allowed the neural signals to become more distinguishable, providing a clearer representation of the underlying EEG activity. The effectiveness of this artifact removal process is visually demonstrated in the figures 5.7 and 5.5, where the preserved fluctuations at other frequencies were retained while the tACS-

induced artifact was significantly reduced. In summary, the combination of SMA and PCA proved to be a powerful technique for effectively separating gross tACS-induced artifacts from the neural EEG signal.

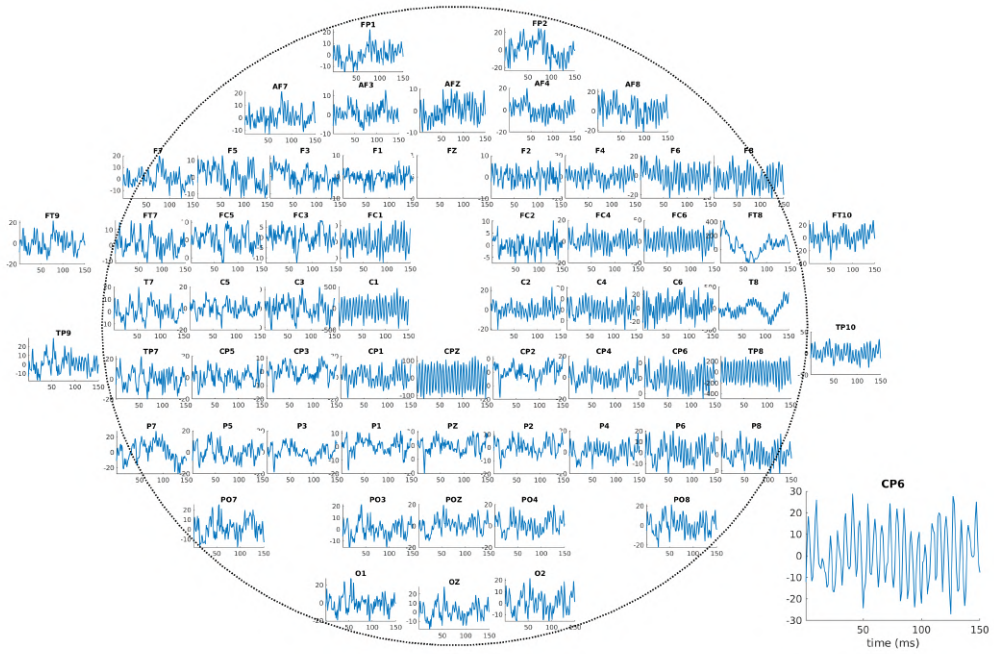

Figure 5.7: EEG voltage potential magnitude scale during tACS condition after artifact rejection.

5.6.1 Topography of tACS induced 40 Hz spectral power

The topographical plot of the 40 Hz power relative to the sham condition showed a distinct increase in the power of the 40 Hz frequency band over the right hemisphere (see Figure 5.8). The difference in global channel average of 40 Hz spectral power during tACS and sham condition was significantly high with $p_{val} < 0.01$ as assessed by random permutation testing (See 2.2.5 for more details). This observation indicates that the tACS stimulation at 40 Hz successfully influenced neural activity in the targeted areas. This result underscores the potential effectiveness of tACS in enhancing the spectral power of neural oscillations in a frequency-specific manner.

The distinct topographical distribution further highlights the spatial specificity of the tACS effect, reinforcing its capability to target particular brain regions.

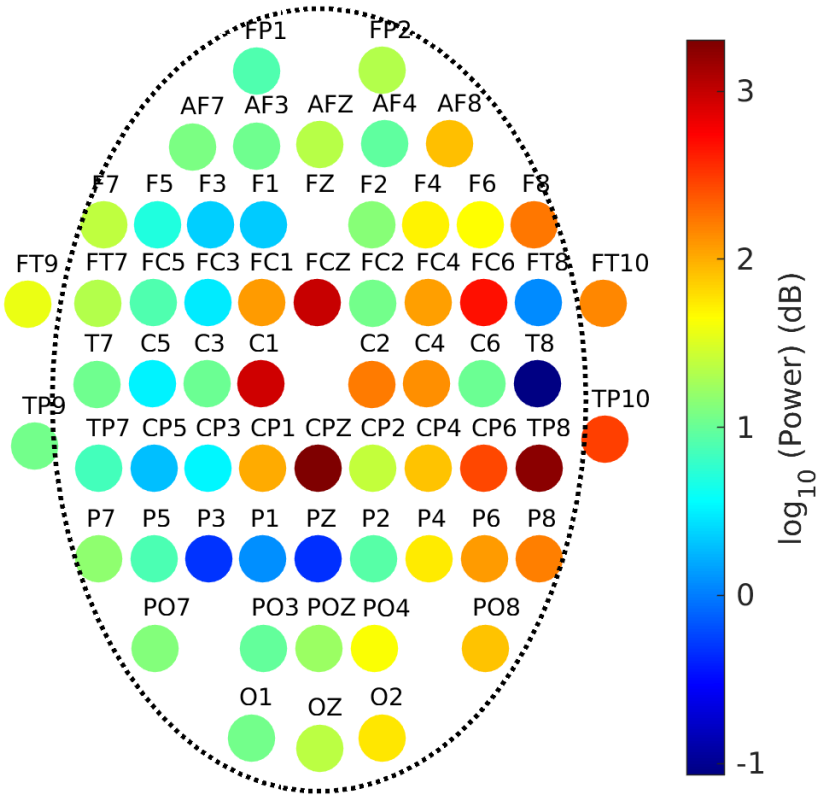

Figure 5.8: Topography of the 40 Hz power during tACS relative to the sham condition.

5.6.2 Presence of entrainment

The subsequent requirement is the assessment of the phase-locking of the 40 Hz steady-state response. This evaluation is essential as the observed increase in 40 Hz power could potentially arise from both phase-locked and non-phase-locked components. The degree of entrainment reflects the ability of tACS to synchronize with and entrain endogenous oscillations in the brain. To conduct this analysis, we epoched

the continuous EEG data into 1-second segments. This segmentation allowed us to estimate the degree of phase alignment through the measurement of the Inter-Trial Phase Coherence (ITPC). The analysis revealed that the ITPC was maximized precisely at the 40 Hz frequency, exhibiting a sharp and narrow peak (see Figure 5.9). This finding suggests a robust phase-locking of the neural oscillations to the 40 Hz tACS stimulation. The high ITPC value signifies that the neural activity during the tACS stimulation at 40 Hz is consistently aligned in phase across different trials. This phase-locking phenomenon implies synchronization between the external tACS input and the ongoing endogenous oscillations in the targeted brain region. The occurrence of this narrow and pronounced peak in the ITPC spectrum at 40 Hz provides compelling evidence for the successful entrainment of neural oscillations by the tACS stimulation. This synchronization underscores the capacity of tACS to modulate and influence neural activity in a frequency-specific manner.

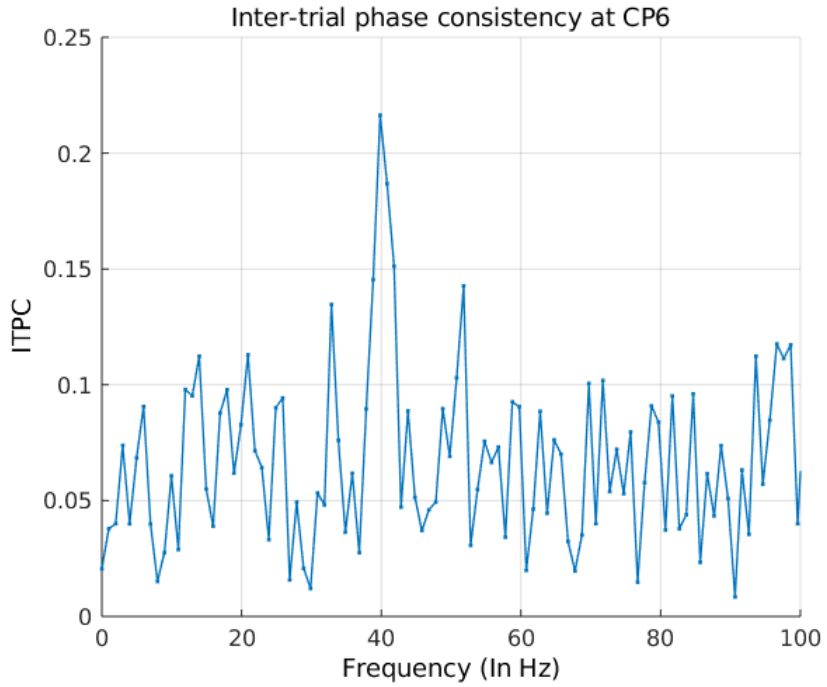

Figure 5.9: Phase-locking across frequency range during tACS stimulation for a arbitrary channel.

However, the ITPC value obtained during the empirical recording of Auditory Steady-State Responses (ASSR) using Amplitude Modulated (AM) stimuli was consistently around 0.5 (See Fig. 2.1) and ITPC value during the tACS stimulation measured at 0.21 (see Figure 5.9). The lower ITPC value at 40 Hz may potentially stem from various factors. One plausible explanation is the existence of distinct internal clocks between the tACS stimulator and the EEG recording system. This temporal misalignment could result in variations in the phase relationship between the tACS application and the EEG data recording, ultimately influencing the calculated ITPC value. Moreover, subtle alterations in electrode impedances over time might contribute to changes in the phase of tACS application across different segments of EEG data. Consequently, the entrained oscillation's phase, when divided into equally segmented data, could be different across trials due to varying tACS application phases at different time points. These inconsistencies in phase alignment across segments may be contributing to the lower ITPC value observed. To address these challenges and attain a more accurate measure of entrainment, it is imperative to explore a method that directly assesses the phase-locking between the administered tACS wave and the recorded EEG signal. This approach would offer a quantifiable metric to precisely evaluate the degree of entrainment. By establishing a direct phase comparison, the impact of potential temporal misalignments and electrode impedance fluctuations on the calculated ITPC value could be mitigated.

5.7 Discussion

The application of transcranial Alternating Current Stimulation (tACS) represents a promising non-invasive technique for modulating endogenous neural oscillations [Hanslmayr et al., 2019, Lakatos et al., 2019]. Sinusoidal currents employed by tACS have the potential to temporally align neural firing patterns and elicit entrainment of

oscillatory activity. Previous studies have demonstrated behavioral effects of tACS, yet the simultaneous investigation of neural activity through EEG poses challenges due to the presence of tACS-induced artifacts. Many studies have been confined to exploring EEG changes before and after stimulation due to the pervasive presence of stimulation artifacts in the EEG data. In this study, we have recorded EEG data during application of 40 Hz sinusoidal current over right auditory cortex. As a prequisite for our main experiment (see 5.1), we showcased how tACS-induced artifacts can be effectively addressed with appropriate methodologies. One key challenge is the tACS-EEG artifact, a quasi-sinusoidal signal with its primary harmonic matching the stimulation frequency and being several orders of magnitude greater than the signal of interest. While common mode rejection by the EEG amplifier can eliminate artifacts that are consistent across all channels (like line noise), our findings indicate the contrary. Furthermore, the existence of non-linear artifacts, which deviate from pure sinusoids [Kasten and Herrmann, 2019], further complicates the situation. Fluctuations in electrode impedance due to factors such as electrode drying, blood circulation, and muscle movements lead to changes in the stimulator's output, effectively modulating the artifact itself [Noury et al., 2016]. Additionally, non-stationary artifacts arising from respiration and heartbeats contribute to the complexity of artifact removal. Addressing these artifact challenges, we demonstrated that EEG signals during tACS can be successfully recovered, thereby eliminating large-scale stimulation artifacts. The utilization of methods like Superposition of Moving Averages (SMA) and Principal Component Analysis (PCA) has enabled the extraction of "clean" EEG data. The preliminary result from the preprocessed data showed tACS-induced spectral power and phase-locking specifically at 40 Hz. Furthermore, the topographical distribution of 40 Hz spectral power are distributed over right channels. In conclusion, our study demonstrates the viability of effectively mitigating tACS-induced artifacts, paving the way for to observe frequency-specific synchro-

nization of neural activity of the primary auditory cortex. This was a preliminary study as sanity check to further study the effect of frequency-specific stimulation of primary auditory cortices and its propagation dynamics in functional hemispheric specialization.

5.8 Future directions

To further refine the tACS paradigm, several requisites are worth noting. Firstly, addressing the variability in tACS phase could be achieved by measuring tACS current simultaneously via an *oscilloscope*. Recording the tACS-generated sine wave provides essential reference information, aiding in the quantification of phase entrainment (see section 5.6.2). Secondly, obtaining an MRI scan of participants could facilitate electrode placement based on a simulated current density distribution in a realistic finite-element head model, optimizing current flow targeting the primary auditory cortices. Thirdly, to enhance temporal alignment between EEG and tACS, multiple triggers in the EEG should be employed, rather than a singular one, maximizing temporal alighnement of tACS-generated sine wave and EEG epochs.

Chapter 6

Conclusion and Summary

At the heart of human perception lies the extraordinary ability to hear, a cornerstone of our sensory experience. Audition commences with the intricate mechanisms of the ear, where sound waves are transduced into neural impulses by the cochlea, an organ orchestrating the initial stages of auditory processing. The auditory pathway carries these impulses through successive processing centres reaching upto the cerebral cortex for specialized and higher-order processing [Hackett, 2011]. This hierarchy is critical for transforming auditory inputs into meaningful perceptions, involves distinct processing stages. At the brainstem, the ascending pathway crosses over, leading to contralateral dominance up to the primary auditory cortices (PAC). These cortices serves as the foundation of cortical processing being the first cortical structures to receive ascending auditory inputs. At the cortical level, there are substantial studies on the functional organisation of auditory processing. The auditory landscape, characterized by speech and music, represents the two most essential modes of auditory communication. One of the widely known attribute of speech and music is their dichotomy and manifestion of the hemispheric specialization. For instance, left hemisphere is known to process speech and language while right hemisphere is dominant during tonal, rhythm and music processing [Zatorre, 2022]. However, prior studies

utilizing neuroimaging techniques have often investigated lateralization in isolation, lacking a comprehensive contextual understanding within the broader hierarchical processing architecture. Particularly, the neural underpinnings and the mechanistic basis of these observed lateralization given the underlying structural pathways remain unanswered.

The study of neural oscillations serves as a crucial approach to understanding auditory processing, given the temporal nature of sound. Neural oscillations synchronize with the temporal patterns of auditory stimuli, forming the basis of auditory perception [Ding et al., 2015]. These oscillations encode various sound attributes, such as pitch, timbre, and rhythm, and their synchronization enables the brain to decode complex auditory information. Oscillations in distinct frequency band are organised at specific processing stages in the brain integrating motor, syntactic, working memory information, constructing a coherent representation of the auditory scene [Kösem and van Wassenhove, 2017b]. The coherence of these oscillations facilitates inter-regional communication emerging as a large-scale functional network [Fries, 2005]. These networks and their dynamics is known to be the fundamental of cognitive functions. Characterization of these functional networks would shed light on the neural underpinnings and mechanistic basis of functional organisation of auditory processing in addition to their asymmetry.

Importantly, the behaviour of these network is naturally contingent upon the underlying structural connectivity (SC), which provides the structural framework for the precise routing of oscillatory activity [Honey et al., 2007]. There has been substantial evidence on the role of SC in information transfer between brain regions [Honey et al., 2007], shaping network topology [Bullmore and Sporns, 2009], and mediating synchronization and coherence of neural activity [Stam et al., 2007]. The white matter strength, which represents the integrity and density of the fiber tracts connecting different brain regions, influences the efficiency and magnitude of in-

formation transfer. In addition, the fiber lengths determine the time constants of information propagation. However, how does a static network subserve the different functional requirements of strengths of coupling and temporal delays during speech and music ? The brain accomplishes this by precisely manipulating the timing and coordination of neural signals through two key factors: conduction velocities and a scaling factor applied to fiber thickness [Cabral et al., 2011]. Conduction velocities, which denote the speed at which neural impulses travel along nerve fibers, play a pivotal role in governing the temporal aspects of neural communication. Varied conduction velocities facilitate the emergence of distinct time delays, thereby shaping the arrival and integration of neural information across disparate regions. This temporal coding ensures the precise synchronization necessary for intricate processing tasks. Additionally, the brain utilizes the scaling factor applied to fiber thickness as a means of regulating synchronization strength. By modulating this factor, the brain can finely adjust the degree of coordination between neural signals. Despite the underlying static structural connectivity within the brain, modulation by conduction velocities and synchronization strength enables the generation of a diverse range of time delays and strengths of information propagation. This understanding enhances our comprehension of the brain's intricate adaptability for specific cognitive demands and environmental stimuli such as speech and music.

Our first study identifies 40 Hz auditory steady-state response (ASSRs) as robust marker to investigate directed networks of tonal processing. We record continuous EEG data from 20 human participants in addition to their individual T1 MRI. During the EEG sessions the participants were presented with 1000 Hz sinusoidal tone amplitude modulated at 40 Hz. There were three auditory conditions 1) Binaural, 2) Monaural left and 3) monaural right condition in addition to resting state EEG recording sessions. We first seek to establish contralateral dominance at the primary auditory cortex level followed by mechanism of well known right hemispheric dom-

inance of 40 Hz ASSRs. We employ power spectrum, source localization, network analysis with global coherence and Granger causality to study functional organization of the brain during processing of 40 Hz ASSRs. We observed stimuli-specific sharp enhancement in phase-locking and spectral power at 40 Hz. Laterality analysis confirms contralateral dominance at the primary-auditory cortex level during monaural conditions and overall right hemispheric dominance. The rise in the Global coherence confirms the presence of underlying large-scale functional network at 40 Hz. Further, the directionality analysis among relevant source regions shows presence of a hierarchical information flow. Particularly, During every stimulation condition, there were causal flows originating from both primary auditory cortices reaching to the right superior temporal gyrus (STG), consequently requiring condition-specific interhemispheric causal flow from the left PAC. Finally, we identify bidirectional communication between right STG and right Broca‘s areas as contributor of right-hemispheric dominance manifested as right hemispheric dominance during tonal processing.

In second study, we aimed to investigate to investigate the frequency-specific outflow from the PAC during speech, melody and ASSR conditions. We employed electroencephalography (EEG) to record neural activity while 30 participants selectively attended to either the speech or melodic content of ecologically valid *a cappella* songs. We reconstruct source activity utilizing subject-specific anatomy of brain and investigate the laterality in the causal outflow from PAC. The findings reveal a common frequency-specific outflow from PAC in both speech and melody conditions, reaching to distinct regions reflecting domain-specific organization of the auditory system. Furthermore, the laterality analysis of causal outflow complies with well-established hemispheric dominance of left hemisphere for speech, right hemisphere for melody, and right hemisphere for ASSR, suggesting role of PAC in hemispheric specializations. This suggests that the observed oscillatory patterns do not encode generic processing of acoustic signal dynamics but instead capture specific linguistic

or musical features. The involvement of distinct regions in processing these acoustic environments indicates specialized and domain-specific organization within the auditory system (Peretz et al., 2015).

In the chapter 4, we explore the mechanistic basis of the hemispheric specialization observed in the chapter 2 and 3. We compute theoretical lateralization indices by integrating diffusion magnetic resonance imaging (dMRI) data from the same participants recorded in chapter 3, to constrain the outflow from the PAC in a neurodynamic whole-brain connectome model. We performed the subject-specific comparative analysis between empirical and theoretical lateralization indices, paving the way for individualized predictions required to establish the robustness of the analysis. Here, we hypothesized that hemispheric lateralization of speech and melody emerge as spatial modes of a collective behaviour exhibited by a large-scale auditory network. Firstly, we validate the frequency-specificity of the neural dynamic model in the comparative analysis with a highly frequency-specific response i.e., ASSR. Our findings revealed that the observed frequency-specific outflow in the brain can be conceptualized as time-delayed phase interactions occurring within the structural connectome. We demonstrate that parametric modulation of conduction speeds that effectively control the transmission delays - a key metric for understanding information processing and control of any biological network, acts as the switch for selection of the spatial mode indexing lateralization of speech and melody. These results provide novel insights into the intricate dynamics of auditory processing and underscore the significant role of structural connectivity in shaping frequency-specific neural responses.

Building upon the findings of our previous studies and to disambiguate between thalamo-cortical and cortico-cortical auditory inputs on corresponding network we undertook a Transcranial Alternating Current Stimulation (tACS) study. By stimulating PAC by tACS we aim to causally modulate large-scale network and exam-

ine how these propagation leads to hemispheric lateralization. In a pilot study, we record EEG while 40 Hz sinusoidal alternating current is applied to a participant's right PAC. The utilization of methods like Superposition of Moving Averages (SMA) and Principal Component Analysis (PCA) has enabled the extraction of "clean" EEG data. The preliminary result from the preprocessed data showed tACS-induced spectral power and phase - locking specifically at 40 Hz. Furthermore, the topographical distribution of 40 Hz spectral power are distributed over right channels. This was a preliminary study as sanity check to further study the effect of frequency-specific stimulation of primary auditory cortices and its propagation dynamics in functional hemispheric specialization. The aim of this pilot to standardise recording and analysis pipeline to remove tACS induced massive artifacts in EEG.

Bibliography

[Abeysuriya et al., 2018] Abeysuriya, R. G., Hadida, J., Sotiropoulos, S. N., Jbabdi, S., Becker, R., Hunt, B. A., Brookes, M. J., and Woolrich, M. W. (2018). A biophysical model of dynamic balancing of excitation and inhibition in fast oscillatory large-scale networks. *PLoS Computational Biology*, 14(2).

[Aboitiz et al., 1992] Aboitiz, F., Scheibel, A. B., Fisher, R. S., and Zaidel, E. (1992). Fiber composition of the human corpus callosum. *Brain Research*, 598(1-2):143–153.

[Agcaoglu et al., 2018] Agcaoglu, O., Miller, R., Damaraju, E., Rashid, B., Bustillo, J., Cetin, M. S., Van Erp, T. G., McEwen, S., Preda, A., Ford, J. M., Lim, K. O., Manoach, D. S., Mathalon, D. H., Potkin, S. G., and Calhoun, V. D. (2018). Decreased hemispheric connectivity and decreased intra- and inter- hemisphere asymmetry of resting state functional network connectivity in schizophrenia. *Brain Imaging and Behavior*, 12(3):615–630.

[Aitkin et al., 1981] Aitkin, L. M., Kenyon, C. E., and Philpott, P. (1981). The representation of the auditory and somatosensory systems in the external nucleus of the cat inferior colliculus. *Journal of Comparative Neurology*, 196(1):25–40.

[Albouy et al., 2020] Albouy, P., Benjamin1, L., Morillon, B., and Zatorre, R. J. (2020). Distinct sensitivity to spectrotemporal modulation supports brain asymmetry for speech and melody. *Science*, 367(6481):1043–1047.

[Andoh et al., 2015] Andoh, J., Matsushita, R., and Zatorre, R. J. (2015). Asymmetric Interhemispheric Transfer in the Auditory Network: Evidence from TMS, Resting-State fMRI, and Diffusion Imaging. *Journal of Neuroscience*, 35(43):14602–14611.

[Angulo-Perkins and Concha, 2019] Angulo-Perkins, A. and Concha, L. (2019). Discerning the functional networks behind processing of music and speech through human vocalizations. *PLoS ONE*, 14(10).

[Attal et al., 2007] Attal, Y., Bhattacharjee, M., Yelnik, J., Cottereau, B., Lefèvre, J., Okada, Y., Bardinet, E., Chupin, M., and Baillet, S. (2007). Modeling and detecting deep brain activity with MEG and EEG. *Annual International Conference of the IEEE Engineering in Medicine and Biology - Proceedings*, pages 4937–4940.

[Avena-Koenigsberger et al., 2017] Avena-Koenigsberger, A., Misic, B., and Sporns, O. (2017). Communication dynamics in complex brain networks. *Nature Reviews Neuroscience*, 19(1):17–33.

[Bauer et al., 2020] Bauer, A. K. R., Debener, S., and Nobre, A. C. (2020). Synchronisation of Neural Oscillations and Cross-modal Influences.

[Baar et al., 2000] Baar, E., Baar-Eroglu, C., Karaka, S., and Schürmann, M. (2000). Gamma, alpha, delta, and theta oscillations govern cognitive processes. *International Journal of Psychophysiology*, 39(2-3):241–248.

[Berger et al., 2019] Berger, B., Griesmayr, B., Minarik, T., Biel, A. L., Pinal, D., Sterr, A., and Sauseng, P. (2019). Dynamic regulation of interregional cortical communication by slow brain oscillations during working memory. *Nature Communications*, 10(1):1–11.

[Bhushan et al., 2012] Bhushan, C., Haldar, J. P., Joshi, A. A., and Leahy, R. M. (2012). Correcting susceptibility-induced distortion in diffusion-weighted MRI using constrained nonrigid registration. In *2012 Conference Handbook - Asia-Pacific Signal and Information Processing Association Annual Summit and Conference, APSIPA ASC 2012*.

[Bohórquez and Özdamar, 2008] Bohórquez, J. and Özdamar, Ö. (2008). Generation of the 40-Hz auditory steady-state response (ASSR) explained using convolution. *Clinical Neurophysiology*, 119(11):2598–2607.

[Brederoo et al., 2020] Brederoo, S. G., Van der Haegen, L., Brysbaert, M., Nieuwenstein, M. R., Cornelissen, F. W., and Lorist, M. M. (2020). Towards a unified understanding of lateralized vision: A large-scale study investigating principles governing patterns of lateralization using a heterogeneous sample. *Cortex*, 133:201–214.

[Bressler and Menon, 2010a] Bressler, S. L. and Menon, V. (2010a). Large-scale brain networks in cognition: emerging methods and principles.

[Bressler and Menon, 2010b] Bressler, S. L. and Menon, V. (2010b). Large-scale brain networks in cognition: emerging methods and principles. *Trends in Cognitive Sciences*, 14(6):277–290.

[Bressler, Steven L and Nakamura, 1993] Bressler, Steven L, C. R. and Nakamura, R. (1993). Episodic multiregional cortical coherence at multiple frequencies during visual task performance. *Nature publishing group*, 366:3.

[Brovelli et al., 2004] Brovelli, A., Ding, M., Ledberg, A., Chen, Y., Nakamura, R., and Bressler, S. L. (2004). Beta oscillations in a large-scale sensorimotor cortical network: Directional influences revealed by Granger causality. *Proceedings of the National Academy of Sciences*, 101(26):9849–9854.

[Bullmore and Sporns, 2009] Bullmore, E. and Sporns, O. (2009). Complex brain networks: Graph theoretical analysis of structural and functional systems. *Nature Reviews Neuroscience*, 10(3):186–198.

[Buzsáki and Chrobak, 1995] Buzsáki, G. and Chrobak, J. J. (1995). Temporal structure in spatially organized neuronal ensembles: a role for interneuronal networks. *Current opinion in neurobiology*, 5(4):504–10.

[Buzsáki and Draguhn, 2004] Buzsáki, G. and Draguhn, A. (2004). Neuronal oscillations in cortical networks. *Science*, 304(5679):1926–1929.

[Buzsáki and Wang, 2012] Buzsáki, G. and Wang, X.-J. (2012). Mechanisms of Gamma Oscillations. *Annual Review of Neuroscience*, 35(1):203–225.

[Buzski, 2006] Buzski, G. (2006). *Rhythms of the brain p220-230*. Oxford university press.

[Cabral et al., 2011] Cabral, J., Hugues, E., Sporns, O., and Deco, G. (2011). Role of local network oscillations in resting-state functional connectivity. *NeuroImage*, 57(1):130–139.

[Cammoun et al., 2015] Cammoun, L., Thiran, J. P., Griffa, A., Meuli, R., Hagmann, P., and Clarke, S. (2015). Intrahemispheric cortico-cortical connections of the human auditory cortex. *Brain Structure and Function*, 220(6):3537–3553.

[Cariani and Baker, 2022] Cariani, P. and Baker, J. M. (2022). Time Is of the Essence: Neural Codes, Synchronies, Oscillations, Architectures. *Frontiers in Computational Neuroscience*, 16:898829.

[Chang et al., 2018] Chang, A., Bosnyak, D. J., and Trainor, L. J. (2018). Beta oscillatory power modulation reflects the predictability of pitch change. *Cortex*, 106:248–260.

[Cimenser et al., 2011] Cimenser, A., Purdon, P. L., Pierce, E. T., Walsh, J. L., Salazar-Gomez, A. F., Harrell, P. G., Tavares-Stoeckel, C., Habeeb, K., and Brown, E. N. (2011). Tracking brain states under general anesthesia by using global coherence analysis. *Proceedings of the National Academy of Sciences*, 108(21):8832–8837.

[Coffey et al., 2016] Coffey, E. B., Herholz, S. C., Chepesiuk, A. M., Baillet, S., and Zatorre, R. J. (2016). Cortical contributions to the auditory frequency-following response revealed by MEG. *Nature Communications*, 7.

[Cohen, 2019] Cohen, M. X. (2019). *Analyzing Neural Time Series Data*. The MIT Press.

[Das et al., 2021] Das, M., Singh, V., Uddin, L. Q., Banerjee, A., and Roy, D. (2021). Reconfiguration of Directed Functional Connectivity among Neurocognitive Networks with Aging: Considering the Role of Thalamo-Cortical Interactions. *Cerebral Cortex*, 31(4):1970–1986.

[Delorme and Makeig, 2004] Delorme, A. and Makeig, S. (2004). EEGLAB: An open source toolbox for analysis of single-trial EEG dynamics including independent component analysis. *Journal of Neuroscience Methods*, 134(1):9–21.

[Desikan et al., 2006] Desikan, R. S., Ségonne, F., Fischl, B., Quinn, B. T., Dickerson, B. C., Blacker, D., Buckner, R. L., Dale, A. M., Maguire, R. P., Hyman, B. T., Albert, M. S., and Killiany, R. J. (2006). An automated labeling system for subdividing the human cerebral cortex on MRI scans into gyral based regions of interest. *NeuroImage*, 31(3):968–80.

[Dhamala et al., 2008] Dhamala, M., Rangarajan, G., and Ding, M. (2008). Analyzing information flow in brain networks with nonparametric Granger causality. *NeuroImage*, 41(2):354–362.

[Dhollander and Connelly, 2016] Dhollander, T. and Connelly, A. (2016). Generating a T1-like contrast using 3-tissue constrained spherical deconvolution results from single-shell (or multi-shell) diffusion MR data. *In: ISMRM Workshop on Breaking the Barriers of Diffusion MRI*, (September):6.

[Di and Biswal, 2019] Di, X. and Biswal, B. B. (2019). Toward Task Connectomics: Examining Whole-Brain Task Modulated Connectivity in Different Task Domains. *Cerebral Cortex*, 29(4):1572–1583.

[Ding et al., 2006a] Ding, M., Chen, Y., and Bressler, S. L. (2006a). 17 Granger Causality: Basic Theory and Application to Neuroscience. *Handbook of Time Series Analysis: Recent Theoretical Developments and Applications*, pages 380–437.

[Ding et al., 2006b] Ding, M., Chen, Y., and Bressler, S. L. (2006b). Granger Causality: Basic Theory and Application to Neuroscience. *Handbook of Time Series Analysis: Recent Theoretical Developments and Applications*, (February):437–460.

[Ding et al., 2015] Ding, N., Melloni, L., Zhang, H., Tian, X., and Poeppel, D. (2015). Cortical tracking of hierarchical linguistic structures in connected speech. *Nature Neuroscience*, 19(1):158–164.

[Ding et al., 2017] Ding, N., Patel, A. D., Chen, L., Butler, H., Luo, C., and Poeppel, D. (2017). Temporal modulations in speech and music.

[Ding et al., 2021] Ding, Y., Zhang, Y., Zhou, W., Ling, Z., Huang, J., Hong, B., and Wang, X. (2021). Neural correlates of music listening and recall in the human brain. *Journal of Neuroscience*, 39(41):8112–8123.

[Fahimi Hnazaee et al., 2020] Fahimi Hnazaee, M., Wittevrongel, B., Khachatryan, E., Libert, A., Carrette, E., Dauwe, I., Meurs, A., Boon, P., Van Roost, D.,

and Van Hulle, M. M. (2020). Localization of deep brain activity with scalp and subdural EEG. *NeuroImage*, 223.

[Farahani et al., 2020] Farahani, E. D., Wouters, J., and van Wieringen, A. (2020). Neural Generators Underlying Temporal Envelope Processing Show Altered Responses and Hemispheric Asymmetry Across Age. *Frontiers in Aging Neuroscience*, 12:431.

[Farahani et al., 2021] Farahani, E. D., Wouters, J., and van Wieringen, A. (2021). Brain mapping of auditory steady-state responses: A broad view of cortical and subcortical sources. *Human Brain Mapping*, 42(3):780–796.

[Feng et al., 2021] Feng, C., Zhu, Z., Cui, Z., Ushakov, V., Dreher, J. C., Luo, W., Gu, R., Wu, X., and Krueger, F. (2021). Prediction of trust propensity from intrinsic brain morphology and functional connectome. *Human Brain Mapping*, 42(1):175–191.

[Filatova et al., 2018] Filatova, O. G., Yang, Y., Dewald, J. P., Tian, R., Maceira-Elvira, P., Takeda, Y., Kwakkel, G., Yamashita, O., and van der Helm, F. C. (2018). Dynamic Information Flow Based on EEG and Diffusion MRI in Stroke: A Proof-of-Principle Study. *Frontiers in Neural Circuits*, 12:397486.

[Finger et al., 2016] Finger, H., Bönstrup, M., Cheng, B., Messé, A., Hilgetag, C., Thomalla, G., Gerloff, C., and König, P. (2016). Modeling of Large-Scale Functional Brain Networks Based on Structural Connectivity from DTI: Comparison with EEG Derived Phase Coupling Networks and Evaluation of Alternative Methods along the Modeling Path. *PLoS Computational Biology*, 12(8):e1005025.

[Fonseca et al., 2015] Fonseca, L. C., Tedrus, G. M. a. S., Rezende, A. L. R. a., and Giordano, H. F. (2015). Coherence of brain electrical activity: a quality of life indicator in Alzheimer's disease? *Arquivos de neuro-psiquiatria*, 73(5):396–401.

[Fries, 2005] Fries, P. (2005). A mechanism for cognitive dynamics: Neuronal communication through neuronal coherence. *Trends in Cognitive Sciences*, 9(10):474–480.

[Friston, 2011] Friston, K. J. (2011). Functional and Effective Connectivity: A Review. *Brain Connectivity*, 1(1):13–36.

[Fuchs et al., 2001] Fuchs, M., Wagner, M., and Kastner, J. (2001). Boundary element method volume conductor models for EEG source reconstruction. *Clinical Neurophysiology*, 112(8):1400–1407.

[Fujioka et al., 2015] Fujioka, T., Ross, B., and Trainor, L. J. (2015). Beta-band oscillations represent auditory beat and its metrical hierarchy in perception and imagery. *Journal of Neuroscience*, 35(45):15187–15198.

[Galambos et al., 1981] Galambos, R., Makeig, S., and Talmachoff, P. (1981). A 40-Hz auditory potential recorded from the human scalp. *Proceedings of the National Academy of Sciences of the United States of America*, 78(4):2643–2647.

[Geweke, 1982] Geweke, J. (1982). Measurement of linear dependence and feedback between multiple time series. *Journal of the American Statistical Association*, 77(378):304–313.

[Ghosh et al., 2008] Ghosh, A., Rho, Y., McIntosh, A. R., Kötter, R., and Jirsa, V. K. (2008). Noise during Rest Enables the Exploration of the Brain's Dynamic Repertoire. *PLoS Computational Biology*, 4(10):e1000196.

[Giraud and Poeppel, 2012] Giraud, A. L. and Poeppel, D. (2012). Cortical oscillations and speech processing: Emerging computational principles and operations.

[Gnanateja et al., 2022] Gnanateja, G. N., Devaraju, D. S., Heyne, M., Quique, Y. M., Sitek, K. R., Tardif, M. C., Tessmer, R., and Dial, H. R. (2022). On the Role of Neural Oscillations Across Timescales in Speech and Music Processing.

[Gotts et al., 2013] Gotts, S. J., Jo, H. J., Wallace, G. L., Saad, Z. S., Cox, R. W., and Martin, A. (2013). Two distinct forms of functional lateralization in the human brain. *Proceedings of the National Academy of Sciences of the United States of America*, 110(36):E3435–E3444.

[Gourévitch et al., 2020] Gourévitch, B., Martin, C., Postal, O., and Eggermont, J. J. (2020). Oscillations in the auditory system and their possible role.

[Gramfort et al., 2010] Gramfort, A., Papadopoulo, T., Olivi, E., and Clerc, M. (2010). OpenMEEG: Opensource software for quasistatic bioelectromagnetics. *BioMedical Engineering Online*, 9(1):1–20.

[Granger, 1969] Granger, C. W. J. (1969). Investigating Causal Relations by Econometric Models and Cross-spectral Methods. *Econometrica*, 37(3):424.

[Griffiths et al., 2000] Griffiths, T. D., Penhune, V., Peretz, I., Dean, J. L., Patterson, R. D., and Green, G. G. (2000). Frontal processing and auditory perception. *NeuroReport*, 11(5):919–922.

[Güntürkün et al., 2020] Güntürkün, O., Ströckens, F., and Ocklenburg, S. (2020). Brain lateralization: A comparative perspective. *Physiological Reviews*, 100(3):1019–1063.

[Hackett, 2011] Hackett, T. A. (2011). Information flow in the auditory cortical network. *Hearing Research*, 271(1-2):133–146.

[Hackett, 2015] Hackett, T. A. (2015). Anatomic organization of the auditory cortex. In *Handbook of Clinical Neurology*, volume 129, pages 27–53. Elsevier B.V.

[Haghighi et al., 2018] Haghighi, S. J., Komeili, M., Hatzinakos, D., and Beheiry, H. E. (2018). 40-Hz ASSR for Measuring Depth of Anaesthesia during Induction Phase. *IEEE Journal of Biomedical and Health Informatics*, 22(6):1871–1882.

[Haldar and Leahy, 2013] Haldar, J. P. and Leahy, R. M. (2013). Linear transforms for Fourier data on the sphere: Application to high angular resolution diffusion MRI of the brain. *NeuroImage*, 71:233–247.

[Halder et al., 2019] Halder, T., Talwar, S., Jaiswal, A. K., and Banerjee, A. (2019). Quantitative evaluation in estimating sources underlying brain oscillations using current source density methods and beamformer approaches. *eNeuro*, 6(4).

[Hanslmayr et al., 2019] Hanslmayr, S., Axmacher, N., and Inman, C. S. (2019). Modulating Human Memory via Entrainment of Brain Oscillations.

[Hari et al., 1989] Hari, R., Hämäläinen, M. S., and Joutsiniemi, S. L. (1989). Neuromagnetic steady-state responses to auditory stimuli. *J Acoust Soc Am*, 86(3):1033–1039.

[Helfrich et al., 2014] Helfrich, R. F., Schneider, T. R., Rach, S., Trautmann-Lengsfeld, S. A., Engel, A. K., and Herrmann, C. S. (2014). Entrainment of Brain Oscillations by Transcranial Alternating Current Stimulation. *Current Biology*, 24(3):333–339.

[Herdman et al., 2002] Herdman, A., Lins, O., Van Roon, P., Stapells, D. R., Scherg, M., and Picton, T. W. (2002). Intracerebral sources of human auditory steady-state responses. *Brain Topography*, 15(69-86).

[Hickok and Poeppel, 2007] Hickok, G. and Poeppel, D. (2007). The cortical organization of speech processing.

[Honey et al., 2007] Honey, C. J., Kötter, R., Breakspear, M., and Sporns, O. (2007). Network structure of cerebral cortex shapes functional connectivity on multiple time scales. *Proceedings of the National Academy of Sciences of the United States of America*, 104(24):10240–10245.

[Hutcheon and Yarom, 2000] Hutcheon, B. and Yarom, Y. (2000). Resonance, oscillation and the intrinsic frequency preferences of neurons.

[Ibrahim et al., 2021] Ibrahim, M. M., Kamran, M. A., Mannan, M. M. N., Jung, I. H., and Kim, S. (2021). Lag synchronization of coupled time-delayed FitzHugh-Nagumo neural networks via feedback control. *Scientific Reports*, 11(1):1–15.

[Jasmin et al., 2019] Jasmin, K., Lima, C. F., and Scott, S. K. (2019). Understanding rostralcaudal auditory cortex contributions to auditory perception.

[Jayakody et al., 2018] Jayakody, D. M., Friedland, P. L., Martins, R. N., and Sohrabi, H. R. (2018). Impact of aging on the auditory system and related cognitive functions: A narrative review.

[Joon Kim et al., 2007] Joon Kim, Y., Grabowecky, M., Paller, K. A., Muthu, K., and Suzuki, S. (2007). Attention induces synchronization-based response gain in steady-state visual evoked potentials. *Nature Neuroscience*, 10(1):117–125.

[Kaas and Hackett, 2000a] Kaas, J. H. and Hackett, T. A. (2000a). Subdivisions of auditory cortex and processing streams in primates.

[Kaas and Hackett, 2000b] Kaas, J. H. and Hackett, T. A. (2000b). Subdivisions of auditory cortex and processing streams in primates. *Proceedings of the National Academy of Sciences*, 97(22):11793–11799.

[Kaas et al., 1999] Kaas, J. H., Hackett, T. A., and Tramo, M. J. (1999). Auditory processing in primate cerebral cortex.

[Kandel and Schwartz, 2014] Kandel, E. R. and Schwartz, J. H. (2014). *Principles of Neural Science*. Mc Graw Hill, fifth edition.

[Karolis et al., 2019] Karolis, V. R., Corbetta, M., and Thiebaut de Schotten, M. (2019). The architecture of functional lateralisation and its relationship to callosal connectivity in the human brain. *Nature Communications*, 10(1):1–9.

[Kasten and Herrmann, 2019] Kasten, F. H. and Herrmann, C. S. (2019). Recovering Brain Dynamics During Concurrent tACS-M/EEG: An Overview of Analysis Approaches and Their Methodological and Interpretational Pitfalls. *Brain Topography*, 32(6):1013–1019.

[Kazanina and Tavano, 2023] Kazanina, N. and Tavano, A. (2023). What neural oscillations can and cannot do for syntactic structure building. *Nature Reviews Neuroscience*, 24(2):113–128.

[Kellner et al., 2016] Kellner, E., Dhital, B., Kiselev, V. G., and Reisert, M. (2016). Gibbs-ringing artifact removal based on local subvoxel-shifts. *Magnetic Resonance in Medicine*, 76(5):1574–1581.

[Kim et al., 2019] Kim, S., Jang, S. K., Kim, D. W., Shim, M., Kim, Y. W., Im, C. H., and Lee, S. H. (2019). Cortical volume and 40-Hz auditory-steady-state responses in patients with schizophrenia and healthy controls. *NeuroImage: Clinical*, 22:101732.

[Klimesch, 2012] Klimesch, W. (2012). Alpha-band oscillations, attention, and controlled access to stored information.

[Koelsch, 2011] Koelsch, S. (2011). Toward a neural basis of music perception - a review and updated model.

[Kohli and Casson, 2015] Kohli, S. and Casson, A. J. (2015). Removal of Transcranial a.c. Current Stimulation artifact from simultaneous EEG recordings by superposition of moving averages. In *Proceedings of the Annual International Conference of the IEEE Engineering in Medicine and Biology Society, EMBS*, volume 2015-Novem, pages 3436–3439. Institute of Electrical and Electronics Engineers Inc.

[Kösem and van Wassenhove, 2017a] Kösem, A. and van Wassenhove, V. (2017a). Distinct contributions of low- and high-frequency neural oscillations to speech comprehension. *Language, Cognition and Neuroscience*, 32(5):536–544.

[Kösem and van Wassenhove, 2017b] Kösem, A. and van Wassenhove, V. (2017b). Distinct contributions of low- and high-frequency neural oscillations to speech comprehension. *Language, Cognition and Neuroscience*, 32(5):536–544.

[Kösem and van Wassenhove, 2017c] Kösem, A. and van Wassenhove, V. (2017c). Distinct contributions of low- and high-frequency neural oscillations to speech comprehension. *Language, Cognition and Neuroscience*, 32(5):536–544.

[Kumar et al., 2016] Kumar, G. V., Halder, T., Jaiswal, A. K., Mukherjee, A., Roy, D., and Banerjee, A. (2016). Large scale functional brain networks underlying temporal integration of audio-visual speech perception: An eeg study. *Frontiers in Psychology*, 7(OCT):1558.

[Kumar et al., 2023] Kumar, N., Jaiswal, A., Roy, D., and Banerjee, A. (2023). Effective networks mediate right hemispheric dominance of human 40 Hz auditory steady-state response. *Neuropsychologia*, 184:108559.

[Kuramoto, 1984] Kuramoto, Y. (1984). *Chemical Oscillations, Waves, and Turbulence*, volume 19 of *Springer Series in Synergetics*. Springer Berlin Heidelberg, Berlin, Heidelberg.

[Lakatos et al., 2019] Lakatos, P., Gross, J., and Thut, G. (2019). A New Unifying Account of the Roles of Neuronal Entrainment. *Current Biology*, 29(18):R890–R905.

[Langers et al., 2005] Langers, D. R., Van Dijk, P., and Backes, W. H. (2005). Lateralization, connectivity and plasticity in the human central auditory system. *NeuroImage*, 28(2):490–499.

[Lee, 2013] Lee, C. C. (2013). Thalamic and cortical pathways supporting auditory processing. *Brain and Language*, 126(1):22–28.

[Lithari et al., 2016] Lithari, C., Sánchez-Garciá, C., Ruhnau, P., and Weisz, N. (2016). Large-scale network-level processes during entrainment. *Brain Research*, 1635:143–152.

[Luo et al., 2006] Luo, H., Wang, Y., Poeppel, D., and Simon, J. Z. (2006). Concurrent Encoding of Frequency and Amplitude Modulation in Human Auditory Cortex: MEG Evidence. *Journal of Neurophysiology*, 96(5):2712–2723.

[Mäkelä and Hari, 1987] Mäkelä, J. P. and Hari, R. (1987). Evidence for cortical origin of the 40-Hz auditory evoked response in man. *Electroencephalography and Clinical Neurophysiology*, 66:539–546.

[Malekmohammadi et al., 2023] Malekmohammadi, A., Ehrlich, S. K., and Cheng, G. (2023). Modulation of theta and gamma oscillations during familiarization with previously unknown music. *Brain Research*, 1800:148198.

[Maris and Oostenveld, 2007] Maris, E. and Oostenveld, R. (2007). Nonparametric statistical testing of EEG- and MEG-data. *Journal of Neuroscience Methods*, 164(1):177–190.

[Maris et al., 2007] Maris, E., Schoffelen, J. M., and Fries, P. (2007). Nonparametric statistical testing of coherence differences. *Journal of Neuroscience Methods*, 163(1):161–175.

[McFadden et al., 2014] McFadden, K. L., Steinmetz, S. E., Carroll, A. M., Simon, S. T., Wallace, A., and Rojas, D. C. (2014). Test-Retest Reliability of the 40 Hz EEG Auditory Steady-State Response. *PLOS ONE*, 9(1):e85748.

[Melynyte et al., 2017] Melynyte, S., Pipinis, E., Genyte, V., Voicikas, A., Rihs, T., and Griskova-Bulanova, I. (2017). 40 Hz Auditory Steady-State Response: The Impact of Handedness and Gender. *Brain Topography*, 31(3):419–429.

[Mišić et al., 2018] Mišić, B., Betzel, R. F., Griffa, A., Reus, M. A. D., He, Y., Zuo, X.-n., Heuvel, M. P. V. D., Hagmann, P., Sporns, O., and Zatorre, R. J. (2018). Network-based asymmetry of the human auditory system. *Cerebral Cortex*, (May):1–14.

[Mišić et al., 2015] Mišić, B., Betzel, R. F., Nematzadeh, A., Goñi, J., Griffa, A., Hagmann, P., Flammini, A., Ahn, Y. Y., and Sporns, O. (2015). Cooperative and Competitive Spreading Dynamics on the Human Connectome. *Neuron*, 86(6):1518–1529.

[Morillon et al., 2010a] Morillon, B., Lehongre, K., Frackowiak, R. S., Ducorps, A., Kleinschmidt, A., Poeppel, D., and Giraud, A. L. (2010a). Neurophysiological origin of human brain asymmetry for speech and language. *Proceedings of the National Academy of Sciences of the United States of America*, 107(43):18688–18693.

[Morillon et al., 2010b] Morillon, B., Lehongre, K., Frackowiak, R. S., Ducorps, A., Kleinschmidt, A., Poeppel, D., and Giraud, A. L. (2010b). Neurophysiological

origin of human brain asymmetry for speech and language. *Proceedings of the National Academy of Sciences of the United States of America*, 107(43):18688–18693.

[Niepel et al., 2020] Niepel, D., Krishna, B., Siegel, E. R., Draganova, R., Preissl, H., Govindan, R. B., and Eswaran, H. (2020). A pilot study: Auditory steady-state responses (ASSR) can be measured in human fetuses using fetal magnetoencephalography (fMEG). *PLoS ONE*, 15(7 July):e0235310.

[Noury et al., 2016] Noury, N., Hipp, J. F., and Siegel, M. (2016). Physiological processes non-linearly affect electrophysiological recordings during transcranial electric stimulation. *NeuroImage*, 140:99–109.

[O'Donnell et al., 2013] O'Donnell, B. F., Vohs, J. L., Krishnan, G. P., Rass, O., Hetrick, W. P., and Morzorati, S. L. (2013). The auditory steady-state response (ASSR): A translational biomarker for schizophrenia. *Supplements to Clinical Neurophysiology*, 62:101–112.

[Oostenveld et al., 2011] Oostenveld, R., Fries, P., Maris, E., and Schoffelen, J.-M. (2011). FieldTrip: Open source software for advanced analysis of MEG, EEG, and invasive electrophysiological data. *Computational intelligence and neuroscience*, 2011:156869.

[Palva et al., 2005] Palva, J. M., Palva, S., and Kaila, K. (2005). Phase synchrony among neuronal oscillations in the human cortex. *Journal of Neuroscience*, 25(15):3962–3972.

[Pandey et al., 2022] Pandey, P., Miyapuram, K. P., and Lomas, D. (2022). Non-Linear Features of β Brain Rhythms Predict Listener-Specific Neural Signature in Naturalistic Music Listening.

[Pandya and Sanides, 1973] Pandya, D. N. and Sanides, F. (1973). Architectonic parcellation of the temporal operculum in rhesus monkey and its projection pattern. *Zeitschrift für Anatomie und Entwicklungsgeschichte*, 139(2):127–161.

[Pang et al., 2023] Pang, J. C., Aquino, K. M., Oldehinkel, M., Robinson, P. A., Fulcher, B. D., Breakspear, M., and Fornito, A. (2023). Geometric constraints on human brain function. *Nature*, 618(7965):566–574.

[Pantev et al., 1989] Pantev, C., Hoke, M., Lütkenhöner, B., and Lehnertz, K. (1989). Tonotopic organization of the auditory cortex: Pitch versus frequency representation. *Science*, 246(4929):486–488.

[Pantev et al., 1996] Pantev, C., Roberts, L. E., Elbert, T., Ross, B., and Wienbruch, C. (1996). Tonotopic organization of the sources of human auditory steady-state responses. *Hear Res*, 101(1-2):62–74.

[Pascual-Marqui, 2007] Pascual-Marqui, R. D. (2007). Discrete, 3D distributed, linear imaging methods of electric neuronal activity. Part 1: exact, zero error localization. *Llinas*.

[Pastor et al., 2002] Pastor, M. A., Artieda, J., Arbizu, J., Marti-Climent, J. M., Pañuelas, I., and Masdeu, J. C. (2002). Activation of human cerebral and cerebellar cortex by auditory stimulation at 40 Hz. *Journal of Neuroscience*, 22(23):10501–10506.

[Pathak et al., 2022] Pathak, A., Sharma, V., Roy, D., and Banerjee, A. (2022). Biophysical mechanism underlying compensatory preservation of neural synchrony over the adult lifespan. *Communications Biology*, 5(1):1–12.

[Peretz et al., 2015] Peretz, I., Vuvan, D., Lagrois, M. É., and Armony, J. L. (2015). Neural overlap in processing music and speech.

[Petkoski et al., 2018] Petkoski, S., Palva, J. M., and Jirsa, V. K. (2018). Phase-lags in large scale brain synchronization: Methodological considerations and in-silico analysis. *PLoS Computational Biology*, 14(7):e1006160.

[Picton, 2013] Picton, T. (2013). Hearing in time: Evoked potential studies of temporal processing.

[Plakke and Romanski, 2014] Plakke, B. and Romanski, L. M. (2014). Auditory connections and functions of prefrontal cortex. *Frontiers in Neuroscience*, (8 JUL).

[Poelmans et al., 2012] Poelmans, H., Luts, H., Vandermosten, M., Ghesquière, P., and Wouters, J. (2012). Hemispheric asymmetry of auditory steady-state responses to monaural and diotic stimulation. *JARO - Journal of the Association for Research in Otolaryngology*, 13(6):867–876.

[Pöppel, 1997] Pöppel, E. (1997). A hierarchical model of temporal perception. *Trends in cognitive sciences*, 1(2):56–61.

[Rauschecker, 2021] Rauschecker, J. P. (2021). Central Auditory Processing. In *Oxford Research Encyclopedia of Neuroscience*. Oxford University Press.

[Rauschecker et al., 1995] Rauschecker, J. P., Tian, B., and Hauser, M. (1995). Processing of complex sounds in the macaque nonprimary auditory cortex. *Science*, 268(5207):111–114.

[Reyes et al., 2005] Reyes, S. A., Lockwood, A. H., Salvi, R. J., Coad, M. L., Wack, D. S., and Burkard, R. F. (2005). Mapping the 40-Hz auditory steady-state response using current density reconstructions. *Hearing Research*, 204(1-2):1–15.

[Reyes et al., 2004] Reyes, S. A., Salvi, R. J., Burkard, R. F., Coad, M. L., Wack, D. S., Galantowicz, P. J., and Lockwood, A. H. (2004). PET imaging of the 40 Hz auditory steady state response. *Hearing Research*, 194(1-2):73–80.

[Riecke et al., 2018] Riecke, L., Formisano, E., Sorger, B., Bakent, D., and Gaudrain, E. (2018). Neural Entrainment to Speech Modulates Speech Intelligibility. *Current Biology*, 28(2):161–169.e5.

[Roberts et al., 2019] Roberts, J. A., Gollo, L. L., Abeysuriya, R. G., Roberts, G., Mitchell, P. B., Woolrich, M. W., and Breakspear, M. (2019). Metastable brain waves. *Nature Communications*, 10(1):1–17.

[Rolls et al., 2015] Rolls, E. T., Joliot, M., and Tzourio-Mazoyer, N. (2015). Implementation of a new parcellation of the orbitofrontal cortex in the automated anatomical labeling atlas. *NeuroImage*, 122:1–5.

[Ross et al., 2005] Ross, B., Herdman, A. T., and Pantev, C. (2005). Right hemispheric laterality of human 40 Hz auditory steady-state responses. *Cerebral Cortex*, 15(12):2029–2039.

[Roß et al., 2002] Roß, B., Picton, T. W., and Pantev, C. (2002). Temporal integration in the human auditory cortex as represented by the development of the steady-state magnetic field. *Hearing Research*, 165(1-2):68–84.

[Sandor and Leahy, 1997] Sandor, S. and Leahy, R. (1997). Surface-Based Labeling of Cortical Anatomy Using a Deformable Atlas. *IEEE Transactions on Medical Imaging*, 16(1):41–54.

[Schirner et al., 2015] Schirner, M., Rothmeier, S., Jirsa, V. K., McIntosh, A. R., and Ritter, P. (2015). An automated pipeline for constructing personalized virtual brains from multimodal neuroimaging data. *NeuroImage*, 117:343–357.

[Scott and McGettigan, 2013] Scott, S. K. and McGettigan, C. (2013). Do temporal processes underlie left hemisphere dominance in speech perception? *Brain and Language*, 127(1):36–45.

[Scrascia et al., 2014] Scrascia, F., Curcio, G., Ursini, F., Trotta, L., Quintiliani, L., Migliore, S., Altamura, C., Pitocco, F., Altavilla, R., Melgari, J. M., Quattrocchi, C. C., and Vernieri, F. (2014). Relationship among Diffusion Tensor Imaging, EEG Activity, and Cognitive Status in Mild Cognitive Impairment and Alzheimer's Disease Patients. *Journal of Alzheimer's Disease*, 38(4):939–950.

[Seghier and Price, 2018] Seghier, M. L. and Price, C. J. (2018). Interpreting and Utilising Intersubject Variability in Brain Function.

[Shattuck and Leahy, 2002] Shattuck, D. W. and Leahy, R. M. (2002). Brainsuite: An automated cortical surface identification tool. *Medical Image Analysis*, 6(2):129–142.

[Shattuck et al., 2001] Shattuck, D. W., Sandor-Leahy, S. R., Schaper, K. A., Rottenberg, D. A., and Leahy, R. M. (2001). Magnetic resonance image tissue classification using a partial volume model. *NeuroImage*, 13(5):856–876.

[Siever, 2007] Siever, D. (2007). *Audio-Visual Entrainment: History, Physiology and Clinical Studies*. The Haworth Medical Press.

[Singhal et al., 2023] Singhal, S., Ghosh, P., Kumar, N., and Banerjee, A. (2023). Parametric separation of phase-locked and non-phase-locked activity. *Journal of neurophysiology*, 129(1):199–210.

[Smith et al., 2012] Smith, R. E., Tournier, J. D., Calamante, F., and Connelly, A. (2012). Anatomically-constrained tractography: Improved diffusion MRI streamlines tractography through effective use of anatomical information. *NeuroImage*, 62(3):1924–1938.

[Smith et al., 2013] Smith, R. E., Tournier, J. D., Calamante, F., and Connelly, A. (2013). SIFT: Spherical-deconvolution informed filtering of tractograms. *NeuroImage*, 67:298–312.

[Sporns, 2010] Sporns, O. (2010). Analysis and Function of Large-Scale Brain Networks. *Society for Neuroscience Short Course III*, pages 1–68.

[Sporns, 2011] Sporns, O. (2011). The human connectome: a complex network. *Annals of the New York Academy of Sciences*, 1224(1):109–125.

[Sporns et al., 2004] Sporns, O., Chialvo, D., Kaiser, M., and Hilgetag, C. C. (2004). Organization, development and function of complex brain networks. *Trends in Cognitive Sciences*, 8(9):418–425.

[Stam et al., 2007] Stam, C. J., Nolte, G., and Daffertshofer, A. (2007). Phase lag index: Assessment of functional connectivity from multi channel EEG and MEG with diminished bias from common sources. *Human Brain Mapping*, 28(11):1178–1193.

[Stange-Marten et al., 2017] Stange-Marten, A., Nabel, A. L., Sinclair, J. L., Fischl, M., Alexandrova, O., Wohlfrom, H., Kopp-Scheinpflug, C., Pecka, M., and Grothe, B. (2017). Input timing for spatial processing is precisely tuned via constant synaptic delays and myelination patterns in the auditory brainstem. *Proceedings of the National Academy of Sciences of the United States of America*, 114(24):E4851–E4858.

[Steinmann and Gutschalk, 2011] Steinmann, I. and Gutschalk, A. (2011). Potential fMRI correlates of 40-Hz phase locking in primary auditory cortex, thalamus and midbrain. *NeuroImage*, 54(1):495–504.

[Toga and Thompson, 2003] Toga, A. W. and Thompson, P. M. (2003). Mapping brain asymmetry. *Nat Rev Neurosci*, 4(1):37–48.

[Tournier et al., 2007] Tournier, J. D., Calamante, F., and Connelly, A. (2007). Robust determination of the fibre orientation distribution in diffusion MRI: Non-negativity constrained super-resolved spherical deconvolution. *NeuroImage*, 35(4):1459–1472.

[Tournier et al., 2004] Tournier, J. D., Calamante, F., Gadian, D. G., and Connelly, A. (2004). Direct estimation of the fiber orientation density function from diffusion-weighted MRI data using spherical deconvolution. *NeuroImage*, 23(3):1176–1185.

[Tustison et al., 2010] Tustison, N. J., Avants, B. B., Cook, P. A., Zheng, Y., Egan, A., Yushkevich, P. A., and Gee, J. C. (2010). N4ITK: Improved N3 bias correction. *IEEE Transactions on Medical Imaging*, 29(6):1310–1320.

[van den Heuvel and Sporns, 2013] van den Heuvel, M. P. and Sporns, O. (2013). Network hubs in the human brain.

[Veraart et al., 2016a] Veraart, J., Fieremans, E., and Novikov, D. S. (2016a). Diffusion MRI noise mapping using random matrix theory. *Magnetic Resonance in Medicine*, 76(5):1582–1593.

[Veraart et al., 2016b] Veraart, J., Novikov, D. S., Christiaens, D., Ades-aron, B., Sijbers, J., and Fieremans, E. (2016b). Denoising of diffusion MRI using random matrix theory. *NeuroImage*, 142:394–406.

[von Conta et al., 2022] von Conta, J., Kasten, F. H., Ćurčić-Blake, B., Schellhorn, K., and Herrmann, C. S. (2022). Characterizing low-frequency artifacts during transcranial temporal interference stimulation (tTIS). *Neuroimage: Reports*, 2(3):100113.

[Wan et al., 2022] Wan, B., Bayrak, ., Xu, T., Schaare, H. L., Bethlehem, R. A., Bernhardt, B. C., and Valk, S. L. (2022). Heritability and cross-species comparisons of human cortical functional organization asymmetry. *eLife*, 11.

[Wang et al., 2015] Wang, L., Uhrig, L., Jarraya, B., and Dehaene, S. (2015). Representation of Numerical and Sequential Patterns in Macaque and Human Brains. *Current Biology*, 25(15):1966–1974.

[Wang, 2010] Wang, X.-J. (2010). Neurophysiological and Computational Principles of Cortical Rhythms in Cognition. *Physiological Reviews*, 90(3):1195–1268.

[Wang et al., 2023] Wang, Y., Siu, T. S. C., and Cheung, H. (2023). Effect of music emotion on mu and beta oscillations. *Psychology of Music*.

[Xie et al., 2018] Xie, H., Calhoun, V. D., Gonzalez-Castillo, J., Damaraju, E., Miller, R., Bandettini, P. A., and Mitra, S. (2018). Whole-brain connectivity dynamics reflect both task-specific and individual-specific modulation: A multitask study.

[Yu and Young, 2000] Yu, J. J. and Young, E. D. (2000). Linear and nonlinear pathways of spectral information transmission in the cochlear nucleus.

[Yurgil et al., 2020] Yurgil, K. A., Velasquez, M. A., Winston, J. L., Reichman, N. B., and Colombo, P. J. (2020). Music Training, Working Memory, and Neural Oscillations: A Review. *Frontiers in Psychology*, 11:478420.

[Zar, 1999] Zar, J. H. (1999). Biostatistical analysis.

[Zatorre, 2022] Zatorre, R. J. (2022). Hemispheric asymmetries for music and speech: Spectrotemporal modulations and top-down influences.

[Zatorre and Belin, 2001] Zatorre, R. J. and Belin, P. (2001). Spectral and temporal processing in human auditory cortex. *Cerebral cortex (New York, N.Y. : 1991)*, 11(10):946–53.

[Zatorre et al., 2002] Zatorre, R. J., Belin, P., and Penhune, V. B. (2002). Structure and function of auditory cortex: Music and speech. *Trends in Cognitive Sciences*, 6(1):37–46.

[Zatorre and Gandour, 2008] Zatorre, R. J. and Gandour, J. T. (2008). Neural specializations for speech and pitch: Moving beyond the dichotomies.

[Zeng et al., 2005] Zeng, F.-G., Nie, K., Stickney, G. S., Kong, Y.-Y., Vongphoe, M., Bhargave, A., Wei, C., and Cao, K. (2005). Speech recognition with amplitude and frequency modulations. *Proceedings of the National Academy of Sciences*, 102(7):2293–2298.

[Zhang et al., 2013] Zhang, L., Peng, W., Zhang, Z., and Hu, L. (2013). Distinct Features of Auditory Steady-State Responses as Compared to Transient Event-Related Potentials. *PLoS ONE*, 8(7):e69164.

List of Publications

- **Neeraj Kumar**, Amit Jaiswal, Dipanjan Roy, Arpan Banerjee. (2023). Effective networks mediate right hemispheric dominance of human 40 Hz auditory steady-state response. Neuropsychologia, 184, 108559. https://doi.org/10.1016/j.neuropsychologia.2023.108559

- G Vinodh Kumar, **Neeraj Kumar**, Dipanjan Roy, Arpan Banerjee. (2018). Segregation and integration of cortical information processing underlying cross-modal perception. Multisensory Research, 31(5), 481-500. https://doi.org/10.1163/22134808-00002574

- Shubham Singhal, Priyanka Ghosh, **Neeraj Kumar**, Arpan Banerjee. (2023). Parametric separation of phase-locked and non-phase-locked activity. Journal of Neurophysiology, 129(1), 199-210. https://doi.org/10.1152/jn.00467.2022

Life is a symphony of rhythms, and the dance of biology is a testament to the exquisite symmetries that exist within nature's grand design.